

Aeroacoustics of pipe systems with closed branches

Devis Tonon¹, Avraham Hirschberg¹, Joachim Golliard² and Samir Ziada³

¹Eindhoven University of Technology, Fluid Dynamics Laboratory, Faculty of Applied Physics, P.O. Box 513, 5600 MB, Eindhoven, The Netherlands

²TNO, P.O. Box 155, 2600 AD, Delft, The Netherlands

³McMaster University, Department of Mechanical Engineering, Hamilton, Ontario, Canada L8S 4L7
email: d.tonon@tue.nl, a.hirschberg@tue.nl

Flow induced pulsations in resonant pipe networks with closed branches are considered in this review paper. These pulsations, observed in many technical applications, have been identified as self-sustained aeroacoustic oscillations driven by the instability of the flow along the closed branches. The fundamental aspects of the flow induced pulsations are discussed, with particular attention to the description of the sound sources. A single mode model for the prediction of the self-sustained oscillations is presented, the "energy balance". This model consists of the evaluation of the amplitude of each acoustic mode of the system by means of a balance between the acoustic source power and the acoustic power losses. The main components of this prediction method are discussed; these are the evaluation of the acoustic behavior of a pipe network and the modeling of the sound sources and the acoustic losses. Several field and scale model examples of pipe systems displaying self-sustained oscillations are presented, in order to discuss the parameters influencing the aeroacoustic behavior of pipe networks. Finally some counter-measures for the prevention of self-sustained oscillations are reviewed and perspectives for future work are considered.

1. INTRODUCTION

1.1. FLOW INDUCED PULSATIONS

Low frequency acoustic pulsations in pipe networks have been observed in many technical applications [1–11]. These pulsations are undesirable not only because of the noise produced but also because of the possibility of mechanical failures in the pipe network. The high amplitude of the acoustic pressure fluctuations results in mechanical stresses that can cause fatigue failure. Lower pulsation levels can already affect volume flow measurements [12] or trigger vibration control equipment. Even when the vibration and pressure pulsation levels do not endanger the system safety and can be tolerated, they still cause additional pressure losses and reduce the efficiency. However small these losses might seem in percentage terms, they constitute, in absolute values, a significant amount of wasted energy.

Forced pulsations, like the pulsations driven by compressors, can be predicted in the design phase by numerical models. A different kind of acoustic pulsations is the aeroacoustic oscillation caused by the instability of the flow in the pipe systems. This kind of pulsations is called self-sustained, or self-excited oscillations.

The flow in a pipe past the opening of a closed branch forms a shear layer, which is one of the main sound sources driving aeroacoustic oscillations in pipe networks. Self-sustained aeroacoustic oscillations of unstable shear layers are due to a feedback mechanism between the hydrodynamic (vortical) flow field, associated with the unstable shear layer, and the acoustic (potential) flow field. Thus, the essential constituents of this feedback excitation mechanism are the shear layer oscillations and the resonant acoustic mode. In this case, the resonant acoustic mode provides the upstream

feedback event which strongly enhances the system oscillations.

1.2. TRAPPED ACOUSTIC MODES

Acoustic resonance of a pipe system occurs when acoustic energy accumulates into a standing wave which is called an acoustic mode of the system. The resonance modes are defined as the eigen-modes of the system [13]. Each mode is described by a complex resonance frequency and a mode shape, corresponding to the eigen-value and the eigen-vector, respectively. The real part of each complex frequency corresponds to the frequency of free oscillation of the system at resonance conditions, while the imaginary part is a measure of the quality factor of the resonance [14].

The resonance behavior of a pipe system depends on the geometry of the system and on the boundary conditions at its terminations. Resonance modes involving the whole system can be defined as global modes [15, 16] of the system and their response depends strongly on the boundary conditions. By contrast, resonance modes involving only a sub-set of the pipe system are referred to as trapped (or localized) modes [15, 16] and are not sensitive to the boundary conditions.

The trapped modes are resonance modes exhibiting zero radiation losses. These modes rarely exist in pipe networks, but more commonly encountered are the nearly trapped modes, for which the radiation losses are small. Trapped and nearly trapped acoustic modes are particularly problematic in industrial applications because they are very liable to flow excitation and can produce excessively high levels of pressure pulsations. Thus, the excitation of these modes often causes severe vibration and noise problems, some of which are briefly discussed in the following section. We will see that closed branches can induce

trapped and nearly trapped modes (Sec. 7).

1.3. EXAMPLES OF FIELD EXPERIENCE

From 1940 to 1960, Oklahoma Gas and Electric Company had problems with the safety valves installed on its boilers. Unusual noise and vibration, coming from these valves were observed by operators. The problem arose with all the re-heater safety valves located on a horizontal portion of the re-heat steam inlet line just before it enters the steam generator, and just downstream of a pipe elbow. The vibration was so severe that within a few months several valves failed. These problems promoted a systematic investigation of the flow induced vibrations in safety valves [2]. This investigation identified the standpipes of the valves, which form a row of closed side branches along a main pipe, as responsible for the occurrence of pulsations.

High amplitude pulsations, one order of magnitude higher than maximum pulsation levels corresponding to safety norms, were observed in 1973 in a compressor station (Fig. 1-a) of the Dutch gas transport system (Ommen, The Netherlands). The ratio of the amplitude of the acoustic velocity to main flow velocity reached 0.4. The pressure pulsation amplitude reached 1.5bar for a static pressure of 60bar and for pipe diameters of 42". These pulsations were identified as aeroacoustic oscillations sustained by the instability of the grazing flow along closed side branches of the pipe system [4]. As the pulsations occurred only above a critical flow velocity, the problem was solved by reducing the local velocity of the flow by means of a by-pass piping.

Peters and Riezebos [6] reported two other similar problems which occurred at a regulating station and at a measurement and control station of the

Dutch gas transport system. In the first case, the pulsations occurred in a section of the pipe network presenting two closed pressure-relieve lines (2" in diameter) along a main pipe (4" in diameter). The source of pulsations was identified to be the instability of the main flow (in the 4" pipe) grazing along the 2" vent lines. The amplitude of the pulsations, measured at the end of the relieve lines was 1.2bar with a static pressure of 60bar. In the case of the measurement and control station, the installation where flow induced pulsations were observed consists of two headers (28" in diameter) and three control sections (8" in diameter). These pulsations were not due to the instability of a grazing flow, but to the instability of the flow entering the 28" low-pressure header, leaving one of the 8" control sections.

Gorter [17] also observed strong pulsations on a long (few meters) side branch of 0.5" diameter along a 12" main pipe. This side branch was used as connection to a manometer, monitoring the static pressure. Pulsations were detected as a result of the associated thermal heating on the wall of the side branch. The paint at the end of the closed side branch would burn off.

In 2002, the steam dryer (Fig. 1-b) in the boiling water reactor (BWR) of Quad Cities Unit 2 (QC2) experienced high cycle fatigue cracks after the reactor's maximum power was increased by approximately 17%. Repairing the

dryer by using thicker plates and stronger welds did not resolve the problem, as the dryer exhibited new cracks upon continued operation [18]. The cracks appeared on the dryer outer plates, which face the inlet nozzles of the main steam lines (MSLs). The steam dryer was therefore replaced with a substantially more robust one which was also instrumented with pressure transducers to provide direct measurements of the pressure fluctuations at numerous locations. During this course of events, the safety relief valves (SRVs) on the MSLs were experiencing high vibration levels, and subsequent inspection for maintenance during a refueling outage showed that some safety valves had been damaged. The pressure measurements on the steam dryer indicated that increasing the steam velocity in the MSLs, related to the increase in the reactor power, excited the acoustic modes in the standpipes of the safety valves, which are mounted on the MSLs. The resonance was so strong that it not only damaged some of the valves, but also propagated upstream in the MSLs and into the reactor dome and damaged the steam dryer. The problem was solved by changing the standpipe geometry to avoid the acoustic resonance at the increased rated power [8, 9, 11].

Turbine by-pass steam piping is another example of side branches which is often encountered in power plants. When the by-pass valve is closed, which

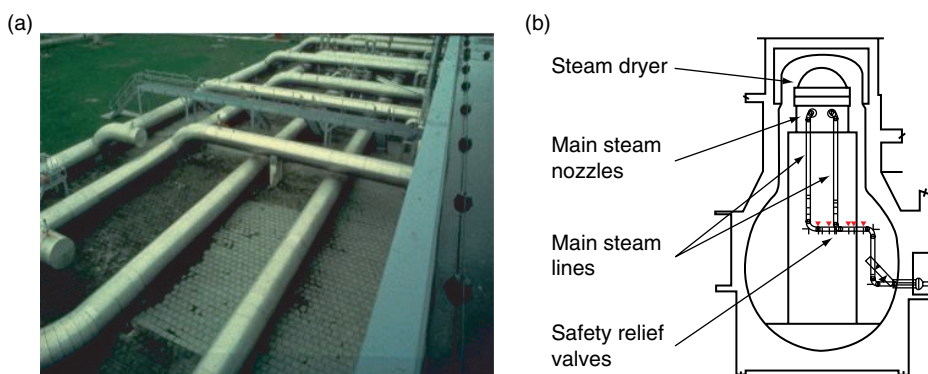


Figure 1: Ommen compressor station (a) and main steam piping layout of the boiling water reactor (BWR) of Quad Cities Unit 2 (b) [9].

is the normal operation mode, the by-pass steam line forms two closed side branches; one branch upstream of the valve connected to the fresh steam pipe and a downstream branch connected to the cold re-heat pipe. Generally, there are multiple by-pass valves for each turbine and consequently multiple side branches in close proximity to each other often exist in power plants. Such pipe arrangements can display trapped or nearly trapped acoustic modes which, as mentioned earlier, are very liable to flow excitation [19]. Serious vibration problems in power plants caused by acoustic resonance in multiple closed side branches were reported by Chen and Stürchler [1] and Gillessen and Roller [20].

1.4. OVERVIEW OF THE PAPER

The present review paper is divided into fourteen sections. In the present section we have introduced the concepts of flow induced pulsations and trapped acoustic modes, and presented some field experiences where these phenomena have been observed. In the following four sections we present the fundamental aspects of the flow induced pulsations in pipe systems with closed branches, these are: the theory of sound produced by vortical disturbances due to shear layer instability (Sec. 2), the description of the hydrodynamic and acoustic conditions for the occurrence of self-sustained oscillations (Sec. 3), the characteristics of the self-sustained oscillations due to the instability of a shear layer (Sec. 4) and the linear stability theory of the shear layer (Sec. 5). Then, in Sec. 6 we present a simple “frequency domain” model to predict the self-sustained oscillations by means of the energy balance technique. In Sec. 7, we describe the prediction of the acoustic behavior of pipe networks and introduce some examples of acoustic resonators displaying self-sustained oscillations. The identification and the modeling of the sound sources in pipe

systems with closed branches are discussed in Sec. 8 and Sec. 9 respectively. Finally, the last five sections present: a qualitative description of the hydrodynamic interaction (Sec. 10), the role of wall vibrations (Sec. 11), some remedial measures for the prevention of self-sustained oscillations (Sec. 12), the design of scale models (Sec. 13) and an overview of some open questions (Sec. 14).

2. VORTEX SOUND

The instability of separated flows such as shear layers, wakes and free jets acts as a source of unsteadiness for flows at high Reynolds numbers. An unsteady flow induces an unsteady force on the walls, associated to vortex shedding. The reaction force of the walls to this hydrodynamic force is a source of sound [21]. The vorticity in a flow field is therefore related to the sound produced [22, 23].

One can qualitatively understand this feature by considering the familiar case of the singing wire: the tone generated by a cylinder of diameter D_{cyl} in a steady cross flow of velocity U . When we assume a potential flow around the cylinder, there is no net force applied by the flow on the cylinder because of the symmetry of the flow field. However, due to viscous effects, vorticity shedding in the cylinder wake breaks the symmetry of the flow field. Above a critical Reynolds number $Re_{D_{cyl}} > 50$ based on the diameter of the cylinder, instability of the wake is observed which results in the formation of periodic vortex shedding at a frequency $f_{vk} \approx 0.2U/D_{cyl}$. This so called von Karman vortex street [24–26] is associated to an oscillating lift force applied by the fluid on the cylinder [27]. The reaction force of the cylinder to this lift force is the source of tone generation, which was studied first by Strouhal [28].

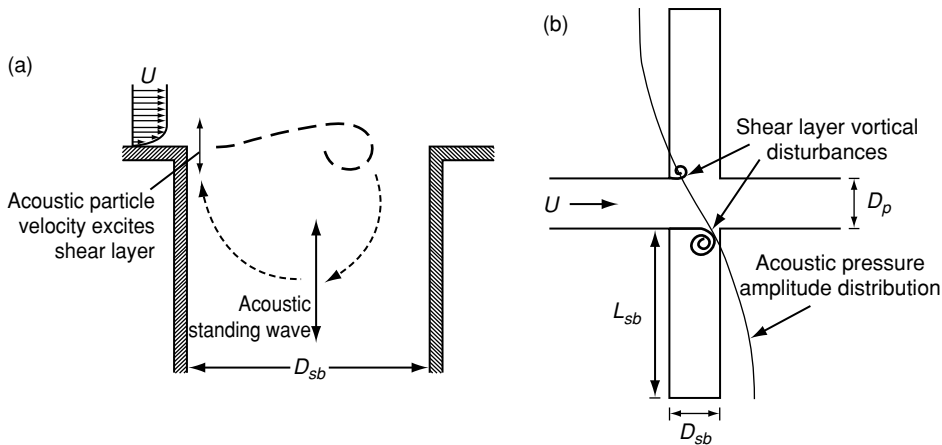


Figure 2: Feedback loop characterizing the self-sustained oscillations (a) and double side branch system in cross configuration (b).

It is essential to realize that the cylinder walls do not need to vibrate in order to generate the sound. However, if a mechanical vibration of the cylinder is induced by the oscillating lift force, this can significantly enhance the spatial coherence of the vortex shedding along the cylinder and result into a stronger tone. This is likely to occur when the cylinder mechanical resonance frequency is close to the natural Strouhal vortex frequency $f_{vk} D_{cyl}/U \approx 0.2$.

A similar lock-in can occur with an acoustic standing wave (resonant mode) when the cylinder is confined in a duct or in a cavity [29–31]. This enhances even more the sound radiation, because the acoustic standing wave provides improved radiation impedance to the sound source. The resulting high amplitude acoustic oscillation controls the vortex shedding. This is an example of a self-sustained oscillation. The global behavior of these kind of oscillations can be described in terms of a feedback loop (Fig. 2-a) consisting of an amplifier (flow instability) coupled to a narrow band filter (acoustic resonance). Reviews of self-sustained oscillations involving a coupling between flow instability and a resonant acoustic field are provided by Rockwell [32], Rockwell and Naudascher [33, 34], Blake [27], Blake and Powell [35], Powell [36], Howe [37–39] and Gloerfelt [40]. These reviews also consider

hydrodynamic instabilities in which acoustic resonance is absent, such as edge tones or shallow cavities oscillations. We restrict ourselves to resonant cavities for which the coupling with an acoustic mode is essential. Please note that we selected the example of the cylinder because it is clear that in this case there is no impingement of the separated flow on a sharp edge. Actually, the concept of sound produced by impingement of a separated flow (such as a shear layer) used in early literature is rather misleading. In contrast to the vortex sound theory described below, it is a verbal conjecture without quantitative predictive value.

A formal relationship between vortex shedding and sound generation has been first established for free field conditions by Powell [22] and generalized by Howe [23, 41, 42]. Howe [41] proposes to use a Helmholtz decomposition of the flow field \vec{u} to define the acoustic field:

$$\vec{u} = \nabla(\varphi_0 + \varphi') + \nabla \times \vec{\psi} \quad (1)$$

where φ_0 is a steady scalar potential, φ' is the unsteady scalar potential and $\vec{\psi}$ is the stream function. The acoustic field \vec{u}' is defined by Howe [41] as the unsteady irrotational part of the velocity field:

$$\vec{u}' \stackrel{def}{=} \nabla \varphi' \quad (2)$$

The ambiguity in the Helmholtz decomposition is in practice removed by the boundary conditions which we impose to the acoustic field.

We consider flows with a high Reynolds number and a low Mach number so that we can neglect friction and heat transfer. Assuming a homentropic flow (uniform entropy), we can use the formulation of Crocco for the momentum equation:

$$\frac{\partial \bar{u}}{\partial t} + \nabla B = -\bar{\omega} \times \bar{u} \quad (3)$$

where $B = |\bar{u}|^2/2 + \int 1/\rho dp$ is the total enthalpy and $\bar{\omega} = \nabla \times \bar{u}$ is the vorticity.

At low Mach numbers, we can neglect the convective effects on the propagation of sound waves. With this assumption one finds the wave equation:

$$\frac{1}{c_0^2} \frac{\partial^2 B}{\partial t^2} - \nabla^2 B = \nabla \cdot (\bar{\omega} \times \bar{u}) \quad (4)$$

where c_0 is the speed of sound.

The last equation shows that the Coriolis force density $\vec{f}_{\text{coriolis}} = -\rho_0 (\bar{\omega} \times \bar{u})$, where ρ_0 is the fluid density, acts as source of sound.

As proposed by Howe [41], the time-averaged acoustic source power $\langle P_{\text{source}} \rangle$ can be estimated using the low Mach number $|\bar{u}|/c_0 \ll 1$ approximation:

$$\langle P_{\text{source}} \rangle = -\rho_0 \left\langle \int_V (\bar{\omega} \times \bar{u}) \cdot \bar{u}' dV \right\rangle \quad (5)$$

where V is the volume in which $\bar{\omega}$ is not vanishing and the brackets $\langle \dots \rangle$ indicate time averaging. The fact that we integrate over space and average over one oscillation period makes this formulation quite robust. Furthermore, it is quite successful because it stresses the dipole character of the sound source, which is dominant in the cases considered [43].

The power transfer from the hydrodynamic field to the acoustic field is due to the pressure difference across the source region which is in phase with the acoustic velocity \bar{u}' . The pressure difference in phase with the acoustic acceleration $d\bar{u}'/dt$ will act as an added mass to the acoustic resonator. This corresponds to the so called “end correction” to the length of the pipe segments, used to predict acoustic resonances of pipe systems by means of a plane wave model [44] (Sec. 7.2).

3. ACOUSTIC AND HYDRODYNAMIC MODES

The flow induced pulsations of double closed side branch systems in cross configuration (Fig. 2-b) have been extensively studied [19, 45–55]. We consider two closed side branches of equal length L_{sb} and diameter D_{sb} connected to a cross-junction with the main pipe of diameter D_p . We use this relatively simple configuration in order to introduce the basic concepts of acoustic and hydrodynamic modes.

The amplitude of the acoustic pressure $|p'_{\text{max}}|$ measured [48] at the closed end of the side branches and the corresponding whistling frequency f are presented as function of the main flow velocity U in Fig. 3-a. The different resonant acoustic modes, corresponding to acoustic standing waves with frequencies $f_n \approx (2n-1)c_0/(4L_{sb})$, $n = 1, 2, 3, \dots$, are clearly observed in Fig. 3-a. Only the odd acoustic modes, consisting of odd multiples of a quarter wavelength in each branch, are resonant because they have a pressure node at the junction.

The resonance modes display an anti-symmetric spatial distribution of the acoustic pressure amplitude at the junction which does not generate plane waves in the main pipe. For frequencies below the cut-off frequency f_{cut} for propagation of non-planar modes in the main pipe, the odd acoustic modes do

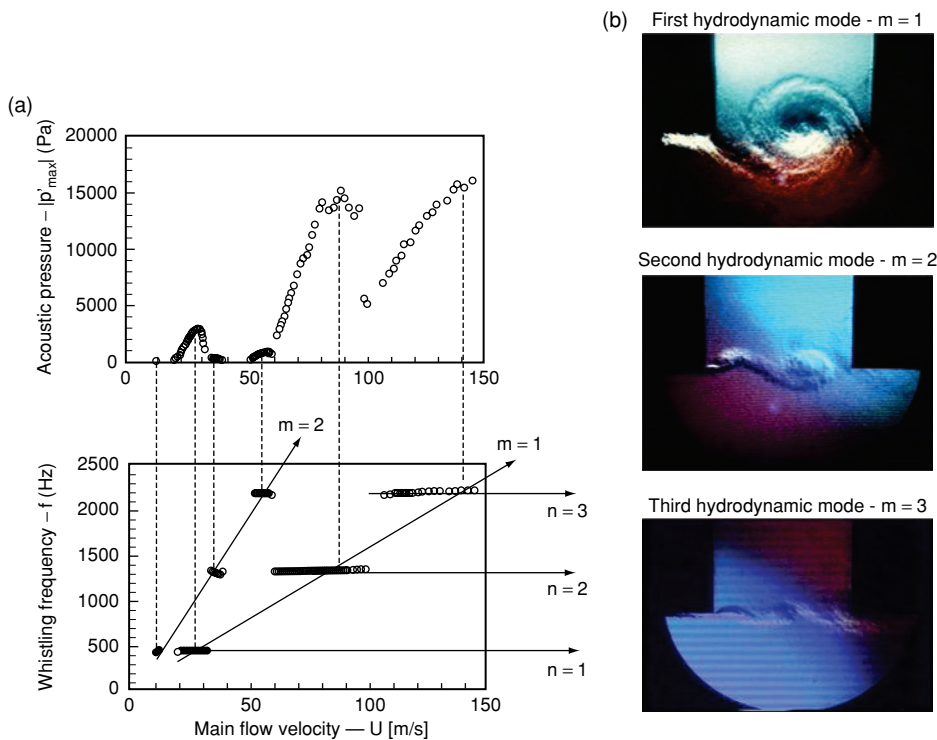


Figure 3: Acoustic measurements [48] (a) and flow visualizations [45] (b) in a double side branch system in cross configuration with sharp edges. The acoustic measurements have been carried out in a system with circular cross section of the pipes and with side branch diameter $D_{sb} = 2.5\text{cm}$, main pipe diameter $D_p = 3\text{cm}$ and side branch length $L_{sb} = 20\text{cm}$. The flow visualizations have been carried out in a system with square cross section of the pipes and with side branch width equal to the main pipe width $W_{sb} = W_p = 6\text{cm}$ and side branch length $L_{sb} = 56.4\text{cm}$. The third hydrodynamic mode, observed in the flow visualizations, corresponds to very low pulsation amplitudes so that it has not been reported in the acoustic measurements.

not radiate into the main pipe. Therefore, these modes are trapped modes, exhibiting negligible radiation losses. In addition, the maximum acoustic velocity of these modes occurs at the branch opening, where the shear layer vortices are formed. Since these vortices are also convected with the flow in a direction which is normal to the acoustic velocity oscillation, the acoustic power production, according to Eq. (5), is at its maximum. These unique features of negligible radiation losses and efficient sound power production make the well-tuned double closed side branch systems in cross configuration very liable to strong flow excited acoustic resonances.

As can be seen from Fig. 3-a, the flow induced pulsations occur in certain intervals of the Strouhal number $Sr_{w_{eff}} = fW_{eff}/U$ based on the effective cavity width W_{eff} . Within each of these intervals, the Strouhal number at which the acoustic pressure $|p'_{max}|$ displays a maximum is referred to as the optimal Strouhal number $Sr_{w_{eff},opt}$. While the optimal Strouhal number is useful to indicate the conditions of maximum pulsation amplitude, in engineering practice one often uses the critical Strouhal number $Sr_{w_{eff},cri}$ that indicates the conditions for the onset of the pulsations, i.e. the highest velocity before the onset of pulsations.

The relevant length scale in problems concerning the aeroacoustic

behavior of pipe systems with closed side branches has been identified by Bruggeman et al. [56] to be the effective cavity width W_{eff} of the side branch at the junction. For a side branch with rectangular cross section $W_{eff} \approx W_{sb} + r_{up}$, where W_{sb} is the width of the side branch and r_{up} the radius of curvature of the upstream edge of the junction (Fig. 14). For side branches with circular cross section of diameter D_{sb} , the effective width is $W_{eff} \approx \pi D_{sb}/4 + r_{eff}$, where $\pi D_{sb}/4$ is the average width of the side branch cross section. This is the width (dimension along the flow direction) of a rectangular opening with the same surface area and the same depth (dimension normal to the flow direction) as the circular opening. Experiments by Bruggeman et al. [56] indicate that for circular cross sections, r_{eff} is the minimum radius of curvature r_{up} of the upstream edge of the junction (Fig. 14).

As can be seen in Fig. 3-a, pulsations occur at a certain acoustic mode n within several, but limited ranges of flow velocity, which correspond to the so called hydrodynamic modes of the shear layer and are referred to in the figure by the integers $m = 1, 2, \dots$. The order of the hydrodynamic mode m indicates the number of vortices formed by the shear layer between the upstream and downstream edges of the side branch opening.

The first hydrodynamic mode $m=1$, corresponding to one vortex in the side branch opening (Fig. 3-b), appears usually at an optimal Strouhal number $Sr_{weff,opt} \approx 0.4$. The convective velocity of the vortex is about $U_{con} \approx 0.4U$ [56], hence the travel time of the vortex across the opening is one oscillation period $T = 1/f$. Please note that at high amplitude oscillations, such as shown in Fig. 3-a, one observes a decrease of $Sr_{weff,opt}$ down to 0.3 [45, 47, 48, 50]. This is due to a decrease of the convective speed as the vortex enters deep into the side branch.

For the second hydrodynamic mode $m = 2$, two vortices are present at the same time in the opening of the side branch (Fig. 3-b), and the time needed by a vortex to travel across the junction is then two oscillation periods, which corresponds to $Sr_{weff,opt} \approx 0.8$.

A third hydrodynamic mode $m = 3$ has been observed by Peters [45] (Fig. 3-b), but it corresponds to very low pulsation amplitudes. It has therefore not been reported by Kriesels et al. [48].

For similar cavity flows, other researchers [32, 33, 40] observed experimentally up to the fifth hydrodynamic mode of the shear layer. Modes higher than the fifth might not appear due to merging of successive vortices in the shear layer, as observed in free shear layers [32, 40, 57].

From Fig. 3-a, it appears that the sound source is most effective when it is operating at the first hydrodynamic mode $m = 1$. Indeed, most of the severe pulsations observed in field experiences correspond to $m = 1$. When the flow velocity is increased gradually, the higher order hydrodynamic modes $m > 1$ are observed before observing the first hydrodynamic mode $m = 1$. Fig. 3-a clearly depicts this feature: each specific acoustic mode ($n = 1, 2, 3, \dots$) is first excited by the second hydrodynamic mode $m = 2$ and then by the first hydrodynamic mode $m = 1$.

In principle, each hydrodynamic mode m could couple with each acoustic mode of the system n . The amplitude of the pulsations increases with the acoustic mode number n simply because, at a fixed Strouhal number $Sr_{weff} = fW_{eff}/U$ (fixed hydrodynamic mode m), a higher frequency implies a higher flow velocity. Hence more flow power $1/2 \rho_0 U^3 (\pi D_{sb}^2/4)$ is available to drive the pulsations [58].

In order to compare the amplitudes of the pulsations, they should be presented in a dimensionless form. It appears that the physically most relevant dimensionless form is to compare the acoustic velocity amplitude

$|\bar{u}'_{jim}|$ at the sound source with the steady main flow velocity U . In the particular case of a resonant closed branch, this corresponds to the ratio $|p'_{\max}|/(\rho_0 c_0 U)$ of the pressure amplitude $|p'_{\max}|$ at a pressure antinode in the closed branch (i.e. at the closed branch termination) divided by the product $\rho_0 c_0 U$ of the characteristic impedance $r_0 c_0$ of the fluid with the main flow velocity U . When presented in this form, the dimensionless amplitude of the pulsations for the first hydrodynamic mode of Fig. 3-a appear to be of order unity, while the pulsation amplitude for the second hydrodynamic mode appears to be an order of magnitude lower.

Based on this dimensionless form, Bruggeman et al. [56] introduced the concept of low, moderate and high amplitude pulsations, which we will discuss in Sec. 8.3.

Using the stagnation pressure $\rho_0 U^2/2$ as characteristic pressure is useful for moderate amplitudes (Sec. 13.2). At high amplitudes scaling with $\rho_0 c_0 U$ appears to be better (Sec. 13.1).

4. SELF-SUSTAINED OSCILLATIONS

Self-sustained oscillations of unstable shear layers can be described by means of a lumped element model as the instability of a feedback loop (Fig. 2-a) involving the unstable hydrodynamic (vortical) flow field and the acoustic (potential) flow field [59–63].

Since self-sustained oscillations involve often only one dominant mode, these kind of oscillations can be described considering a single mode model of the acoustic behavior of the pipe system. Drawing a parallel between the oscillations of mass-spring systems and the aeroacoustic pulsations in pipe systems, each acoustic mode of the pipe system will be described by discussing the oscillations of an independent mass-spring system [64].

The vortex shedding at discontinuities in a pipe system corresponds to an external force \vec{F}_{ext} . This force is triggered by the acoustic velocity and it maintains the oscillations. In a mass-spring system this force is considered proportional to the velocity of the mass (corresponding to the acoustic velocity), so that it can maintain self-sustained oscillations.

The amplitude and phase responses of a forced mass-spring system are represented in Fig. 4 in terms of the velocity of the mass $d\bar{x}/dt$. The amplitude of this response has a maximum at a frequency f close to the natural frequency of the free oscillation regime f_n . This maximum corresponds to the resonance condition of the forced oscillation regime. The quality factor Q is defined as the ratio $f_n/\Delta f_n$ of the resonance frequency and the width of the resonance peak 3dB below the peak amplitude. The phase φ_{ac} between the excitation force \vec{F}_{ext} and the velocity of the mass $d\bar{x}/dt$ changes from $\varphi_{ac} = -\pi/2$ at low frequencies, where the response of the mass is quasi-static, towards $\varphi_{ac} = \pi/2$ at high frequencies, where the mass movement is opposite in sign to the excitation. When there is no damping, the phase transition is abrupt and occurs at $f = f_n$. As the damping increases (the quality factor Q decreases) the transition becomes more gradual. This phase transition around the resonance frequency is essential to understand the behavior of self-sustained oscillations.

For periodic oscillations the total time delay along the feedback loop should be an integer number of the oscillation period. From this oscillation condition we can determine the whistling frequency f of the self-sustained oscillations:

$$\frac{2\pi f W_{eff}}{U_{con}} + \varphi_{ac} = 2\pi m \quad (6)$$

where the first term of the left side is the phase delay due to convection and φ_{ac} is

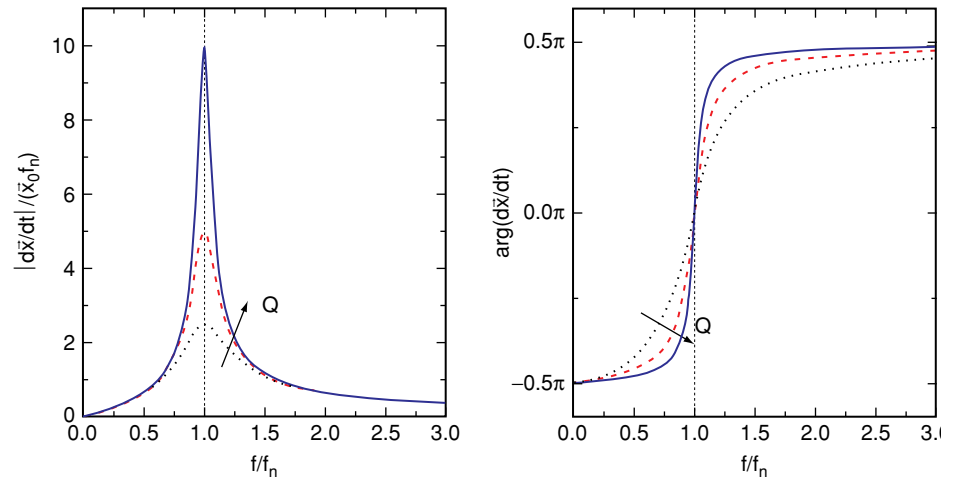


Figure 4: Amplitude response (left) and phase response (right) of a forced mass-spring system for different values of the quality factor $Q = 2.5, 5, 10$. The dimensionless amplitude $|d\bar{x}/dt|/(\bar{x}_0 f_n)$ and the phase $\arg(d\bar{x}/dt)$ of the velocity oscillations are presented in function of the dimensionless frequency f/f_n , where \bar{x}_0 is the rest position of the system and f_n is the natural frequency of the free oscillation regime.

the phase between the excitation force due to vortex shedding (which can be expressed as a source pressure related to the sound source) and the acoustic velocity at the source position.

The convective velocity U_{con} depends on the amplitude of the oscillation. For high amplitudes the vortex path enters deep into the closed branch, resulting into a decrease of the convective velocity. This decrease results into a lowering of the Strouhal number for maximum pulsation level (optimal Strouhal number) [45, 47, 48, 50]. As explained in Sec. 2, the flow also involves an acoustical inertia. This inertia corresponds to the added mass term experienced by an oscillating object placed in a flow [65]. In our case the added mass term is taken into account by the end corrections to the length of the pipe segments (Sec. 7.2). We neglect the amplitude dependence of these end corrections. This implies that the observed oscillation frequency at maximum pulsation level will differ slightly from the passive resonance frequency in the absence of main flow.

The optimal oscillation condition corresponds to acoustic resonance $f \approx f_n$ and implies $\varphi_{ac} \approx 0$. When the flow

velocity U is changed the phase delay due to convection is modified because the convective velocity $U_{con} \propto U$ changes. Furthermore the oscillation condition (Eq. (6)) is not satisfied anymore at the resonance frequency f_n . By adjusting the oscillation frequency f , the system can reach any phase in the range $-\pi/2 < \varphi_{ac} < \pi/2$ which leads to the matching of the oscillation condition (Eq. (6)), allowing whistling within a finite velocity range (Fig. 3-a) for a given hydrodynamic and acoustic mode. By shifting away from the resonance, the amplitude of the response of the system is reduced. The oscillation frequency f increases gradually with increasing flow velocity. For velocities below the value for optimal oscillation condition, the oscillation amplitude increases with increasing the flow velocity. When the optimal flow velocity is reached a further increase implies a decrease of the response of the acoustic mode and, as a consequence, a reduction of the pulsation amplitude. When losses become too large, the oscillation stops or an oscillation involving other hydrodynamic or acoustic modes becomes dominant (Fig. 3-a).

When the resonator has a high quality factor Q , the frequency change due to change in flow velocity U remains very small for a given acoustic mode. We therefore observe a typical stepwise increase in frequency f (Fig. 3-a) rather than a gradual increase of frequency f with increasing flow velocity U .

As will be explained in Sec. 5 a stable limit cycle of the oscillation of a feedback system cannot be achieved when all the elements of the loop display a linear behavior. A non-linear saturation mechanism is essential to obtain a stable periodic oscillation at finite amplitude [60].

The changes in hydrodynamic and acoustic modes can display hysteresis [47, 56]. This implies that the oscillations modes will appear, respectively disappear, at different flow velocities U . This is common for non-linear systems.

5. THE SHEAR LAYER INSTABILITY AND SATURATION

The shear layer instability is the source of unsteadiness that acts as the amplifier in the feedback loop generating self-sustained oscillations (Fig. 2-a). The growth of vortical disturbances in the shear layer separating the main pipe flow from the stagnant fluid in the closed side branch has been extensively studied by means of the linearized stability theory since Rayleigh [66].

The effect of finite momentum thickness of the velocity profile of the mean flow on the spatial amplification and convective velocity (phase speed) of hydrodynamic waves in an inviscid parallel free shear layer has been predicted by Michalke [67]. The nature of the coupling between the shear layer and the acoustic field at the flow separation point at $x = 0$, where the shear layer is formed, is not addressed in the analysis of Michalke [67]. For a given initial harmonic perturbation of

the vorticity field at position $x = 0$, the theory predicts an exponential spatial growth $e^{-\alpha_i x}$. The predicted influence of the mean flow velocity profile on the spatial growth of unstable waves has been confirmed by experiments [68]. The predicted spatial amplification exponent $-\alpha_i \theta_s$ [67] is shown in Fig. 5 as a function of the Strouhal number $Sr_\theta = f \theta_s / U$ based on the shear layer momentum thickness θ_s .

For low frequencies or thin shear layer compared to the hydrodynamic wavelength, the theory predicts an integral amplification over one wavelength by a factor $e^{2\pi}$. This low frequency limit is indicated by the dotted line in Fig. 5. Furthermore, the theory predicts that for frequencies above:

$$\frac{f \theta_s}{U} = 0.04 \quad (7)$$

the perturbations are not amplified. Therefore, hydrodynamic waves with wavelength $\lambda_h = 0.4U/f$ shorter than about ten times the shear layer momentum thickness θ_s are not amplified by the shear layer and cannot be self-sustained. This implies that when the main flow velocity is increased monotonically, the highest hydrodynamic mode to appear is determined by the critical ratio λ_h / θ_s of hydrodynamic wavelength λ_h to momentum thickness θ_s , as discussed above. The Strouhal number above which $-\alpha_i \theta_s < 0$ has been confirmed experimentally [68].

The exponential growth of vorticity perturbations with increasing distance from the flow separation point is only observed as long as the shear layer perturbations are very small. For large perturbations, the shear layer is observed to roll-up into coherent vortex structures as can be seen from the flow visualizations in Fig. 3-b.

The concentration of the shear layer vorticity into discrete vortices, clearly observed in Fig. 3-b, is the non-

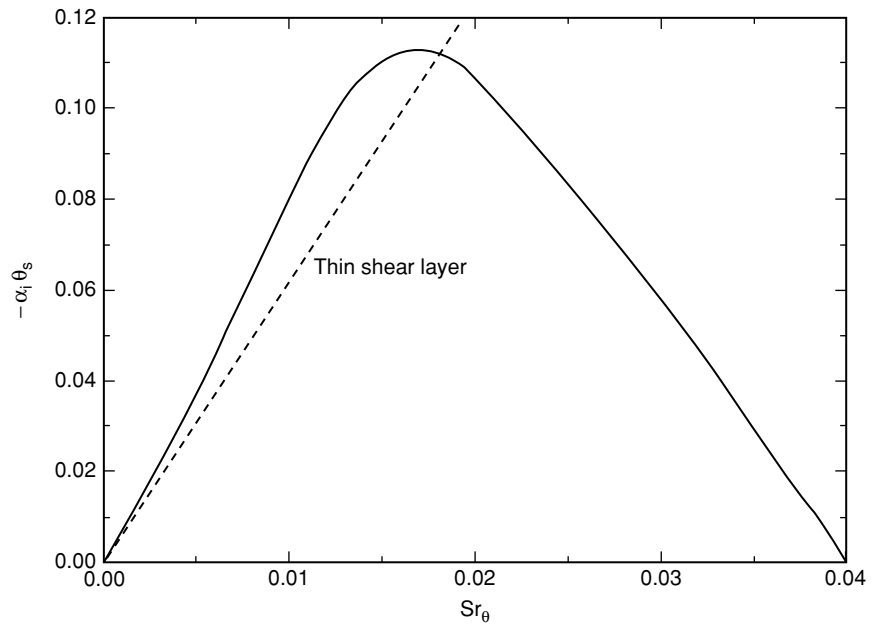


Figure 5: Amplification rate $-\alpha_i \theta_s$ for a shear layer with finite thickness as function of the Strouhal number based on the shear layer momentum thickness Sr_θ [67].

linear saturation mechanism which explains the stabilization of the feedback loop oscillation at finite pulsation amplitude [56, 60, 69]. As the perturbation amplitude becomes very large, $|\bar{u}'_{jun}|/U = O(1)$, another non-linearity appears, which is caused by the acoustically induced flow separation at the downstream edge and the amplitude dependence of the rate of vortex shedding at the upstream edge. This effect is referred to as “vortex damping” and has been predicted by Howe [39] and by Disselhorst and van Wijngaarden [70]. Furthermore, it has been experimentally demonstrated by Graf and Ziada [71, 72] and Ziada [47]. At yet higher amplitudes, non-linear wave steepening, which generates radiation losses, can become significant [45, 48, 50, 73, 74]. This wave steepening leads eventually to the formation of acoustic shock waves [45, 50, 73, 74].

6. ENERGY BALANCE

In general, prediction of the self-sustained oscillations can be achieved by means of the classical “time-domain”

approach in which the equations of motion are integrated numerically. However, if the oscillations are harmonic, we can use a “frequency-domain” approach, in which we consider the steady oscillations in the frequency domain. In the following we describe two “frequency-domain” methods, the single mode model of Bruggeman et al. [56] and the less formal energy balance approach.

A formal procedure to determine the self-sustained oscillation behavior of a pipe system with closed branches has been obtained by Bruggeman et al. [56, 75]. This consists of a single mode model for the low frequency sound production by vortical non-homogeneities in a pipe system with low Mach number flow. The propagation of low frequency sound in a two-dimensional duct system was studied by means of the method of matched asymptotic expansions [75]. An integral formulation of the problem of sound produced by aeroacoustic sources in T-junctions was derived using the formula of Green. The Green’s function was determined as proposed by Howe [23, 76] by coupling a locally incompressible potential flow model at the junctions to

a plane wave model (Sec. 7.2) in the pipe segments. The Green's function was expanded in terms of modes of the pipe system. The resulting expansion was solved with the method of vander Pol and the source terms were modeled analytically. This results into a set of coupled second order differential equations, one for each mode. This approach has been inspired by the approach proposed by Fletcher [60] for wind instruments. Assuming that a single mode is dominant yields a single second order equation as used by Bruggeman et al. [56, 75] and by Dequand et al. [50].

A less formal method for the prediction of the self-sustained oscillations is the energy balance approach. This method assumes that at fixed flow conditions only a single acoustic mode of the pipe network is dominating and that each resonance has a high quality factor so that the oscillation frequency f corresponds, in first approximation, to that of an acoustic mode f_n of the system. The evaluation of the mode amplitude, that is the amplitude of the steady harmonic oscillation, is carried out through a balance between the time-averaged acoustic source power $\langle P_{source} \rangle$ and the time-averaged acoustic power losses $\langle P_{loss} \rangle$, in order to satisfy the acoustic energy balance of the whole system. The acoustic source power $\langle P_{source} \rangle$ is modeled by using the formulation of Howe (Eq. (5)). Acoustic losses $\langle P_{loss} \rangle$ are due to different contributions, the most important are: radiation of acoustic waves $\langle P_{rad} \rangle$, visco-thermal dissipation by friction and heat transfer $\langle P_{v-th} \rangle$, non-linear radiation losses due to wave steepening $\langle P_{rad-nl} \rangle$, energy transfer to wall vibrations $\langle P_{wall} \rangle$ and sound absorption by vortex shedding $\langle P_{vort} \rangle$ at pipe discontinuities. In principle, the last effect is included in the theory of vortex sound (Eq. (5)). However, in some cases, simplified (quasi-steady) theories can be used,

which do not involve details of the flow [77–80].

7. GLOBAL ACOUSTIC BEHAVIOR OF A PIPE SYSTEM

7.1. CLOSED BRANCHES AS ACOUSTIC DELIMITERS

We consider self-sustained acoustic pulsations in pipe systems involving a resonant acoustic field. This resonant field can be described in first approximation as a standing wave of the system. This standing wave is localized in space by acoustic delimiters.

Acoustic delimiters in a pipe system are discontinuities in the system inducing strong reflections. These can be for example a sudden area expansion, an open pipe termination, an orifice or a choked valve. The aeroacoustic response of such acoustic delimiters has been extensively discussed in literature [77–90].

An interesting type of acoustic delimiter is the closed branch. This is composed by a pipe segment connected on one side to a junction (usually a T-junction or a cross-junction) and closed at the other side.

The closed branch of length L_{cb} acts as “perfect” reflector at frequencies $f_n \approx (2n - 1) c_0 / [4(L_{cb} + \delta_{cb})]$, $n = 1, 2, 3, \dots$. The so called end correction δ_{cb} takes into account the inertia of the acoustic flow at the junction. In absence of mean flow this end correction has been evaluated by Benade [91], Keefe [92, 93], Nederveen [94], Bruggeman [75] and Dubos et al. [95]. For these critical frequencies f_n below the cut-off frequency for non-planar waves $f_n < f_{cut}$, the standing wave patterns display a pressure node at the junction.

7.2. LOW FREQUENCY MODELING

For a global prediction of the standing wave pattern of a complex pipe system with closed branches, we assume that the relevant oscillations have frequencies below the cut-off frequency

f_{cut} for non-planar wave propagation, so that only plane waves propagate in the various pipe segments composing the system. Within pipes with circular cross section, the first evanescent pipe mode decays in space, for low Helmholtz numbers $He_D = 2\pi f D / c_0 \ll 1$ based on the pipe diameter D , as $e^{-2\pi f_{cut} x / c_0} \approx e^{-3.68 x / D}$. Hence, the plane wave assumption is quite accurate within one diameter from the junction.

When calculating the standing wave behavior of a pipe system (resonance modes), we neglect the sound sources in the system. Then, for low Helmholtz numbers $He_D \ll 1$, at each junction in the pipe system the difference in fluctuations of the total enthalpy B' between points in different sections of the junction, at about one pipe diameter from the junction, is negligible. This result is derived by using the linearized form of the Bernoulli equation (integral of momentum equation along a streamline assuming a potential acoustic flow):

$$\frac{p'_1}{\rho_0} + U_1 u'_1 = \frac{p'_2}{\rho_0} + U_2 u'_2 = \dots = \frac{p'_N}{\rho_0} + U_N u'_N \quad (8)$$

where 1, 2, ... N are the indices of the different pipe segments meeting at the junction (Fig. 14), p' and u' are the acoustic pressure and the acoustic velocity of the plane waves, U is the main flow velocity and ρ_0 is the fluid density.

The set of equations is then complemented by the linearized integral mass conservation law:

$$\sum_{j=1}^N \left(\rho_0 u'_j + \frac{p'_j}{c_0^2} U_j \right) \hat{n}_j S_j = 0 \quad (9)$$

where the index j refers to the different pipe segments meeting at the junction, \hat{n} is the unit vector of the different sections of the junction (directed outwards the junction), S is the cross sectional area of each pipe meeting at the junction and c_0 is the speed sound.

To obtain more explicit results we assume harmonic waves so that the d'Alembert solution for plane waves in pipe segments can be introduced in the form:

$$\begin{aligned} p'_j &= p_j^+ \exp[i(\omega t - k_j^+ x_j)] + p_j^- \exp[i(\omega t + k_j^- x_j)] \\ u'_j &= \frac{p_j^+ \exp[i(\omega t - k_j^+ x_j)] - p_j^- \exp[i(\omega t + k_j^- x_j)]}{\rho_0 c_0} \end{aligned} \quad (10)$$

where $\omega = 2\pi f$ is the angular frequency, p^\pm is the complex amplitude of the wave traveling in the positive/negative direction and $k^\pm = \omega / (c_0 \pm U)$ is the wave number.

In these equations, we assume the origin of the coordinates of each pipe segment to be at the junction which we consider. The positive direction is chosen outwards from the junction. The set of equations is mathematically closed by imposing the acoustic boundary conditions at the boundaries of the pipe system.

The visco-thermal losses can be taken into account in the model by incorporating them in the wave number k^\pm , in absence of main flow as discussed by Kirchhoff [96], Rayleigh [66], Tijdeman [97], Kergomard et al. [98, 99] and Pierce [44] and in presence of main flow as proposed by Ronneberger and Ahrens [100], Peters et al. [84] and Allam and Åbom [101]. The radiation losses can be included in the boundary conditions by imposing a radiation impedance. Other acoustic losses, as the wall vibrations, the non-linear losses due to wave steepening and the vortex shedding at pipe discontinuities are difficult to model analytically.

Using linear models for the acoustic boundary conditions at the boundaries of the pipe system, one obtains a homogeneous set of linear equations. Non-trivial solutions of this system of equations correspond to eigen-values f_n for which the determinant of the homogeneous set of equations vanishes.

As mentioned in Sec. 6, we adopt a single mode approach for the

description of the aeroacoustic behavior of a pipe system. Furthermore, we assume that the oscillation frequency of each mode is well approximated by the real part $\text{Re}(f_n)$ of the corresponding eigen-value f_n . Justification for this assumption is that we are mostly interested in oscillations with a high quality factor Q , so that $\text{Re}(f_n)/\text{Im}(f_n) \gg 1$. We will further use the spatial distribution of each mode, the eigenvector, to calculate the acoustic power generated by the sources $\langle P_{\text{source}} \rangle$ and the acoustic power losses $\langle P_{\text{loss}} \rangle$. This provides an energy balance, which allows the prediction of the amplitude of a stable limit cycle oscillation (Sec. 6).

7.3. SINGLE CLOSED BRANCH RESONATOR

7.3.1. Single deep side branch

Considering a single closed side branch of diameter D_{sb} along an infinite main pipe of diameter D_p , at low frequencies, the pressure reflection coefficient R_p for plane waves traveling in the side branch towards the junction p_{sb}^- is:

$$R_p = \frac{p_{sb}^+}{p_{sb}^-} = \frac{D_{sb}^2 - 2D_p^2}{D_{sb}^2 + 2D_p^2} \quad (11)$$

where p_{sb}^\pm is the complex amplitude of the reflected/incoming wave (Eq. (10)) and we assumed anechoic pipe terminations of the main pipe.

In the limit of small side branch diameter compared to the main pipe diameter $D_{sb} \ll D_p$, the pressure reflection coefficient (Eq. (11)) is close to that of an ideal open end $R_p \approx -1$, so that the closed side branch can be considered as an isolated resonator. At the frequencies corresponding to the resonances of the closed side branch $f_n \approx (2n - 1)c_0/(4L_{sb})$, $n = 1, 2, 3, \dots$, the system can be excited, displaying self-sustained oscillations.

Deep and narrow closed side branches are widely used for pressure measurements along gas transport systems. Gasunie has experienced

strong flow induced pulsations in these kinds of configurations (Sec. 1.3).

In studies on the aeroacoustic behavior of single deep side branch resonators [8, 9, 55, 102, 103], measurements are often carried out on a deep side branch ($L_{sb}/D_{sb} > 1$) placed in the test section ($D_p/D_{sb} > 1$) of a closed loop wind tunnel. When $L_{sb}/D_p < 1$, the system is acoustically similar to a cavity radiating sound into a free space [61]. In that case, the radiation impedance Z of this side branch can be approximated by the radiation impedance of a flanged open pipe termination:

$$\frac{Z}{\rho_0 c_0} = \frac{1}{8} \left(\frac{2\pi f D_{sb}}{c_0} \right)^2 \quad (12)$$

The pressure reflection coefficient R_p for plane waves traveling in the side branch towards the junction p_{sb}^- is then:

$$R_p = \left(\frac{Z}{\rho_0 c_0} - 1 \right) / \left(\frac{Z}{\rho_0 c_0} + 1 \right) \quad (13)$$

In the single deep side branch resonators, near the transverse acoustic resonances of the system composed by the closed branch and the main pipe $f_n \approx 1/2nc_0/(D_p + L_{sb})$, $n = 1, 2, 3, \dots$, strong deviations from the free field conditions, described above, are observed. In particular, the acoustic field displays a localized (trapped) mode.

Flow induced resonance in deep cavities has been reviewed, among others, by Rockwell and Naudascher [33], Rockwell [32] and Gloerfelt [40]. The related whistling of a Helmholtz resonator in grazing flow has been studied by Panton [104] and Dequand et al. [105, 106]. These papers provide a systematic discussion of the influence of the geometry of the cavity edges on the whistling behavior.

7.3.2. Impact of downstream boundary conditions

We now consider a pipe system (Fig. 6) composed of a single T-junction

forming a closed side branch with $D_p/D_{sb} \approx 1$. The pipe system is furthermore delimited upstream by a settling chamber and downstream by an open pipe termination.

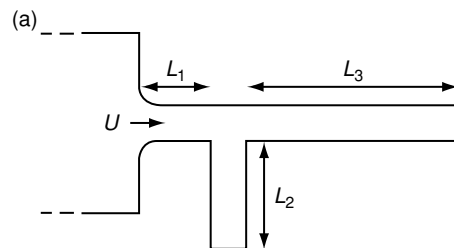
When the side branch diameter is of the same order of magnitude as that of the main pipe $D_p/D_{sb} \approx 1$, the closed branch is not an isolated resonator on its own because the pressure reflection coefficient R_p for waves traveling in the side branch towards the junction p_{sb}^- is very low. In this particular case, the reflection coefficient is $R_p \approx -1/3$, which implies that only 10% of the wave energy is reflected. Since the rest of the energy is radiated into the main pipe, the upstream and the downstream acoustic boundary conditions of the main pipe are clearly critical.

For length L_j ($j = 1, 2, 3$) of the pipe segments composing the system of the same order of magnitude, it is interesting to note that the acoustic modes of the system will not necessarily involve a resonance of the closed side branch segment $L_{sb} = L_2$.

The global acoustic behavior of this pipe system is strongly influenced by the upstream and the downstream acoustic boundary conditions of the main pipe. In a well designed (smooth) nozzle of the settling chamber, acoustic losses due to convective effects are negligibly small. The upstream boundary condition is then a reflection coefficient of unity for the acoustical energy [84, 107]:

$$R_{E,up} = \left(\frac{B_1^-}{B_1^+} \right)^2 = R_{p,up}^2 \left(\frac{1+M}{1-M} \right)^2 \approx 1 \quad (14)$$

where B_1^\pm is the complex amplitude of the total enthalpy fluctuation of the



incoming/reflected waves at the main pipe inlet and $M = U/c_0$ is the Mach number of the flow through the main pipe.

At the downstream side, when the pipe termination has sharp edges, the acoustical energy reflection coefficient for plane waves traveling in the main pipe towards the open end is [84, 107]:

$$R_{E,down-sharp} = \left(\frac{B_3^-}{B_3^+} \right)^2 \approx \left(\frac{1-M}{1+M} \right)^2 \quad (15)$$

where B_3^\pm is the complex amplitude of the total enthalpy fluctuation of the incoming/reflected waves at the main pipe outlet.

We see from Eq. (15) that even moderate Mach numbers will result into strong sound absorption at a downstream open pipe termination with sharp edges. As demonstrated by Bechert [108] and Hofmans et al. [109, 110], convective absorption can be used to design an orifice plate which at low Strouhal numbers behaves as an anechoic pipe termination for a critical Mach number. A multiple orifice configuration can be used to obtain an anechoic behavior in a wide range of flow Mach numbers and acoustic frequencies [80]. This is a robust way to avoid pulsations, at the cost of significant pressure losses.

A small rounding r_{nozzle} of the edges of the downstream pipe termination dramatically modifies the acoustic behavior of the single side branch system. At low Strouhal numbers St_{weff} the acoustic losses are globally reduced. In this case the acoustical energy reflection coefficient of the downstream termination is close to unity [84]:

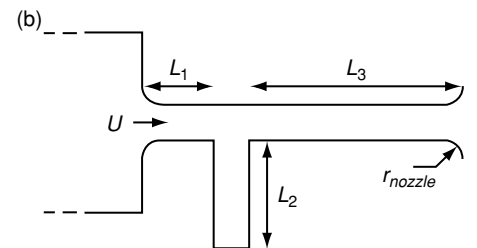


Figure 6: Single side branch resonator with open pipe termination presenting sharp edges (a) and a rounded edges (b).

$$R_{E,down-round} = \left(\frac{B_3^-}{B_3^+} \right)^2 \approx 1 \quad (16)$$

For Strouhal numbers based on the radius of curvature of the rounded termination $Sr_r = fr_{nozzle}/U \approx 0.2$, acoustic energy production can be observed at this termination [35, 74, 84, 111].

For a single side branch resonator, in Fig. 7 we compare the pulsation amplitude observed with a round edged downstream termination, obtained by means of a lip-shaped nozzle, with the pulsation amplitude observed with a sharp edged termination [74]. An order of magnitude difference between these amplitudes is observed.

When the downstream main pipe segment has a length L_3 related to the closed branch length L_2 by:

$$L_3 = \frac{2j}{2n-1} L_2, \quad j=1, 2, 3, \dots, \quad n=1, 2, 3, \dots \quad (17)$$

the acoustic standing wave in the single side branch system has a pressure node

at the T-junction and the resonance frequencies are $f_n \approx (2n - 1)c_0/(4L_2)$. If the upstream main pipe segment L_1 has an arbitrary non-resonant length, then the resonant acoustic field is localized in the side branch L_2 and the downstream pipe segment L_3 . This means that the upstream acoustic boundary condition does not influence the acoustic modes. This is the geometry of the single side branch systems whose whistling behaviors are presented in Fig. 7.

We conclude that one should be careful in drawing any conclusion from single side branch experiments for which there is not detailed information about the acoustic boundary conditions and about the geometry of the pipe terminations.

7.4. DOUBLE CLOSED BRANCH RESONATOR

In the present discussion on double closed branch resonators, we consider pipe systems comprising junction

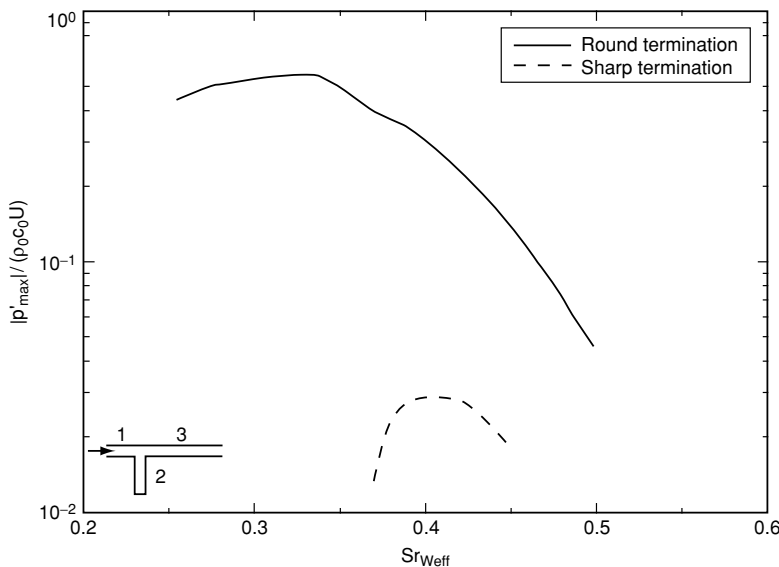


Figure 7: Effect of the downstream pipe termination on the dimensionless pulsation amplitude $|p'_{max}|/(\rho_0 c_0 U)$ of the quarter wavelength resonance $f_1 \approx c_0/(4L_2)$. Single side branch system of Fig. 6-a ($L_1 = 0.18m$, $L_2 = 0.59m$, $L_3 = 1.21m$, $W_1 = W_2 = W_3 = 0.06m$) with square cross section of the pipes and sharp edges of the junction (dashed line) [56]. Single side branch system of Fig. 6-b ($L_1 = 0.12m$, $L_2 = 0.44m$, $L_3 = 0.82m$, $W_1 = W_2 = W_3 = 0.06m$, $r_{nozzle} = 0.03m$) with square cross section of the pipes and sharp edges of the junction (solid line) [74].

elements with diameter of the main pipe D_p equal to the diameter of the side branch D_{sb} .

A double closed branch resonator is formed by two T-junctions placed along a main pipe, with each junction connected to a closed pipe segment, or by a cross-junction connected to two closed branches (Fig. 8). In such configurations, the acoustic field can display trapped modes which are confined to the closed pipe segments and the pipe segment between them. This occurs at the resonance frequencies $f_n \approx (2n-1)c_0/(4L_2)$ when:

$$\begin{aligned} L_3 &= \frac{2j}{2n-1}L_2, \quad j=0, 1, 2, 3\dots, \quad n=1, 2, 3\dots \\ L_4 &= \frac{2i-1}{2n-1}L_2, \quad i=1, 2, 3\dots \end{aligned} \quad (18)$$

Tonon et al. [112] have carried out systematic experiments in different double closed branch resonators (Fig. 8) with circular pipes of 3.36cm diameter and atmospheric pressure. A global overview of the maximum pulsation amplitudes observed in these systems is presented in Tab. 1. These configurations represent all the possible

double closed branch resonators for the case of a tandem configuration with $L_2 = L_4 \approx L_3/2$ ($i = n$ and $j = 2n-1$) and for the case of a cross configuration with $L_2 = L_4$ and $L_3 = 0$ ($i = n$ and $j = 0$). The differences between the various configurations, exhibiting the same acoustic behavior, are a difference in the direction of the main flow and a difference in the local acoustic flow of the junctions.

The double closed branch configurations usually studied in literature are the system with two closed side branches in tandem configuration (Fig. 8-a) and the system with two side branches in cross configuration (Fig. 8-1). Although these configurations have been recognized as the main sources of pulsation in pipe networks, strong flow induced pulsations have been measured also for other configurations, as illustrated in Tab. 1. However, from the overview presented in Fig. 8 and Tab. 1 it is clear that the configuration generating the highest amplitude of acoustic pulsations is the double side branch system in cross configuration (Fig. 8-1). This system is such an excellent and robust resonator, so that even 10% of geometrical deviation from

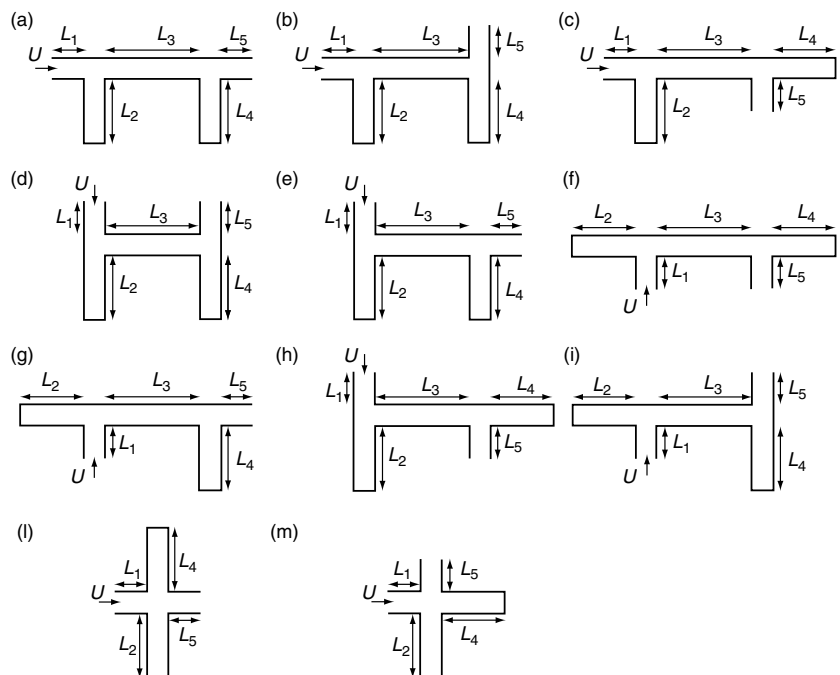


Figure 8: Double closed branch resonators in tandem configuration (a), (b), (c), (d), (e), (f), (g), (h), (i) and in cross configuration (l), (m) [112].

Table 1: Maximum dimensionless pulsation amplitude $|p'_{\max}|_{\max}/(\rho_0 c_0 U)$, corresponding to the maximum pulsation measured in the velocity range $M = U/c_0 = 0 \text{ } \Pi \text{ } 0.25$, in the different double closed branch resonators of Fig. 8. The amplitude $|p'_{\max}|$ is measured at the end of the two closed branches: $|p'_{\max}| = |p'_{\max}|_2 = |p'_{\max}|_4$. The lengths of the pipe segments are: $L_1 = 7.41\text{cm}$, $L_2 = L_4 = 9.91\text{cm}$, $L_3 = 16.64\text{cm}$, $L_5 = 6.36\text{cm}$. Each pipe segment has circular cross section of diameter $D_1 = D_2 = D_3 = D_4 = D_5 = 3.36\text{cm}$. The upstream and the downstream edges of each T-junction and cross-junction are rounded (Fig. 14, $r_{\text{up,down}} = 3.3\text{mm}$, $r_{\text{up,down}}^{u,l} = 3.3\text{mm}$) [112].

Configuration	$\frac{ p'_{\max} _{\max}}{\rho_0 c_0 U}$	Configuration	$\frac{ p'_{\max} _{\max}}{\rho_0 c_0 U}$
(a)	$1.8 \cdot 10^{-1}$	(g)	$8.1 \cdot 10^{-3}$
(b)	$1.8 \cdot 10^{-1}$	(h)	$6.2 \cdot 10^{-2}$
(c)	$7.4 \cdot 10^{-2}$	(i)	$5.7 \cdot 10^{-3}$
(d)	$7.7 \cdot 10^{-3}$	(l)	$8.9 \cdot 10^{-1}$
(e)	$1.5 \cdot 10^{-2}$	(m)	$1.9 \cdot 10^{-1}$
(f)	$7.7 \cdot 10^{-3}$		

the ideal geometry for resonance is not always sufficient to kill the strong whistling (Sec. 12.1).

The double side branch system in tandem configuration has been extensively studied [19, 46, 49, 56, 113, 114]. Strong pulsations at atmospheric pressure have been usually observed in laboratory experiments for $i = n = 1$ and $j = 1$ (Eq. (18)). For higher frequencies, the visco-thermal losses become more important and the measured pulsations are usually substantially weaker. However, in industrial gas transport systems, the pipe diameters are large and the static gas pressure p_0 is high. As a consequence visco-thermal losses are very low and many more whistling modes can appear.

Typical pulsation amplitudes in double side branch systems in tandem configuration (Fig. 8-a) are lower than that of double side branch systems in cross configuration (Fig. 8-l). While the two systems exhibit similar acoustic and hydrodynamic characteristics, the visco-thermal losses in the pipe segment L_3 and the differences in the aeroacoustic sources, due to differences in the local acoustic field patterns at the junctions, are responsible for the lower pulsation amplitudes in the tandem configuration.

An interesting result, obtained by Ziada and Bühlmann [19], is that two closed side branches in close proximity $L_2 = L_4 \gg L_3$ have an aeroacoustic behavior very similar to that of the double side branch system in cross configuration (Fig. 9).

It is interesting to note that resonances of the upstream L_1 or the downstream L_5 pipe segments can significantly affect the response of a non-symmetric resonant double closed branch system. As an example, we show in Fig. 10 the pulsation amplitudes of two double side branch systems in tandem configuration (Fig. 8-a) presenting respectively a long outlet main pipe L_5 and a long inlet main pipe L_1 . The experiments have been carried out for each system by varying the length of the upstream side branch L_2 at fixed length of the downstream side branch L_4 [115]. The acoustic resonances of the upstream pipe segment L_1 and of the downstream pipe segment L_5 are clearly observed in Fig. 10 as dips in the evolution of the pulsation amplitude as function of the length L_2 . The same effect has been found in the field experiments at Westerbork (Fig. 11) [115]. In these experiments we observe a dip in the amplitude of the pulsations measured at

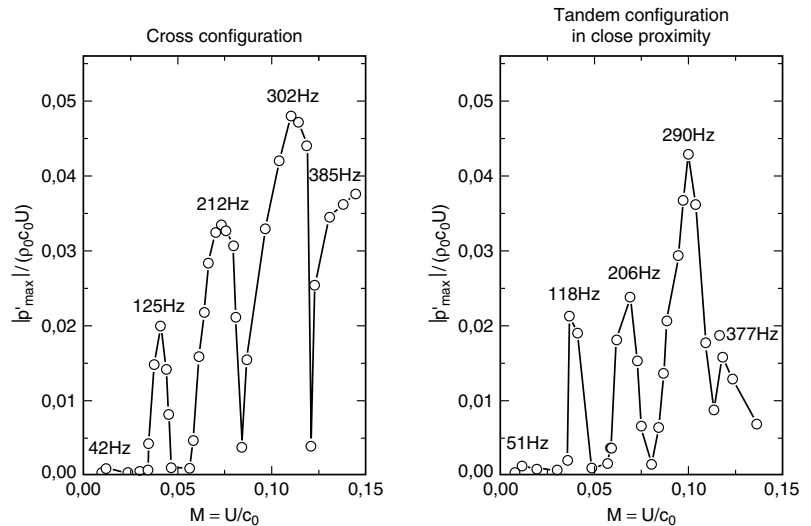


Figure 9: Dimensionless pulsation amplitude $|p'_{max}|/(\rho_0 c_0 U)$ as function of the Mach number $M = U/c_0$ [19]. The amplitude $|p'_{max}|$ is measured at the end of the two closed branches: $|p'_{max}| = |p'_{max}|_2 = |p'_{max}|_4$. Double side branch system in cross configuration of Fig. 8-l ($L_1 = 5.05m$, $L_2 = L_4 = 2m$, $L_5 = 1.7m$, $D_1 = D_5 = 0.089m$, $D_2 = D_4 = 0.051m$) with circular cross section of the pipes and sharp edges. Double side branch system in tandem configuration of Fig. 8-a ($L_1 = 5.05m$, $L_2 = L_4 = 2m$, $L_3 = 0.119m$, $L_5 = 1.7m$, $D_1 = D_3 = D_5 = 0.089m$, $D_2 = D_4 = 0.051m$) with circular cross section of the pipes and sharp edges.

the end of the upstream side branch each time the length of this side branch L_2 matches a resonance frequency of the

165m long pipe of 30" diameter placed upstream of the double side branch system (Fig. 11).

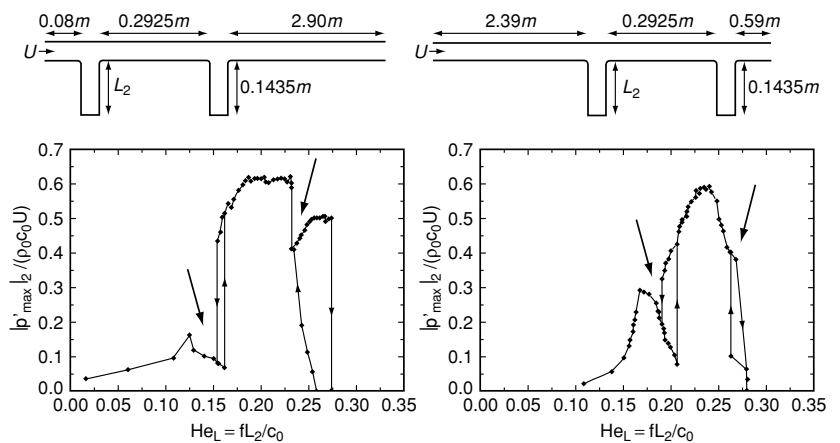


Figure 10: Pulsation amplitudes of double side branch systems in tandem configuration presenting respectively a long outlet main pipe L_5 (left) and a long inlet main pipe L_1 (right) as function of the length of the upstream side branch L_2 . The pipes have circular cross section of diameter 30mm, the junctions have rounded edges $r_{up,down} = 3mm$ and the measurements have been carried out at 10bar [115]. The dimensionless pulsation amplitude $|p'_{max}|_2/(\rho_0 c_0 U)$, measured at the closed end of the upstream side branch L_2 , is presented as function of the dimensionless whistling frequency $He_L = fL_2/c_0$. Downstream or upstream pipe resonances are indicated by the arrows.

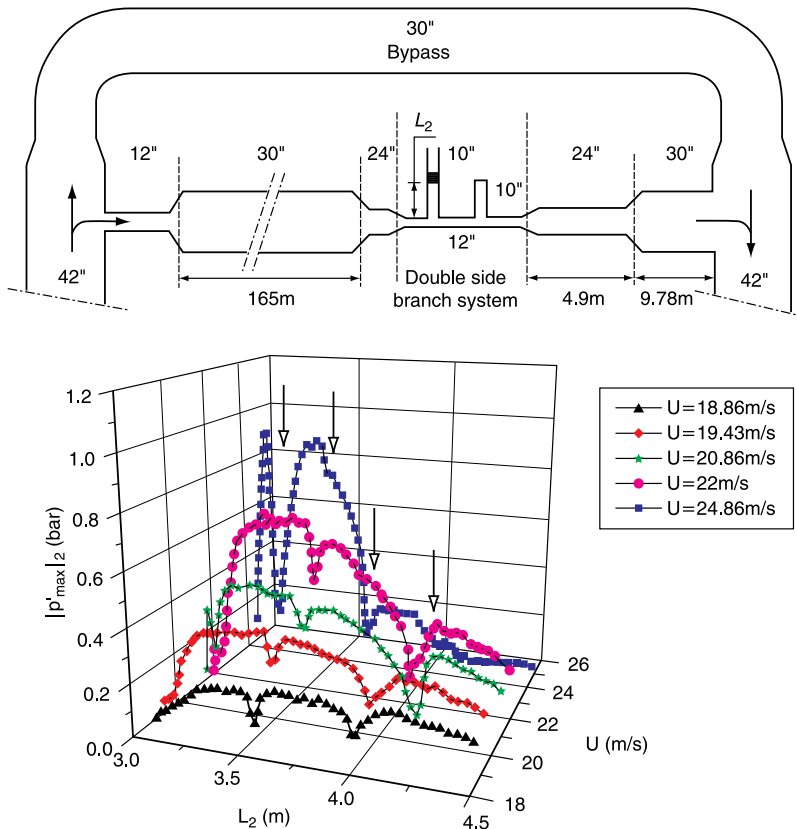


Figure 11: Pulsation levels $|p'_{\max}|_2$ as function of the flow velocity U and the length of the upstream side branch L_2 in the field experiments of Westerbork [115]. The pressure fluctuation is measured at the closed end of the upstream side branch L_2 . The pipes have circular cross section, the junctions have rounded edges $r_{up,down} = 2.5''$ and the measurements have been carried out at 60 bar. We observe dips in amplitude each time the length L_2 of the upstream side branch corresponds to a resonance mode of the upstream pipe of 165 m length and 30'' diameter. Resonances of the upstream pipe are indicated by the empty arrows.

7.5. MULTIPLE CLOSED BRANCH RESONATOR

7.5.1. Multiple deep side branches

The global acoustic behavior of multiple deep side branch systems with more than two side branches is difficult to predict intuitively. These systems display some acoustic similarities with single or double side branch systems. However they show some peculiarities so that they cannot be acoustically reduced to a collection of simpler elements [116].

In Fig. 12-b we show a survey of pulsation frequencies and dimensionless amplitudes observed in a section of the compressor station of

Ommen [4, 117]. This section presents two separate sets of six equally spaced closed side branches along a main pipe, formed respectively at the suction side and at the discharge side of six compressors (Fig. 12-a). The investigation of the aeroacoustic behavior of the discharge side of the compressor station has been carried out by Tonon et al. [116] in an atmospheric scale model with pipe diameters of $D_p = D_{sb} = 3.36\text{cm}$. These scale model experiments provided a good prediction of maximum pulsation amplitudes observed in field data. Furthermore, higher Strouhal numbers were observed than in field experiments.

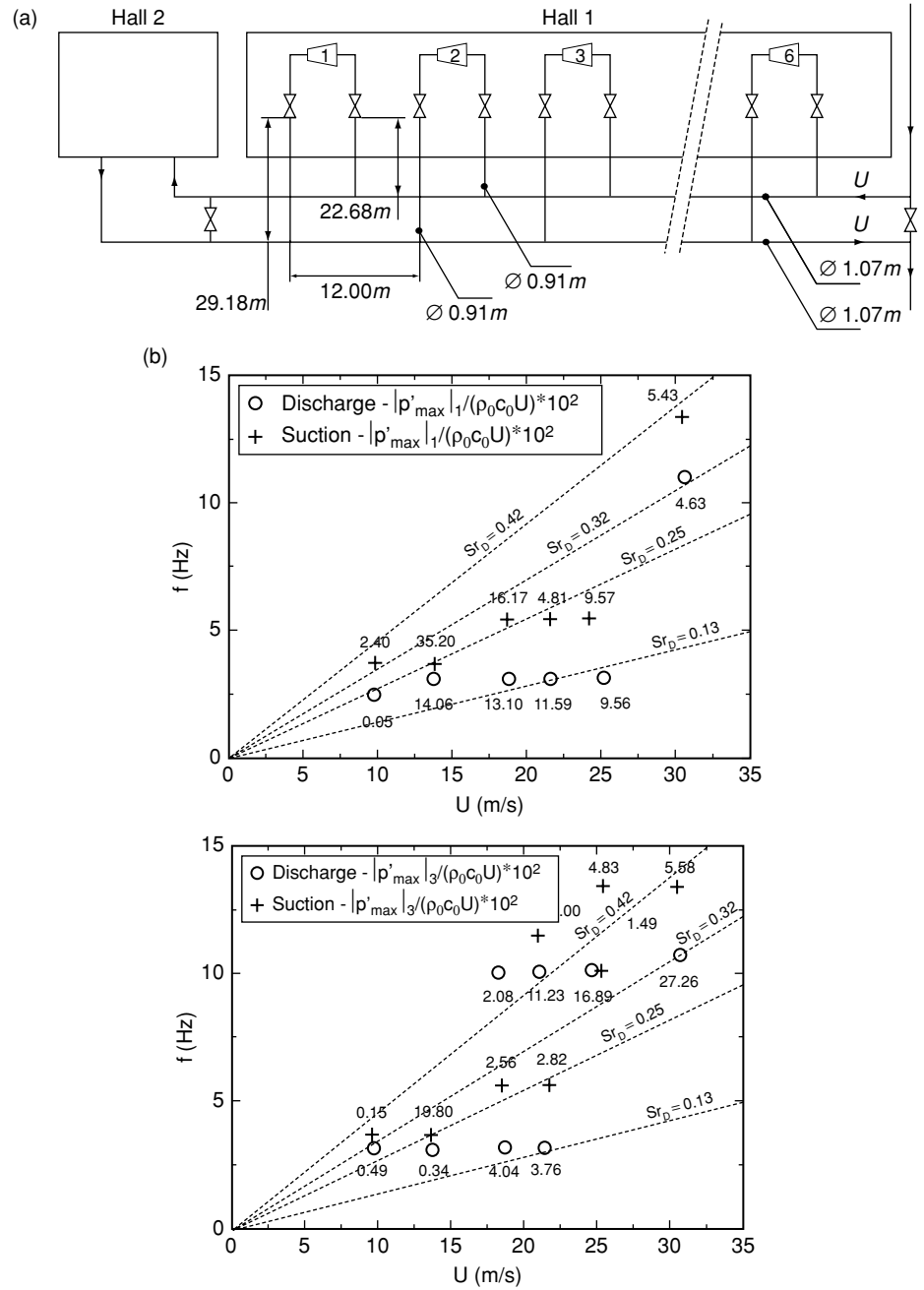


Figure 12: Section of the compressor station Ommen [4] displaying flow induced pulsations (a). Pulsation frequencies f and dimensionless pressure fluctuation amplitudes at the closed end of side branch 1 $|p'_{\max}|_1/(\rho_0 c_0 U)$ and side branch 3 $|p'_{\max}|_3/(\rho_0 c_0 U)$ of the suction and the discharge sides of the compressor section (b). The gas compressed at the station is natural gas from Groningen [117] with pressure $p_0 = 60\text{ bar}$ and temperature $T_0 = 278\text{ K}$. The edges of all the junctions are rounded $r_{\text{up,down}} = 9.1\text{ cm}$. The Strouhal number is based on the side branch diameter $Sr_D = fD_{\text{sb}}/U$.

One would expect that the very strong pulsations, observed in the six side branch systems described above, are due to the fact that the side branches have all exactly the same length. Detuning the length of the side

branches seems a logical approach to avoid strong pulsations. As discussed in Sec. 12.1 this approach does not always reduce sufficiently the pulsation levels. Using spoilers, as discussed in Sec. 12.3 is a promising alternative to detuning.

7.5.2. Multiple shallow side branches

A row of shallow closed side branches, presenting length comparable with the diameter $L_{sb}/D_{sb} = O(1)$, placed along a main pipe of length L_{mp} with both terminations open, displays self-sustained oscillations very similar to those found in corrugated pipes [118–120]. The low frequency pulsation amplitudes will be typically of the order $|p'_{main}|/(\rho_0 c_0 U) = O(10^{-2})$ and appear around $Sr_{weff} = 0.6$ (Fig. 13).

At low frequency, the acoustic modes of the multiple shallow side branch systems correspond to the longitudinal global pipe modes of these systems [118–120]. These modes have frequencies $f_n \approx n c_{eff}/(2L_{mp})$, $n = 1, 2, 3, \dots$, where the effective speed of sound [121] is:

$$c_{eff} = c_0 \sqrt{\frac{V_{mp}}{V_{mp} + V_c}} \quad (19)$$

This formula is obtained assuming that the inertia in the acoustic flow is not affected by the side branches, while

the cavity volume V_c is added to the main pipe volume V_{mp} to account for the effect of the compressibility [118, 120].

An interesting aspect of the multiple shallow side branch systems is that, as the main flow velocity U increases, one reaches a Brillouin zone and finds a frequency gap in which the system does not whistle [118].

As in the case of the single closed branch resonator (Sec. 7.3.2), the system of multiple shallow side branches excites a global mode rather than a trapped mode. It is therefore very sensitive to the upstream and downstream boundary conditions.

8. SOUND SOURCES

8.1. MAIN FLOW CONFIGURATIONS

8.1.1. Main flow configurations of a T-junction

The main geometrical characteristics of a T-junction (Fig. 14-a) are the diameter of the main pipe D_p , the diameter of the side branch D_{sb} and the radius of

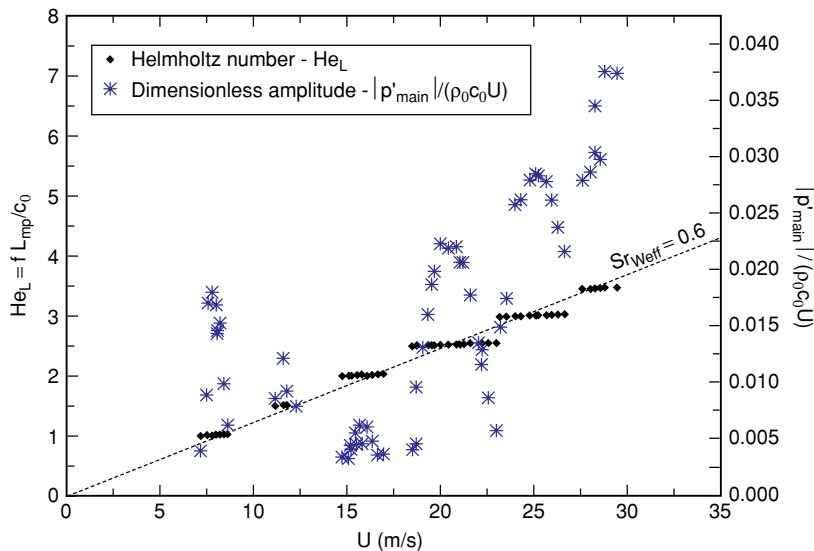


Figure 13: Pulsation behavior of a multiple shallow side branch system composed by 15 side branches of 3.36cm depth along a main pipe of $L_{mp} = 1.5m$ length [118]. The side branches are equispaced along the main pipe and the junctions present sharp edges. The pipes have circular cross section with diameter of 3.36cm. The dimensionless whistling frequency $He_L = f L_{mp}/c_0$ and the dimensionless pulsation amplitude $|p'_{main}|/(\rho_0 c_0 U)$ are presented as function of the flow velocity U . The pressure fluctuation amplitude $|p'_{main}|$ is the amplitude of the longitudinal global pipe mode of the system.

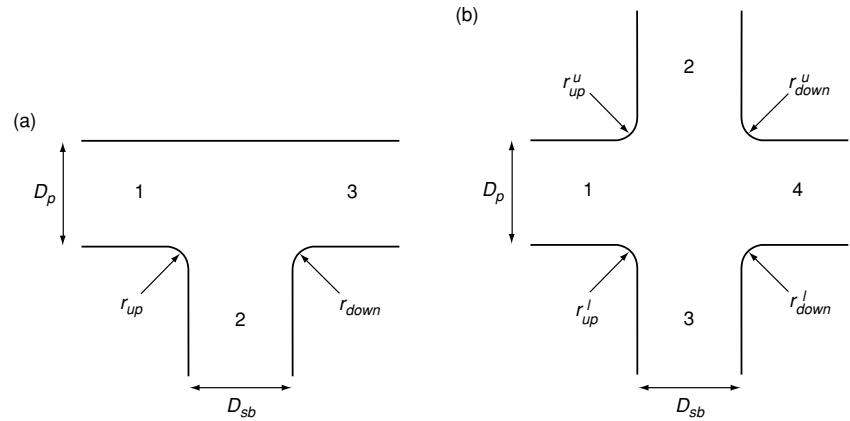


Figure 14: Main geometrical characteristics of a T-junction (a) and of a cross-junction (b).

curvature $r_{up,down}$ of the edges of the junction. The three pipe segments meeting at the T-junction are called upstream main pipe (segment 1), downstream main pipe (segment 3) and side branch (segment 2).

T-junction elements with $D_{sb}/D_p = O(1)$ are common in pipe systems [5, 6, 19, 45, 46, 56, 71, 72, 74, 113, 122]. We therefore start our discussion on the main flow configurations of a T-junction by considering side branches with diameter D_{sb} close to the main pipe diameter D_p . A commonly used ratio is $D_{sb}/D_p = 0.8$.

When one of the pipe segments (branches) is closed, flow separation occurs at the T-junction and a shear layer is formed. Coupling of the shear layer instability with the acoustic field provides a mean to transfer energy between the steady main flow and the acoustic flow. Acoustical energy can be produced or absorbed depending on the flow and acoustic conditions.

In most technical applications of pipe networks, the pipes have circular cross sections. Practical exceptions are air conditioning systems, in which rectangular cross sections are not unusual. Also for research purposes (flow visualization, laser Doppler anemometry, ...) experiments have been carried out in pipes with rectangular cross sections. While the flow within circular pipes is essentially three dimensional, the global aeroacoustic behavior is the same as for rectangular

pipes [56] when D_{sb}/D_p is close to unity. For example, the optimal Strouhal number $Sr_{W_{eff,opt}}$ for the maximum of pulsation amplitude for circular pipes can be translated into that for rectangular pipes by introducing the concept of effective (average) cavity width W_{eff} (Sec. 3). The observed pulsation levels for circular pipes are, in the moderate amplitude range (Sec. 8.3), typically a factor two lower than for rectangular pipes. For high amplitudes (Sec. 8.3), the geometry of the cross sections will mainly affect the amplitude as a result of the stronger sensitivity of rectangular cross sections to wall vibrations. The coupling with wall vibrations tends to lower the pulsation levels [56], as discussed in Sec. 11.

At each T-junction we can distinguish three main flow configurations, depending on which of the pipe segments is closed (Fig. 15-a) [6, 74, 113, 122].

In flow configuration (T-a) the side branch is closed. The main flow travels from the upstream pipe 1 to the downstream pipe 3 and it separates from the upstream edge to form a shear layer between the main flow and the stagnant fluid in the closed side branch.

In flow configuration (T-b) the main flow turns from the upstream pipe 1 into the side branch 2 because the downstream main pipe segment 3 has closed pipe termination. In this case, flow separation can occur at three places: the upstream edge, the downstream edge

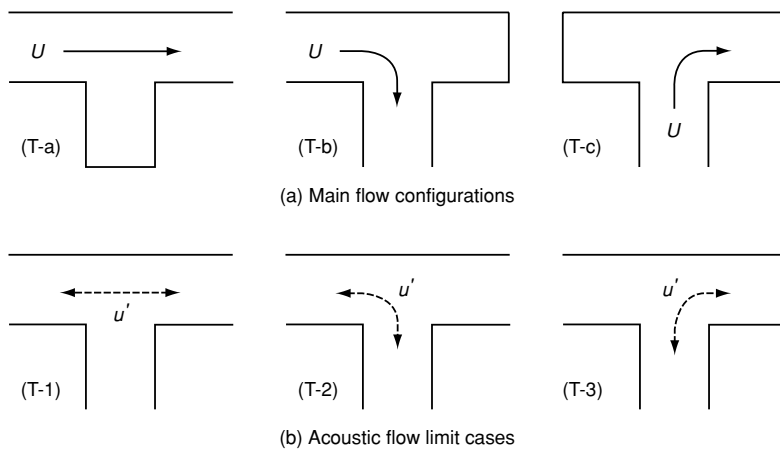


Figure 15: Definition of main flow configurations (a) and acoustic flow limit cases (b) in a T-junction.

and on the wall opposite to the side branch. When the edges of the junction are sharp $r_{up,down}/D_{sb} = 0$ flow separation will certainly occur at both edges and a free jet will be formed into the side branch. For values of $r_{up,down}/D_{sb} \geq 0.1$ [123] the flow separation at the edges is strongly reduced. The flow separation at the wall opposite to the side branch always occurs because of the deceleration of the flow in the closed downstream pipe 3. The position at which this separation occurs is difficult to predict. In contrast to separation at a sharp edge, this separation point is expected to move under the influence of acoustic perturbations.

In flow configuration (T-c) the upstream main pipe 1 is closed. The main flow turns from the side branch 2 into the downstream main pipe 3 and flow separation occurs at the outer side of the flow bend (upstream edge). Flow separation at the interior of the flow bend will occur if the downstream edge is sufficiently sharp. In view of the associated energy losses, separation at the inner side of the flow bend is usually avoided by choosing a large radius r_{down}/D_{sb} . In that case, due to the Coanda effect, the jet flow formed by separation at the upstream edge is expected to remain attached to the wall at the inner side of the bend.

In the case of side branches with diameter D_{sb} considerably smaller than the main pipe diameter D_p , the main

flow configurations are different from those described above. The main difference between narrow side branches $D_{sb}/D_p \ll 1$ and wide side branches $D_{sb}/D_p = O(1)$ is that in the main flow configuration (T-c) a free jet is formed in the main pipe. Furthermore, in technical applications, the radius of curvature $r_{up,down}$ of the edges of a T-junction with a narrow side branch are usually relatively large compared to the side branch diameter D_{sb} , values of $r_{up,down}/D_{sb} = O(1)$ are common. These cases have not yet been studied.

The evaluation of the efficiency of the main flow configurations described above as sound sources can be qualitatively (roughly) carried out by evaluating the experimental results of closed branch systems. From the experiments on the double closed branch resonators of Fig. 8, presented in Tab. 1, it is evident that the configuration (T-a) is the major pulsation driver, since the highest pulsations are observed only in systems presenting this main flow configuration in one of the junctions. However, these experimental results do not provide information about the efficiency of flow configurations (T-b) and (T-c) as sound sources. A quantitative and more complete evaluation of the sound sources will be obtained by means of source modeling. We will discuss this topic in Sec. 9.

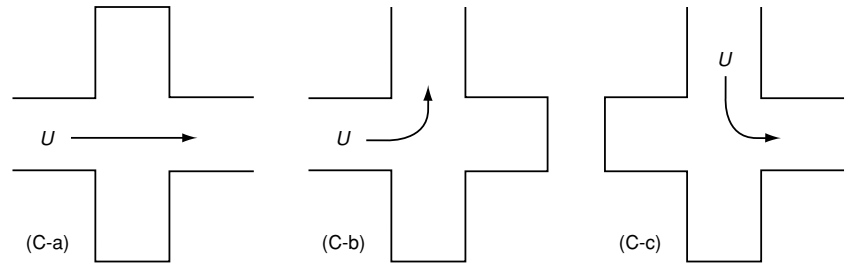


Figure 16: Definition of main flow configurations in a cross-junction.

8.1.2. Main flow configurations of a cross-junction

The main geometrical characteristics of a cross-junction (Fig. 14-b) are the diameter of the main pipe D_p , the diameter of the side branches D_{sb} and the radius of curvature $r_{up,down}^{u,l}$ of the edges of the junction. The four pipe segments meeting at the cross-junction are called upstream main pipe (segment 1), downstream main pipe (segment 4), upper side branch (segment 2) and lower side branch (segment 3).

At each cross-junction we can distinguish three main flow configurations, depending on which couple of pipe segments is closed (Fig. 16). We start our discussion on the main flow configurations of a cross-junction by considering side branches with a diameter D_{sb} close to the main pipe diameter D_p , as commonly found in technical applications $D_{sb}/D_p = O(1)$.

In flow configuration (C-a) both the side branches are closed. The main flow travels from the upstream pipe 1 to the downstream pipe 4 and it separates from the upstream edges to form two shear layers between the main flow and the stagnant fluid in the two closed side branches. This configuration is, from the hydrodynamic point of view, similar to the main flow configuration (T-a) of T-junction elements (Fig. 15-a).

In flow configuration (C-b) the main flow turns from the upstream pipe 1 into one of the side branches (2 or 3). The downstream main pipe segment 4 and the other side branch (3 or 2) have both a closed pipe termination. Due to the geometrical symmetry of the cross-configuration, there are no fluid

dynamic differences between the cases in which the main flow enters the upper side branch 2 or the lower side branch 3.

In flow configuration (C-c) the main flow turns from one of the side branches (2 or 3) into the downstream main pipe 4. This configuration is similar to flow configuration (C-b) for $D_{sb}/D_p = O(1)$.

In the case of narrow side branches $D_{sb}/D_p \ll 1$, the flow configuration (C-c) is substantially different from flow configuration (C-b). The main difference is that a free jet is formed in the main pipe. This configuration has not been studied until now.

Analyzing the results of the experiments on the double closed branch resonators of Fig. 8, presented in Tab. 1, we can observe that the configuration (C-a) is a driver of high amplitude oscillations. However, a quantitative and more complete evaluation of the sound source will be obtained by means of source modeling (Sec. 9).

8.2. LOCAL ACOUSTIC FIELD OF T-JUNCTIONS AND CROSS-JUNCTIONS

As defined by Howe [23, 41, 42], the acoustic field is a potential flow (Eq. (2)). At low frequencies, only plane waves propagate along straight pipe segments. At a distance of about one pipe diameter from a junction, the acoustic field is uniform and can be described in terms of two plane waves travelling in opposite directions (Sec. 7.2). This uniform acoustic velocity field drives within the junction a potential flow, which in first order approximation is incompressible.

It is important to realize that the shape of the edges is crucial in the local acoustic field distribution. At a sharp edge, the acoustic velocity is locally singular. This is a consequence of the definition of the acoustic flow as potential flow. Furthermore, the edge shape is crucial in the aeroacoustic behavior because it determines the flow separation and the consequent vortex shedding.

From the energy corollary of Howe (Eq. (5)) we see that at a sharp edge we combine the ideal conditions for a strong interaction between the acoustic and the hydrodynamic flow fields. We need therefore an accurate description of the acoustic field near such singularities. A modal expansion of the solution of the equation of Helmholtz as proposed by Keefe [92] and Dubos et al. [95] will diverge at such singularities. This is therefore not a suitable approach. Assuming a locally incompressible two-dimensional potential flow one can obtain some insight by using complex function theory with conformal mapping [56]. This corresponds to the use of a low frequency Green's function as proposed by Howe [23, 76]. For a more general case, as for pipes with a circular cross section and junctions with rounded edges, one has to use a numerical method to determine the detailed acoustic flow.

An important result, concerning the effect of the edge shape on the aeroacoustic behavior of junction elements, was obtained by Bruggeman et al. [56]. This was the demonstration of the crucial role of the shape of the upstream edge of the T-junctions for a tandem of two closed side branches (Fig. 8-a, $L_2 = L_4 \approx L_3/2$). A sharp upstream edge considerably reduces the pulsation amplitudes. In contrast with this, the downstream edge geometry was found to be less critical. The effect observed by Bruggeman et al. [56] on T-junctions has been confirmed for cross-junctions [45, 48] and for Helmholtz resonators in grazing flow [105, 106].

8.2.1. Acoustic flow limit cases of a T-junction

The acoustic flow distribution in T-junction elements is usually quite complex. For the sake of simplicity some authors [74, 113] distinguish three limit cases. These acoustic flow limit cases, presented in Fig. 15-b, consist of an acoustic flow oscillating between two of the three pipe sections of the T-junction.

The strongest pulsations in the double closed branch systems in tandem configuration of Fig. 8 display type (T-2) and (T-3) cases. The type (T-1) case (grazing acoustic flow) is dominant in the case of a long row of shallow closed side branches discussed in Sec. 7.5.2.

The main flow configurations (T-a), (T-b) or (T-c) (Fig. 15-a) combined with the acoustic flow limit cases (T-1), (T-2) or (T-3) (Fig. 15-b) form nine limit cases which we denote by (T-a1), (T-a2), (T-a3), (T-b1), (T-b2), (T-b3), (T-c1), (T-c2) and (T-c3).

For wide side branches, $D_{sb}/D_p = O(1)$, the limit case (T-a2) presents a local acoustic field near the edges that is essentially different from that of the case (T-a3). This is due to the much larger acoustic velocity at the interior of the bend than at the exterior. As shown by Bruggeman [58], the (T-a2) limit case with sharp edges has a local acoustic velocity at the upstream edge that is a factor 3 higher than at the downstream edge. This is the opposite for the (T-a3) limit case. A spoiler placed at the upstream edge of the limit case (T-a2) will therefore be much more efficient than a spoiler at the upstream edge of the limit case (T-a3) [56]. This asymmetry disappears for narrow side branches $D_{sb}/D_p \ll 1$.

8.2.2. Acoustic flow limit cases of a cross-junction

As for the case of T-junctions, in cross-junction elements we can distinguish many limit cases of acoustic flow distribution.

Despite the variety of the combinations between the main flow configurations (Fig. 16) and the acoustic flow limit cases that can be obtained for a cross-junction, the only case discussed in literature is the limit case of an acoustic flow oscillating normal to the main flow, which is grazing along two opposite closed side branches. We will refer to this case as the (C-a1) limit case. The acoustic flow is symmetric with respect to the side branch axis, which is quite different from all the cases discussed for the T-junction. We therefore expect a different aeroacoustic source behavior.

8.3. LOW, MODERATE AND HIGH AMPLITUDE OSCILLATIONS

From the analysis of flow configuration (T-a) (Fig. 15), Bruggeman et al. [56] observed three different behaviors of the shear layer depending on the dimensionless pulsation amplitude $|\bar{u}'_{jun}|/U = |p'_{max}|/(\rho_0 c_0 U)$.

For low acoustic velocities at the sound source $|\bar{u}'_{jun}|/U \ll 1$, the amplitude of the perturbations of the shear layer increases exponentially with the distance x from the upstream edge of the junction. This amplification is of the order of $e^{2\pi f x/U_{con}}$, where U_{con} is the convective velocity of the vorticity in the shear layer (Sec. 3). This corresponds to an amplification by a factor $e^{2\pi} \approx 535$ over one hydrodynamic wavelength. Hence, perturbations in the main flow velocity as small as $|\bar{u}'_{jun}|/U = O(10^{-3})$ induce perturbations in the velocity field of the shear layer of order unity for the first hydrodynamic mode $m = 1$. For such large perturbations, a linear theory is not valid.

This provides the condition $|\bar{u}'_{jun}|/U < 10^{-3}$ for a linear behavior of the shear layer upon acoustic perturbations for $m = 1$. For higher hydrodynamic modes $m > 1$, this condition is even more restrictive, $|\bar{u}'_{jun}|/U < 10^{-3m}$.

In the linear regime (very low pulsation amplitudes) the strength of the sound source is linear with the pulsation amplitude, this implies that the acoustic source power $\langle P_{source} \rangle$ scales quadratically with the pulsation amplitude $|\bar{u}'_{jun}|$. The acoustic power losses $\langle P_{loss} \rangle$, due to visco-thermal damping $\langle P_{v-th} \rangle$ and acoustic radiation $\langle P_{rad} \rangle$ also depend quadratically on the pulsation amplitude $|\bar{u}'_{jun}|$. In general, one would therefore expect the system to be either stable ($\langle P_{source} \rangle$ lower than $\langle P_{loss} \rangle$) or unstable ($\langle P_{loss} \rangle$ lower than $\langle P_{source} \rangle$). This implies either an exponential decay respectively growth in time of perturbations. An exact balance (Sec. 6) between acoustic source power $\langle P_{source} \rangle$ and acoustic power losses $\langle P_{loss} \rangle$, if it is achieved, implies neutral stability (Fig. 17-a). Hence an energy balance, if satisfied at one amplitude, would be satisfied at any other amplitude.

In the low amplitude regime $|\bar{u}'_{jun}|/U = O(10^{-3})$, the strength of the sound source is almost linear with the pulsation amplitude and the acoustic source power $\langle P_{source} \rangle$ is almost quadratic with the pulsation amplitude $|\bar{u}'_{jun}|$. The acoustic losses $\langle P_{loss} \rangle$ remain quadratic with the pulsation amplitude $|\bar{u}'_{jun}|$. The balance (Sec. 6) between acoustic source power $\langle P_{source} \rangle$ and acoustic power losses $\langle P_{loss} \rangle$ determines the pulsation amplitude (Fig. 17-b). However, the acoustic pulsations in the low amplitude regime are quite unstable. A marginal increase of the acoustic losses can make them disappear.

Pulsation amplitudes of $10^{-2} < |\bar{u}'_{jun}|/U < 10^{-1}$ have been defined by Bruggeman et al. [56] as the moderate amplitude regime. For moderate amplitudes, non-linearity induces a concentration of the vorticity, shed at the upstream edge, into coherent vortex structures. These discrete vortices are clearly observed in flow visualizations (Fig. 3-b) [32, 34, 45, 47, 48, 58, 124–126]

and numerical simulations [45, 48, 50, 74, 113, 127, 128].

In the moderate amplitude regime, the perturbation of the shear layer at the upstream edge is relatively small $O(10^{-1})$, so that the acoustic field only triggers the concentration of vorticity into discrete vortices. The amount of vorticity shed (circulation of the vortices) and the path of the vortices are not strongly affected by the amplitude of the acoustic pulsation and the source strength is therefore almost independent of the amplitude of the acoustic field.

At moderate amplitudes, the formation of a new vortex is observed

[56, 122, 129] each time that the acoustic velocity changes direction from outside the side branch towards the inside of the side branch at the upstream edge of the junction. The vortical structures are then convected downstream with a velocity proportional to the main flow velocity $U_{con} \approx 0.4U$ [56]. For the limit cases (T-a2) and (T-a3), this determines the Strouhal condition for maximum pulsations amplitude $Sr_{W_{eff,opt}} \approx 0.4$. The acoustic source power $\langle P_{source} \rangle$ is linear with the pulsation amplitude $|\bar{u}'_{jun}|$, while the acoustic power losses $\langle P_{loss} \rangle$ are still quadratic. Hence, the oscillation amplitude is stable (Fig. 18-a).

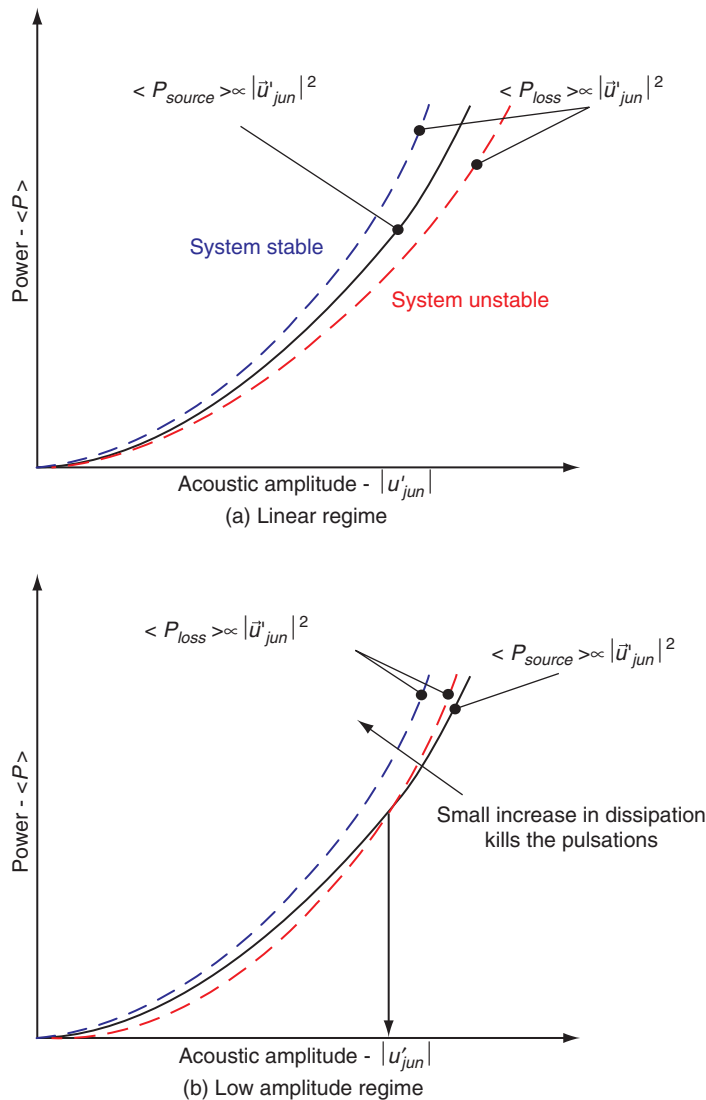


Figure 17: Energy balance of the self-sustained oscillations. Qualitative representation of the acoustic source power $\langle P_{source} \rangle$ (solid line) and the acoustic power losses $\langle P_{loss} \rangle$ (dashed line) in the linear (very low amplitude) regime (a) and in the low amplitude regime (b).

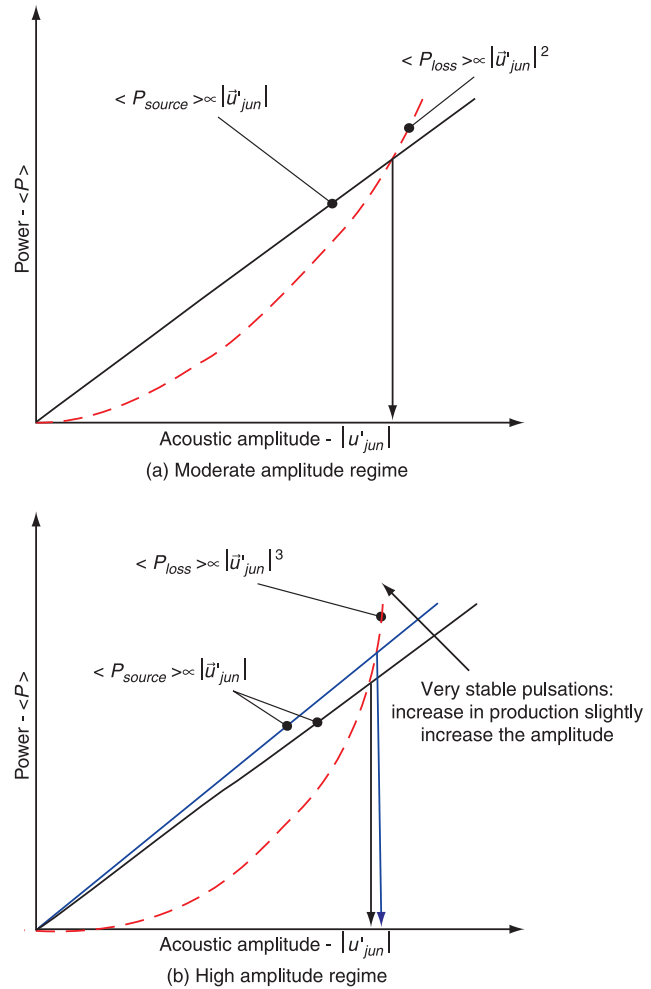


Figure 18: Energy balance of the self-sustained oscillations. Qualitative representation of the acoustic source power $\langle P_{source} \rangle$ (solid line) and the acoustic power losses $\langle P_{loss} \rangle$ (dashed line) in the moderate amplitude regime (a) and in the high amplitude regime (b).

High pulsation levels, with acoustic velocity at the sound source of the order of magnitude of the main flow velocity $|\bar{u}'_{jun}|/U = O(1)$, are usually observed in pipe systems with negligible visco-thermal and radiation losses. Under such conditions, the pulsation amplitude becomes almost independent of the static pressure in the system and details of the geometry of the junction become essential. As explained by Howe [39], in the limit of such high pulsation levels, there is a balance between sound production by vortices $\langle P_{source} \rangle$, that scales linearly with the pulsation amplitude $|\bar{u}'_{jun}|$, and sound absorption by vortex shedding (vortex damping) $\langle P_{vort} \rangle$, that scales with the third power of the pulsation amplitude $|\bar{u}'_{jun}|$. This is due to the effect of the acoustic field on the amount of vorticity shed at

the upstream edge and on its effect on the path of the vortices. Also the sound absorption due to “spurious” vortex shedding at the downstream edge becomes increasingly important at large pulsation amplitudes. Besides vortex damping, the transfer of energy to higher harmonics as a result of the non-linear wave steepening can result into acoustic losses $\langle P_{rad-nl} \rangle$.

These high pulsation levels are likely to occur when the upstream edge of the junction is rounded [48, 50, 51, 56], because the initial sound absorption due to vortex shedding (vortex damping) is lower with a rounded edge than with a sharp edge (Sec. 8.2). In some cases, however, configurations with sharp edges can display high pulsation levels (Fig. 3-a).

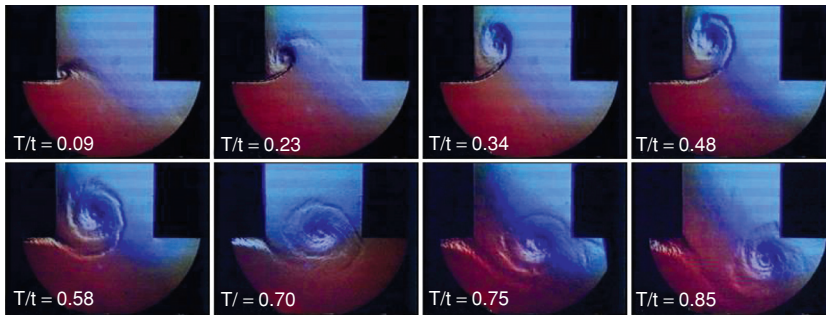


Figure 19: Periodic vortex formation in the double side branch system in cross configuration of Fig. 8-1 with sharp edges and square cross section of the pipes ($L_2 = L_4 = 0.564\text{m}$, $W_1 = W_2 = W_4 = W_5 = 0.06\text{m}$, $U = 35\text{m/s}$, $f = 1/T = 156\text{Hz}$, $Sr_{\text{Weff}} = 0.27$, $|\bar{u}'_{\text{jun}}|/U = 0.76$) [45]. The time at which the acoustic velocity changes direction from outside the side branch towards the inside of the side branch at the upstream edge of the junction is $t/T = 0$. Please note that the vortex does not impinge on the downstream edge of the junction.

In the high amplitude regime the path of the vortices (Fig. 19) are significantly influenced by the amplitude of the acoustic field [45, 48, 50, 56]. The vortices enter quite deep into the side branch rather than following the line of the unperturbed shear layer. This may qualitatively explain the decrease of the optimal Strouhal number $Sr_{\text{Weff},\text{opt}}$ observed by Bruggeman et al. [56] and by Ziada [47]. Deeper in the side branch the convective velocity of the vortices U_{con} is lower than at the junction. This increases the travel time of the vortices across the junction for a given main flow velocity U . A higher flow velocity U is then needed to make the vortex reach the downstream edge of the junction within an oscillation period. This implies a decrease of the optimal Strouhal number for maximum pulsations, that, for high amplitude pulsations, is typically $Sr_{\text{Weff},\text{opt}} \approx 0.3$.

In the high amplitude regime, the pulsations continue below Strouhal numbers for which they would have disappeared at low or moderate amplitudes. As a consequence hysteresis is observed [47, 56]. This means that the strong pulsations of a given mode (acoustic and hydrodynamic) disappear at a higher velocity upon flow acceleration than the velocity at which they reappear

upon flow deceleration. Furthermore, these transitions are abrupt (on-off).

At high amplitude oscillations, the phase of the oscillation period, at which a new vortex is shed, changes compared to the case of moderate amplitude oscillations. This shift in phase for the generation of a new vortex can almost reach a quarter of the oscillation period [45].

In field experiments, as high Reynolds numbers are not unusual, one should suspect the occurrence of turbulence in the acoustic boundary layers in the closed branches. For an acoustic laminar boundary layer thickness $\delta_v \approx \sqrt{\mu/(\rho_0 \pi f)}$, where m is the dynamic viscosity of the fluid, turbulence is expected when $\rho_0 \delta_v |\bar{u}'|/\mu > 350$ [130]. The transition from laminar to turbulent acoustic boundary layers has been reported as potential amplitude limiting effect in thermoacoustic devices [52]. However, this effect has never been reported in laboratory experiments on flow induced pulsations.

9. SOURCE MODELING

9.1. EXPERIMENTAL CHARACTERIZATION OF THE SOUND SOURCES

The whistling of a flute presents many similarities with the pulsation of a pipe

system with closed branches. In a flute, the sound is generated by the instability of the free jet formed by blowing across the mouth of the instrument. The jet oscillation couples with the acoustic resonances of the pipe, leading to a feedback mechanism similar to that occurring in pipe systems with closed branches.

The early models of the aeroacoustic behavior of a flute, based on the assumption that the jet and the resonant acoustic field form a feedback loop, consist of predicting the oscillations condition (oscillation threshold) by means of the linear theory. These models have been established by imposing a match between the resonator impedance and the source impedance.

A first method to determine the source impedance in a flute has been introduced by Coltman [131]. Assuming a harmonic oscillation, he generalized the impedance balance to non-linear systems. He developed a measurement technique to measure the source impedance, defined as the pressure difference across the mouth of the instrument divided by the acoustic volume flux through the mouth. In these experiments, the frequency and the amplitude of the acoustic field have been imposed by a loudspeaker placed at the end of the pipe of the flute. Measurements have been carried out as a function of the acoustic frequency, the amplitude of the acoustic field and the velocity of the jet at the mouth of the flute. In a complex representation the measured impedance is, for a given amplitude of the acoustic field, a spiral in the complex plane around the origin. The real part is in phase with the acoustic volume flow oscillation and therefore provides the energy transfer between the flow field and the acoustic field.

An experimental technique to characterize the sound source in a single side branch configuration (Fig. 6-a, $L_1 \ll L_2 \approx L_3/2$), in which the (T-a3) limit case prevails (Fig. 15), has been proposed

by Bruggeman et al. [56, 58]. This method consists of applying an energy balance between sound production and acoustic dissipation (Sec. 6). The acoustic source power $\langle P_{source} \rangle$ is then determined by measuring the acoustic power losses $\langle P_{loss} \rangle$. These losses are evaluated by using a two microphone method to measure the acoustic radiation at the main pipe terminations $\langle P_{rad} \rangle$ and the theory of Kirchhoff [96] to estimate the visco-thermal damping $\langle P_{v-th} \rangle$. By carrying out this kind of measurements for various values of radiation losses at the downstream termination, Bruggeman et al. [56, 58] found that, at moderate amplitudes, the acoustic source power $\langle P_{source} \rangle$ scales linearly with the acoustic amplitude $|\vec{u}'_{jun}|$ (Sec. 8.3).

For a double side branch system in cross configuration (Fig. 8-1), Peters [45] and Kriesels et al. [48] obtained, by means of the technique introduced by Bruggeman et al. [56, 58], an acoustic source power $\langle P_{source} \rangle$ showing saturation at high amplitudes.

Using a method similar to that used by Coltman [131], Graf and Ziada [71, 72] carried out measurements for characterizing the source impedance in double side branch systems in cross configuration [71] and tandem configuration [72]. A unique feature of these experiments is that the source impedance was determined for circular branches exposed to fully developed turbulent flow in the main pipe, which is similar to the geometrical and flow conditions in industrial applications. In these experiments, a loudspeaker was used to excite the system at the resonance frequency of the branches, and each series of measurements was carried out at fixed pulsation amplitude, while the Strouhal number was varied by changing the flow velocity in the main pipe. The source impedance $Z_s = 2 \Delta p_s / (\rho_0 U |\vec{u}'_{jun}|)$, where Δp_s is the acoustic source pressure across the shear layer and \vec{u}'_{jun} is the acoustic velocity at the branch opening, results in a spiral

evolution in the complex plane (Fig. 20). An important aspect of the experiments carried out by Graf and Ziada [71, 72] is the quantitative evaluation of the non-linear saturation of the shear layer disturbances (Sec. 8.3). Furthermore, the results indicate, in the moderate amplitude regime, a square root dependence of the acoustic source power $\langle P_{source} \rangle$ on the pulsation amplitude $|\bar{u}'_{jun}|$, rather than a linear dependence, as proposed by Bruggeman et al. [56, 58]. Using the empirical data of Graf and Ziada [71, 72] allows predicting the pulsation behavior of double side branch systems, for various depths of the side branches and static pressures. Typical accuracy of these predictions is about 20% in amplitude. Since the measurements of Graf and Ziada [71, 72] have been carried out only for junctions with sharp edges and in view of the accuracy in the prediction of pulsation amplitudes, this would call for a systematic reproduction of these measurements for T-junctions and cross-junctions with rounded edges,

which are common in industrial applications.

More recently, Oshkai and Yan [53] and Oshkai et al. [54], proposed a combination of digital particle image velocimetry (DPIV), acoustic pressure measurements and phase-locking techniques in order to provide insight into the mechanism of acoustic power generation in a double side branch system in cross configuration (Fig. 8-1).

9.2. LINEAR MODELS

The first attempt to predict self-sustained oscillations was to use the results of Michalke's theory [67] in linear models applied to flow induced cavity noise [59, 61, 78, 132–134]. In these models, a Kutta-like condition has been used at the upstream edge, where flow separation occurs, to estimate the perturbation of the shear layer due to acoustic oscillation. The spatial amplification of the perturbation has been calculated by using the stability theory of Michalke [67] for inviscid

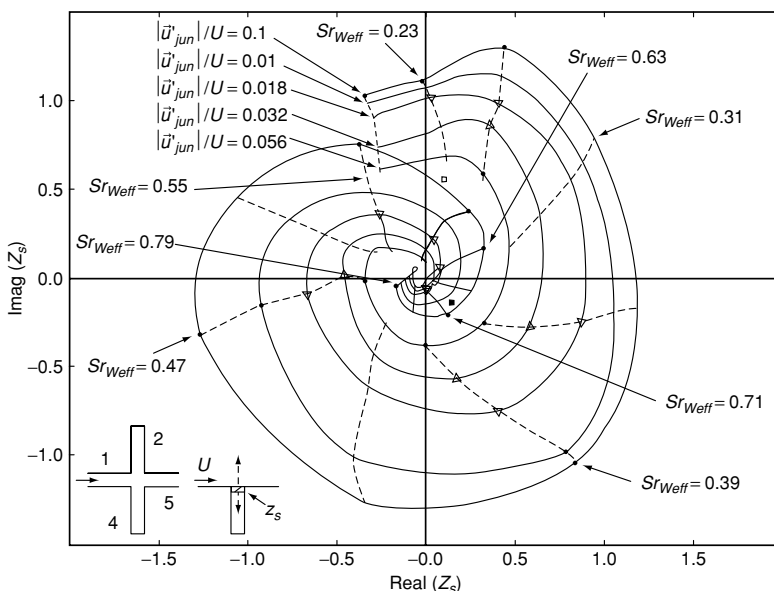


Figure 20: Complex representation of the source impedance of the (C-a1) limit case for small and moderate pulsation amplitudes. The solid lines are spirals of constant acoustic velocity $|\bar{u}'_{jun}|/U$, the dashed lines represent constant Strouhal number Sr_{Weff} and the symbols indicate measured data points. Measurements have been carried out in a double side branch system in cross configuration with sharp edges and circular cross section of the pipes. $L_2 = 0.64\text{m}$, $L_4 = 0.68\text{m}$, $L_5 = 2.1\text{m}$, $D_1 = D_5 = 89\text{mm}$, $D_2 = D_4 = 51\text{mm}$ (Fig. 8-1) [71].

parallel free shear layers (Sec. 5). The source of sound has been then assumed to be a dipole located at the downstream edge and resulting from the “impact” of the shear layer disturbances on this edge. These linear models do not explain essential effects, such as the influence of the shape of the upstream edge of the cavity on the pulsation behavior. One should furthermore realize that the impingement of the shear layer disturbances on the downstream edge is not essential for the sound production (Sec. 2 and Fig. 19).

An alternative linear model has been introduced by Elder [135], in which the shear layer is assumed to act as an oscillating “membrane” driving the cavity oscillations.

Möhring [136], Crighton [137] and Howe [39] proposed various formulations to predict the linear response of an infinitely thin shear layer. The formulation of Howe [39], considering the case of grazing flow along a thin walled orifice, combines the membrane concept of Elder [135] with an integral formulation of the Kutta condition at the upstream edge of the orifice. In agreement with experimental evidence, the singularity at the downstream edge does not seem to be crucial in the predicted source of sound. Furthermore, this formulation does predict the occurrence of limited Strouhal ranges for sound production, as confirmed by measurements carried out by Kooijman et al. [138]. These experimental results, in terms of source impedance, are however quite different from the results of the formulation of Howe [39]. Furthermore, they show a strong dependence of the Strouhal ranges for sound production and of the acoustic amplitude on the structure of the boundary layer upstream of the separation point and on the shape of the edges of the cavity. A quantitative theoretical prediction of the effect of the boundary layer structure on the source impedance is not yet available.

Recently, Åbom et al. [139, 140] proposed to include the effect of vortex-sound interaction in linear multi-port models in order to predict self-sustained oscillations. Multi-port models are linear aeroacoustic models, which split the problem in a passive part, the scattering matrix, and an active part describing the sound sources. The active part, representing the vortex-sound interaction has been included as part of the passive data expressed by means of the scattering matrix. This approach leads to scattering matrices that contains information about linear damping or amplification of sound by vortex-sound interaction.

9.3. SINGLE VORTEX MODEL

9.3.1. Single vortex model with calculated path and circulation

The model of Howe [23], for the aeroacoustic behavior of a flute, presents a first attempt to describe the sources of sound in a flute in terms of vortex sound. In his model, Howe [23], focused on the effect of vortex shedding at the sharp downstream edge of the mouth of the flute, the labium. Assuming that the vorticity can be concentrated into a single line vortex, the circulation of the vortex is determined by a Kutta condition imposed at the edge of the labium. While Howe [23] predicts that this vortex produces acoustical energy, experiments show that it absorbs sound [141, 142].

The idea of Howe [23] has been applied by Bruggeman et al. [56, 58] to a T-junction with sharp edges, in order to describe the vortex formed at the upstream edge. This model fails because the vortex circulation and its convective speed diverge as the vortex approaches the downstream wall of the T-junction. Attempts by Peters [45] to improve this single vortex model were not successful. While this model is not able to describe the vortex formed at the upstream edge, it can however be used to predict the sound absorption at high amplitudes by

vortex shedding at a sharp downstream edge of the T-junction.

9.3.2. Single vortex model with imposed path and calculated circulation

Based on detailed flow measurements in the opening of a Helmholtz resonator, Nelson et al. [124] proposed a simplified vortex model in which a line vortex is assumed to be formed, at the upstream edge of the cavity, each time the acoustic flow turns into the cavity. The circulation of this vortex is assumed to correspond to the integral of the vorticity shed at the upstream edge and the vortex is assumed to be convected downstream at a constant speed U_{con} , along a straight line between the upstream and the downstream edges. As the vortex flow is assumed to be independent of the oscillation amplitude this is a moderate amplitude model. Using this vortex model in combination with vortex sound theory [23], Nelson et al. [62] provide a qualitative explanation of the sound generation in a Helmholtz resonator.

An attractive aspect of the model of Nelson et al. [62, 124] is that it opens the way for analytical models of the sound sources at junction elements. A first analytical solution has been obtained by Hirschberg and Rienstra [143] by assuming a uniform acoustic flow normal to the vortex path. This corresponds roughly to the condition found at T-junctions and cross-junctions with rounded edges.

Combining the model of Hirschberg and Rienstra [143] with analytical models for the acoustic losses yields a surprisingly reasonable prediction of the pulsation amplitude for the first hydrodynamic mode. However, for higher hydrodynamic modes, this model tends to overestimate drastically the pulsation amplitudes. Furthermore, the model does not predict the amplitude dependence of the optimal Strouhal number $Sr_{W_{eff,opt}}$. In fact, this

Strouhal number is imposed by the convective velocity U_{con} which is introduced in the model as an empirical parameter [50, 143].

For the case of a sharp edged T-junction, Bruggeman et al. [56, 58] used the vortex model of Nelson et al. [62, 124] in combination with vortex sound theory [23] to explain the essential differences in the aeroacoustic behavior of the (T-a1), (T-a2) and (T-a3) limit cases (Fig. 15). This model provided a qualitative explanation of the effect of the edge shape on the whistling behavior of a double side branch system in tandem configuration (Fig. 8-a, $L_2 = L_4 \approx L_3/2$).

9.3.3. Single vortex model with imposed path and distributed vorticity

While the model of Nelson et al. [62, 124] in combination with vortex sound theory [23] provides a good insight in the aeroacoustic behavior of junction elements, it fails to give accurate quantitative predictions. The sharp edges imply a singularity of the acoustic field, which in combination with the imposed straight path of the vortices results in an overestimation of the acoustic source power $\langle P_{source} \rangle$ by almost a factor of five. This interaction between the singularity in the vortex model (line vortices with concentrated vorticity) and the singularity in the acoustic field can be avoided by assuming a distributed vorticity along a line segment, as proposed by Bruggeman [58], or by removing the downstream singularity in the acoustic flow distribution, as proposed by Dequand et al. [50]. Both these modifications reduce the overestimation by about a factor two.

Kook and Mongeau [63] proposed a modified model of Nelson et al. [62, 124] in which, in order to take into account the diffusivity of the vortices travelling downstream, a vortex concentration parameter has been

introduced. This empirical parameter has been estimated, for the case of a Helmholtz resonator, by using absolute cavity pressure amplitudes obtained experimentally over a range of free stream velocities. This vortex model has been then implemented in a feedback loop model, where the flow excitation and the acoustic response are approximately modeled as a forward gain function and as a backward gain function respectively.

9.3.4. Quasi-steady limit

An essential limitation of the single vortex models, is that they are not suitable to describe the low Strouhal number limit $Sr_{weff} \ll 1$. In this limit one can use a quasi-steady model in which the sound source is defined as the steady linear perturbation in total enthalpy across the junction ΔB_s .

An attempt to predict the aeroacoustic behavior of T-junctions at low Strouhal numbers has been done by Hofmans [74]. He developed analytical models for the quasi-steady behavior of sharp edged T-junctions, which provide predictions in good agreement with experiments from literature [144].

9.4. MODELS BASED ON THE NUMERICAL SOLUTION OF THE FLOW FIELD

Source models based on the numerical solution of the flow field have been developed by many authors. These models consist of two main steps. The first step is to solve numerically the flow field, imposing the acoustic field as boundary condition. The second step is to use the solution of these numerical calculations to evaluate the sources of sound.

9.4.1. Vortex blob simulations

Early work [145–147] on models based on the numerical solution of the flow field has been carried out using frictionless flow simulations based on discrete vortex methods. These models,

applied to various resonators (parallel plates, double diaphragm, Hartman generator), successfully determine the Strouhal conditions for optimal sound production by vortex shedding $Sr_{weff,opt}$.

Solving the flow field by means of the vortex blob method as developed by Chorin and Bernard [148] and used by Krasny [149, 150], several authors [45, 48, 74, 113] obtained predictions of the acoustic source power $\langle P_{source} \rangle$ in T-junctions and cross-junctions for various main flow configurations and acoustic flow limit cases.

Assuming a moderate amplitude behavior (Sec. 8.3), Hofmans [74] obtained the Strouhal number dependence of the acoustic source power $\langle P_{source} \rangle$ for all the nine limit cases of a T-junction with sharp edges. In these calculations, Hofmans [74] neglected the effect of vortex shedding at the downstream edge. Simulations in which this effect was taken into account did not indicate this was an important effect at moderate amplitudes.

For the (T-a3) limit case in a single side branch system (Fig. 21-a), at moderate amplitudes, the pulsation amplitudes predicted using the results of the simulations [74] in an energy balance, agreed within 10% with the measurements of Bruggeman [58] (Fig. 21-b). For the (T-a1) limit case in a multiple shallow side branch system, the model of Hofmans [74] implemented in an energy balance predicts exactly the observed optimal Strouhal number $Sr_{weff,opt}$ but overestimates the pulsation amplitude by a factor four [118].

The moderate amplitude assumption used by Hofmans [74] implies to assume the acoustic source power $\langle P_{source} \rangle$ to be linearly proportional to the acoustic amplitude $|\vec{u}'_{jun}|$. For high pulsation amplitudes this is not a correct assumption, so that when the pulsation amplitude becomes large, separate calculations should be carried out for various amplitudes. Using such simulations in combination

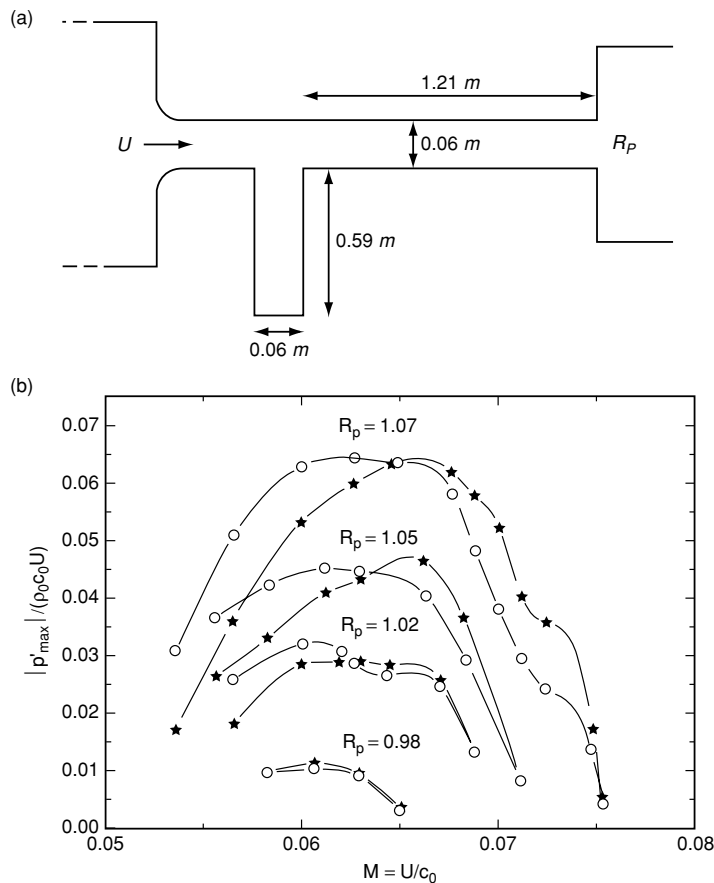


Figure 21: Experimental setup used by Bruggeman [58] to measure the pulsation levels of a single side branch system as function of main flow velocity U and pressure reflection coefficient R_p (a). Dimensionless pulsation amplitude $|p'_{max}|/(\rho_0 c_0 U)$ at the end of the closed side branch as function of the main flow Mach number $M = U/c_0$ for various reflection conditions R_p (b). The pipes have square cross section and the junction has sharp edges. Experimental results by Bruggeman [58] (stars) and predictions by means of an energy balance implementing the numerical results of the vortex blob method of Hofmans [74] (empty circles).

with an energy balance, Hofmans [74] predicted the pulsation amplitude for a single side branch configuration terminated by a horn (Fig. 6-b). The acoustic response of the horn placed at the downstream open termination $\langle P_{rad} \rangle$ was measured by means of a two microphone method. The visco-thermal losses $\langle P_{v-th} \rangle$ were calculated following the theory of Kirchhoff [96] and the acoustic losses due to non-linear wave steepening $\langle P_{rad-nl} \rangle$ were estimated. The predicted pulsation amplitude agrees within 30% with the experimental results (Fig. 22). Hofmans [74] assumes that these discrepancies

are due to the sound absorption by wall vibrations (Sec. 11).

Using the same numerical method as Hofmans [74], Kriesels et al. [48] obtained a prediction of the effect of the rounding of the edges on the acoustic source power $\langle P_{source} \rangle$ generated by vortex shedding in T-junctions and cross-junctions. In these simulations, the flow separation point was taken to be fixed at the end of the upstream main pipe segment, just before the upstream edge. The results of the simulations are shown in Fig. 23 for moderate pulsation amplitudes. At high pulsation amplitudes the simulations did not give reasonable results because the fixed

separation point assumption fails for rounded edges. The results obtained for moderate amplitudes agree qualitatively with the experimental observations of Dequand et al. [50].

The same vortex blob method as the one of Hofmans [74] and Kriesels et al. [48] has been used by Peters and Bokhorst [113], by means of which they obtained the prediction of the acoustic source power $\langle P_{source} \rangle$, at moderate amplitudes, for the (T-c1) and (T-c2) limit cases with sharp and rounded edges (Fig. 24).

9.4.2. Laminar and incompressible numerical simulations

Using a commercial solver, for the laminar, incompressible and two-dimensional Navier-Stokes equations, Martínez-Lera et al. [151] predicted the sound sources in sharp edged T-junctions for the limit cases (T-a1), (T-a2) and (T-a3). The use of

incompressible simulations limits the validity of this approach to low frequencies, but it avoids the appearance of spurious numerical resonances when using a limited numerical domain. This approach eliminates then the extreme difficulty to implement non-reflecting boundary conditions at the limits of the numerical domain. The Reynolds number based on the side branch diameter $Re_{D_{sb}} = UD_{sb}/\nu$ for which the calculations have been carried out is low, $Re_{D_{sb}} < 3000$. As the simulations are two-dimensional, the effect of turbulence has been excluded. The encouraging results of these simulations, summarized below, call for further work along this line.

In a first step, Martínez-Lera et al. [151] considers the Strouhal dependence of the source impedance Z_s in the linear (very low amplitude) limit. The results obtained are very similar to the experimental results of Graf and

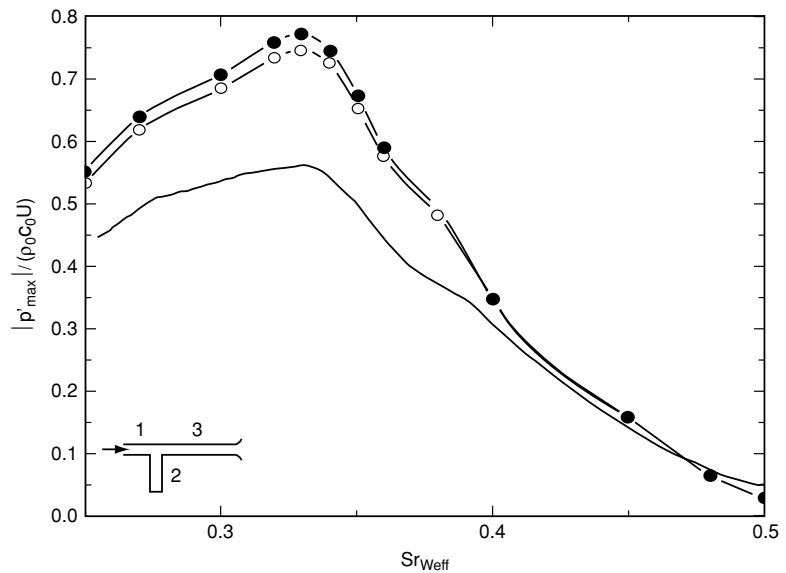


Figure 22: Dimensionless pulsation amplitude $|p'_{max}|/(\rho_0 c_0 U)$ at the end of the closed side branch of the single side branch system of Fig. 6-b ($L_1 = 0.12\text{m}$, $L_2 = 0.44\text{m}$, $L_3 = 0.82\text{m}$, $W_1 = W_2 = W_3 = 0.06\text{m}$, $r_{nozzle} = 0.03\text{m}$) with square cross section of the pipes and sharp edges of the junction, as function of the Strouhal number based on the effective cavity width $Sr_{W_{eff}}$. Experimental results (solid line) and predictions by means of an energy balance (circles) implementing the numerical results of the vortex blob method of Hofmans [74]. The energy balance is implemented without non-linear losses due to wave steepening (full circles) and with non-linear losses due to wave steepening (empty circles).

Ziada [71, 72] discussed in Sec. 9.1. Furthermore, these results display a dependence of the source impedance Z_s on the boundary layer thickness of the main flow, similar to that observed for an orifice subjected to grazing flow [88, 90]. An interesting aspect of the method introduced by Martínez-Lera et al. [151] is that the full range of acoustic frequencies is obtained in a single numerical simulation by means of a random perturbation of the steady solution.

In a second step, Martínez-Lera et al. [151] calculates the acoustic source power $\langle P_{source} \rangle$ for different pulsation amplitudes $|\bar{u}'_{jun}|/U$. The simulations clearly show the saturation effect predicted by Bruggeman [58] and observed by Graf and Ziada [71, 72].

The moderate amplitude case with $|\bar{u}'_{jun}|/U = 2 \cdot 10^{-1}$, for the (T-a3) limit

case, does agree well with the vortex blob simulations of Hofmans [74].

Using a methodology similar to that introduced by Martínez-Lera et al. [151], Nakiboglu et al. [152] investigate the dependence of the optimal Strouhal number $Sr_{W_{eff,opt}}$ on the diameter ratio D_{sb}/D_p for the (T-a1) limit case. It appears that the ratio of boundary layer thickness to pipe diameter determines the optimal Strouhal number $Sr_{W_{eff,opt}}$. Predicted optimal Strouhal numbers agree well with the available experimental data [120, 153]. The effect of boundary layer thickness also agrees with the observation of Elder et al. [61] and Golliard [154] on orifices subjected to grazing turbulent boundary layer flow. The method used by Nakiboglu et al. [152] is also successful in predicting the effect of cavity edge geometry on the acoustic source power $\langle P_{source} \rangle$ [128].

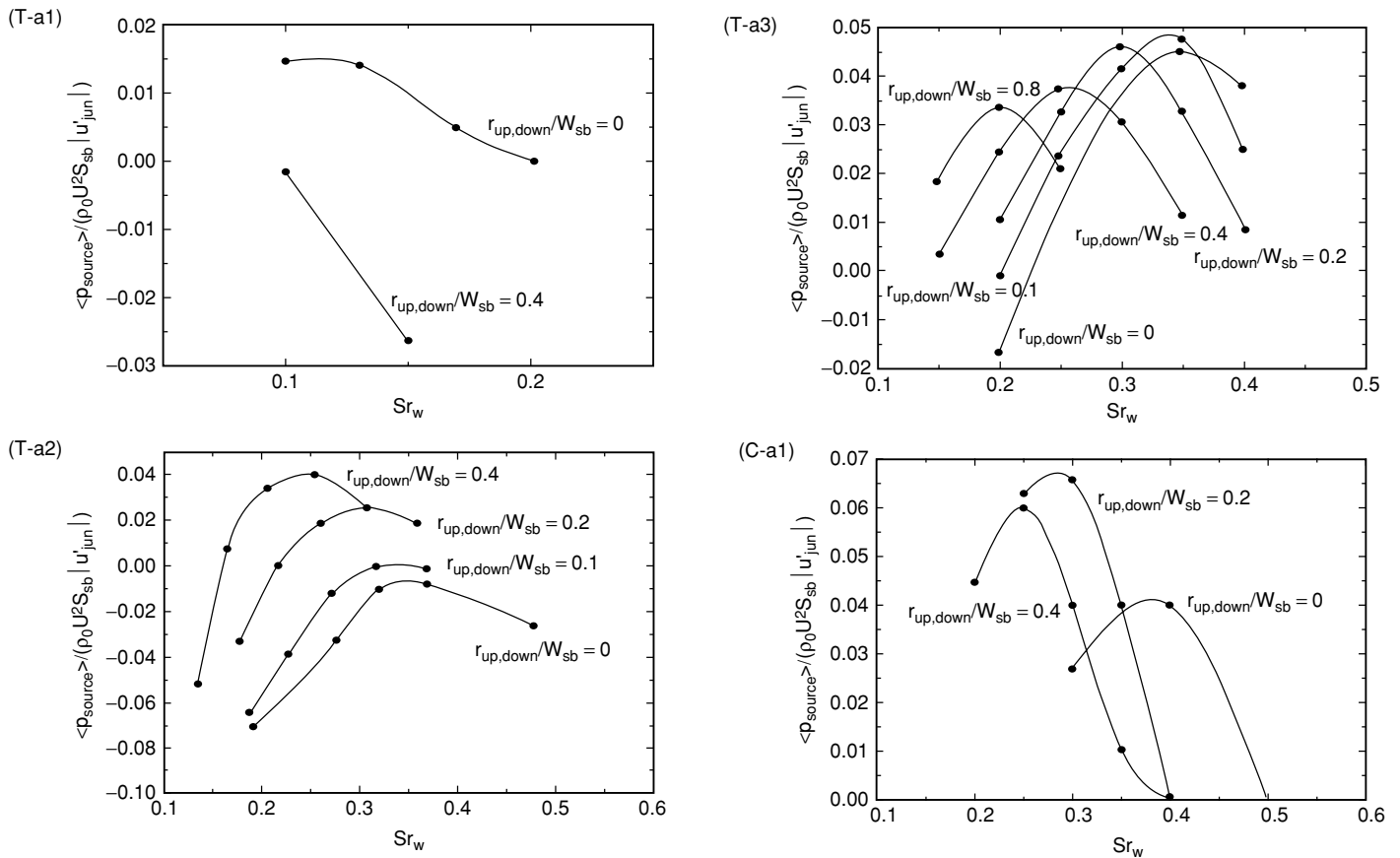


Figure 23: Dimensionless time-averaged acoustic source power $\langle P_{source} \rangle / (\rho_0 U^2 S_{sb} |\bar{u}'_{jun}|)$, where S_{sb} is the cross sectional area of the side branch, as function of the Strouhal number Sr_w based on the side branch width W_{sb} for the (T-a1), (T-a2), (T-a3) and (C-a1) limit cases with various shapes of the edges. Results of the vortex blob simulation carried out by Kriesels et al. [48].

9.4.3. Unsteady, turbulent and compressible numerical simulations

Numerical simulations of the flow field in sharp edged cross-junctions have been carried out by Radavich et al. [127] by means of an unsteady, turbulent and compressible solver. The results of these numerical simulations have been then processed by means of the analogy of Howe [41], in order to identify the regions of sound production. The results of these simulations, compared with experiments on a double side branch systems in cross configuration (Fig. 8-1), show that the method is capable of reproducing the physics of the flow-acoustic coupling and of predicting the flow conditions when this coupling occurs.

Recently, Föller et al. [155] investigated the aeroacoustic behavior of T-junctions with flow configuration (T-a) by means of Large Eddy Simulations (LES) in combination with system identification techniques (SI). The coefficients of reflection and transmission of plane acoustic waves and the production and absorption of acoustic energy due to the interaction of the unstable shear layer with the impinging acoustic waves, determined through the LES/SI methodology, compares favorably with available experimental data [140].

A drawback of the compressible simulations is that special care should be taken in implementing non-reflecting boundary conditions at the limits of the numerical domain.

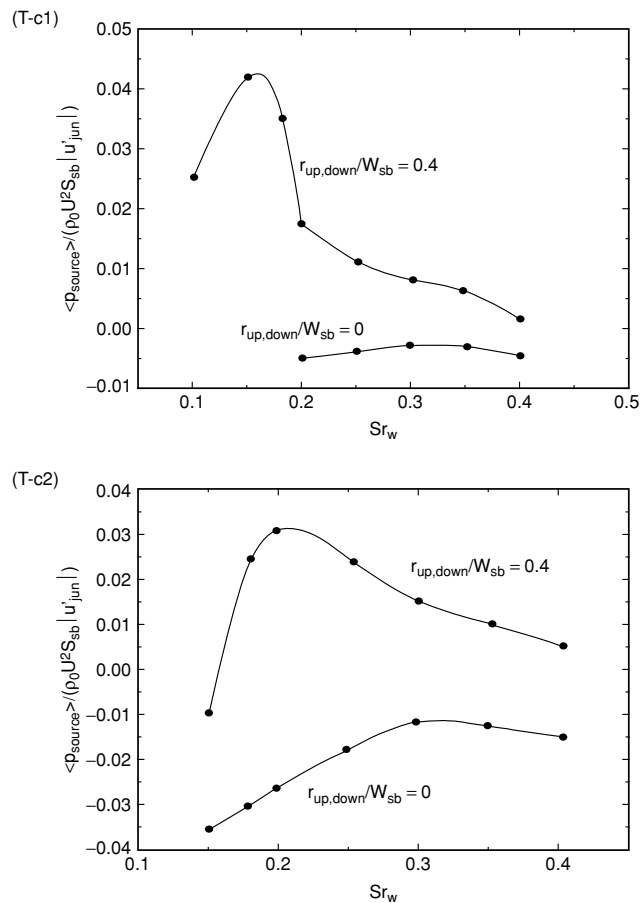


Figure 24: Dimensionless time-averaged acoustic source power $\langle P_{source} \rangle / \rho_0 U^2 S_{sb} |\bar{u}'_{jun}|$, where S_{sb} is the cross sectional area of the side branch, as function of the Strouhal number Sr_w based on the side branch width W_{sb} for the (T-c1) and the (T-c2) limit cases with sharp and rounded edges. Results of the vortex blob simulation carried out by Peters and Bokhorst [113].

9.5. DIRECT NUMERICAL SIMULATIONS (DNS) AND COMPRESSIBLE EULER SIMULATIONS

Full numerical models for the aeroacoustic behavior of pipe systems are based on the numerical solution of the flow by means of CFD codes, in which the solution includes both the main flow field and the acoustic field.

The aeroacoustic behavior of cavities subjected to grazing flow have been recently studied by Gloerfelt et al. [156] by means of direct numerical simulations (DNS). Besides the great advantage of having an accurate solution of the flow, including the main flow field and the acoustic field, a clear disadvantage is that these simulations are computationally expansive and are limited to resonators of limited size. Such simulations have not yet been achieved for T-junctions or cross-junctions. However, DNS does not seem suitable to compute the aeroacoustic behavior of complex pipe systems where the sources are compact and the resonators can typically extend over several acoustic wavelengths.

Using a dedicated compressible Euler solver, Dequand et al. [50] obtained a prediction of the pulsation behavior of a double side branch system in cross configuration (Fig. 8-1). In these numerical simulations, both sharp edges and chamfered edges have been considered. An interesting observation, confirmed by experiments, is that the chamfered edges behave as the rounded edges.

The numerical simulations of Dequand et al. [50] predict pulsation amplitudes which are 40% higher than the amplitudes observed experimentally in pipes with square cross section. This is partially expected to be due to the effect of wall vibrations in experiments.

The modeling of self-sustained oscillations in T-junctions and cross-junctions by solving the Euler equations gives reasonable results because, apart

from the upstream boundary layer, self-sustained cavity oscillations are essentially non-viscous phenomena. Furthermore, the imposed description of the upstream boundary layer into an Euler model leads to a satisfactory description of the phenomenon. A clear advantage of this kind of simulations is the reduced computational cost, compared to a DNS.

Using another Euler code, Lafon et al. [7] studied numerically the self-sustained oscillations in a steam line with a cavity (isolation valve). In this work two different computations have been carried out. In the first one a uniform mean flow profile was assumed at the inlet of the numerical domain. In the second one, a boundary layer obtained from experimental data was introduced in the numerical computation as an upstream boundary condition. This boundary layer profile appears to be essential to recover the experimentally observed coupling between the shear layer instability and the acoustic modes of the pipe system.

10. HYDRODYNAMIC INTERACTION

Hydrodynamic interaction between two side branches in close proximity has been observed by Ziada and Bühlmann [19]. This interaction results into a dependence of the pulsation amplitude on the angle between the planes defined by the main pipe and each side branch separately. This effect has been observed to be weak.

The influence of the distance between two side branches in tandem configuration on the pulsation amplitude, which has been reported in literature [19], is mainly due to an increase of radiation losses rather than to hydrodynamic interaction. In a study of the interaction between two Helmholtz resonators, Derks and Hirschberg [157] observed that the hydrodynamic interaction becomes

important only for distances lower than the width of the cavity opening.

When two closed side branches are placed in a cross configuration, they can produce a pulsation level which is higher than that of a tandem of two closed side branches placed next to each other. This is expected to be due to the reduced sound production of the downstream side branch in the tandem configuration, that presents a (T-a2) limit case (Fig. 23). In a cross configuration, if the side branch diameter is comparable to the main pipe diameter $D_{sb}/D_p = O(1)$, a significant hydrodynamic interaction can be observed between the two shear layers at the junction between each side branch and the main pipe [53, 54].

A strong hydrodynamic interaction has been observed [49] between a bend with a radius of curvature $3D_p$ of three pipe diameters and a closed side branch, placed just downstream of the bend. This is due to the formation of a jet in the bend. This non-uniformity of the flow influences the effective grazing flow velocity at the junction between the main pipe and the closed side branch for distances up to $10D_p$ downstream of the bend. When the closed side branch is placed in the direction of the interior of the bend, the effective grazing flow velocity is decreased and this results in a reduction of the optimal Strouhal number $Sr_{W_{eff,opt}}$, the critical Strouhal number $Sr_{W_{eff,cri}}$ and the pulsation amplitude. When the closed side branch points towards the exterior of the bend, the effective grazing flow velocity is increased and this results in an increase of the optimal Strouhal number $Sr_{W_{eff,opt}}$, the critical Strouhal number $Sr_{W_{eff,cri}}$ and the pulsation amplitude. The same effect has been observed to occur for a tandem of two side branches downstream of a bend [19]. However, this effect is less important for a system of two side branches in cross configuration downstream of a bend [46, 49]. Coffman and Bernstein [2]

observed strong hydrodynamic interaction between a row of closed side branches (standpipes of safety valves) and an upstream sharp bend.

Our recent experiments on double side branch systems in tandem and cross configuration show a strong reduction of the pulsation amplitude when these systems are placed a few pipe diameters ($\approx 3D_p$) downstream of a sharp bend with radius of curvature of $D_p/2$. We expect this effect to be similar to that of an orifice plate, discussed by Ziada [46] (Sec. 12.3).

11. INFLUENCE OF WALL VIBRATIONS

Wall vibrations can be significant amplitude limiting losses. In laboratory experiments with pipes with rectangular cross sections one should suspect them because rectangular cross sections are easily deformed by pressure fluctuations. In full scale pipes, vibrations can also become crucial because pipe walls become relatively thin as one increases the pipe diameter.

Large scale experiments carried out by Gasunie at Westerbork confirm the significant role of wall vibrations as amplitude limiting losses [4, 17]. These experiments have been carried out measuring the pulsation level in a double side branch system in tandem configuration with and without stiffening elements. By increasing the rigidity of the setup, the pulsation amplitude was increased by about 50% (Fig. 25). This confirms the hypothesis that wall vibrations have a significant effect.

An accurate prediction of pulsation amplitudes in pipe networks where the wall vibrations are significant requires an estimation of the transfer of acoustic power from the acoustic field to the pipe structure $\langle P_{wall} \rangle$. We propose here a simple model for the evaluation of the order of magnitude of these losses.

At low frequencies the coupling between the acoustic waves and the pipe

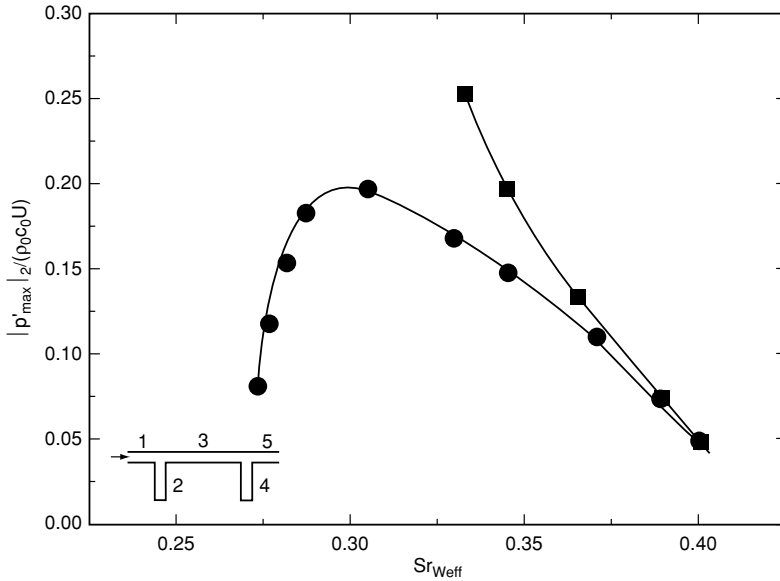


Figure 25: Effect of the wall vibrations on the pulsation level of the double side branch system in tandem configuration of Westerbork [4, 17]. The pipes have circular cross section and the junctions have rounded edges (Fig. 8-a, $L_2 = L_4 = 3.73\text{m}$, $L_3 = 7.29\text{m}$, $D_1 = D_3 = D_5 = 0.305\text{m}$, $D_2 = D_4 = 0.254\text{m}$, $r_{up,down} = 0.25D_2$, $\rho_0 = 54\text{kg/m}^3$ and $c_0 = 388.5\text{m/s}$). The dimensionless pulsation amplitude $|p'_{max}|_2 / (\rho_0 c_0 U)$, measured at the closed end of the upstream side branch L_2 , is presented as function of the Strouhal number Sr_{Weff} for the system without stiffening elements (circles) and with stiffening elements (squares). Measurements on the stiffened system could not be carried out below $Sr_{Weff} \approx 0.33$ for safety reasons.

wall vibrations is limited at discontinuities. At such points the acoustic pressure is not uniform and can drive lateral displacements of the pipe. We focus on the case of a system composed by a closed side branch along an infinitely long free pipe (Fig. 26).

If we assume a quarter wavelength resonance in the side branch $f_1 \approx c_0 / (4L_{sb})$, the junction between the main pipe and the side branch is at a pressure node while the end of the side branch is at a pressure antinode. The fluctuating pressure p'_{max} at the end of the side branch induces a periodical force $F_{vib} = S_{sb} p'_{max}$, which is transmitted by the side branch walls and pulls the main pipe periodically. This force is not compensated by pressure fluctuations at the junction because there is a pressure node at this point (Fig. 26).

The time-averaged acoustic power transferred from the acoustic field to the pipe structure $\langle P_{wall} \rangle$ is found from:

$$\langle P_{wall} \rangle = \frac{1}{T} \int_0^T F_{vib} \frac{dy(x = x_{sb})}{dt} dt \quad (20)$$

where $T = 1/f$ is the period of the acoustic oscillation, $y(x = x_{sb})$ is the lateral displacement of the main pipe at the side branch position $x = x_{sb}$.

The lateral displacement y of an infinite pipe under the influence of a point force F_{vib} applied at $x = x_{sb}$ has been evaluated by Morse [14]. Introducing the results of this theory in Eq. (20), the time-averaged acoustic power transferred to wall vibrations can be expressed as:

$$\langle P_{wall} \rangle = \frac{|F_{vib}|^2 2\pi f}{8EI_p k_p^3} \quad (21)$$

where E is the Young's modulus of the pipe, I_p is the moment of inertia of the pipe with respect to its neutral axis and k_p is the wave number of the vibrations

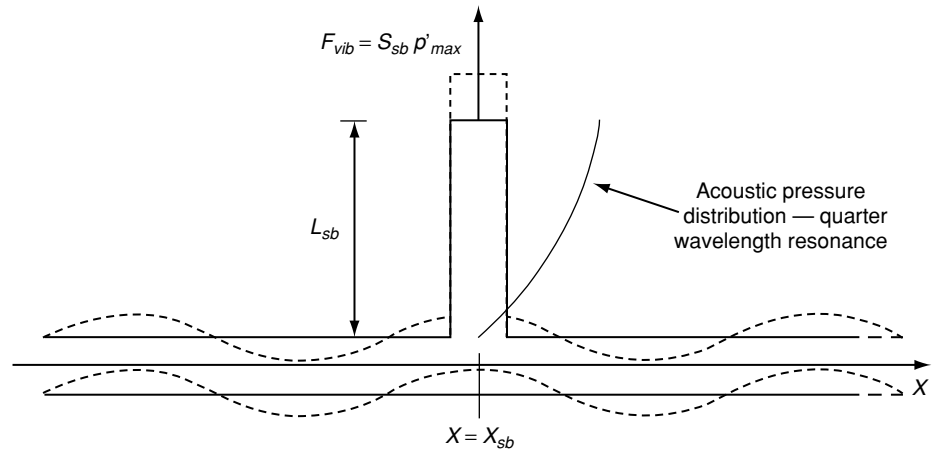


Figure 26: System composed by a closed side branch along an infinitely long free pipe. In the condition of a quarter wavelength resonance of the side branch, the fluctuating pressure p'_{max} at the end of the side branch induces a periodical force $F_{vib} = S_{sb} p'_{max}$ which is transmitted by the side branch walls and pulls the main pipe periodically.

along the main pipe. This wave number is given by:

$$k_p = \left(\frac{\rho_p S_p}{EI_p} \right)^{\frac{1}{4}} \sqrt{2\pi f} \quad (22)$$

where ρ_p and S_p are respectively the density and the cross sectional area of the main pipe.

In most cases the mass of the side branch or the mass of a compressor attached to the side branch will significantly affect the movement of the system. This mass m_p can be taken into account in the expression of the periodical force which is transmitted by the side branch walls and pulls the main pipe periodically, so that $F_{vib} = S_{sb} p'_{max} - m_p d^2y(x = x_{sb})/dt^2$. The time-averaged acoustic power transferred to wall vibrations, taking into account the attached mass, is then:

$$\langle P_{wall} \rangle = \frac{1}{2} S_{sb}^2 |p'_{max}|^2 \frac{2\pi f (4EI_p k_p^3)}{(4EI_p k_p^3 + 2\pi f m_p)^2 + (2\pi f)^4 m_p^2} \quad (23)$$

12. REMEDIAL MEASURES FOR THE PREVENTION OF THE SELF-SUSTAINED OSCILLATIONS

Self-sustained aeroacoustic pulsations can appear either in new pipe networks

or in existing networks when the operation conditions are modified. A typical example is the appearance of flow induced pulsations as a consequence of the increase in the operational flow speed in gas transport systems. Indeed, severe self-sustained oscillations are more likely to occur at high velocities than at low velocities. Pulsations are expected to occur in any pipe system containing closed branches when the flow velocity exceeds a critical value.

A proper aeroacoustic design of a pipe network avoids the operational conditions which may lead to the occurrence of self-sustained oscillations. This can be achieved by following the aeroacoustic design charts, as those presented by Ziada and Shine [49] and Bruggeman et al. [56]. These charts are constructed by using the results obtained in scale model experiments. Each scale model (i.e. single closed branch, double side branch system, ...) is tested to investigate the effects of the flow and design parameters on the critical Strouhal number $Sr_{Weff,cri}$ at which acoustic resonances are initiated. The use of the design charts is useful to determine the flow velocity in the system above which self-sustained oscillations can be expected.

Whenever design rules (design charts) cannot be fulfilled, or in the case of modification of the operational conditions, the maximum pulsation amplitudes should be estimated. If this amplitude is not acceptable, additional remedial measures can be implemented to mitigate the pulsation intensity or eliminate it altogether. These remedial measures are: detuning the branches by making them of different lengths, inserting anti-vortex elements in the branch inlet or adding upstream spoilers in the main pipe. Active control methods have also been shown to be effective, however, to date, only under laboratory conditions. In the following, these remedial measures are briefly discussed.

12.1. DETUNING OF THE LENGTH OF THE CLOSED BRANCHES

If resonance conditions cannot be avoided for piping systems with closed branches, the pulsation intensity can be reduced by detuning the length of the closed branches, by making one branch shorter (or longer) than the other. However, the effect of detuning the branches is strongly dependent on the specific geometry of the piping system, including the diameter ratio D_{sb}/D_p , the distance between the closed branches, the branch arrangement (i.e. whether the pipe system includes double or multiple branches and whether they are in the tandem or the cross configuration) and the geometry of the upstream and downstream pipe segments.

For double side branch systems arranged in the tandem [19, 46] and in the cross configurations [71, 72], the pulsation amplitude has been observed to decrease by an order of magnitude when the lengths of the branches were detuned by about 10% (Fig. 27-a). In all these experiments, two absorption silencers were installed at both ends of the test section to make the main pipe acoustically less reactive and, therefore,

reduce the influence of the main pipe on the acoustical response of the side branches.

For the case of short side branches with small diameter ratios D_{sb}/D_p , which are liable to resonance even in the single configuration, detuning the branches may be less effective. For example, Arthurs and Ziada [55] showed that introducing a relatively small offset in the length of two branches generates two distinct tones, corresponding to the different lengths of the branches. Although the tone amplitudes of the detuned branches were reduced to about 25% of those observed for tuned branches, this reduction may not be sufficient, especially when the higher order acoustic modes are of concern for short side branches with small diameter ratio D_{sb}/D_p .

In some cross configurations (Fig. 27-b) with rounded edges and diameter ratio $D_{sb}/D_p = 1$, Tonon et al. [158] found that even a change of 30% in length of one of the side branches (L_2 was changed while keeping $L_4 = 13cm$) was not sufficient to reduce by an order of magnitude the pulsations of the system. The robustness of these resonators has been found to be due to the influence of the main pipe on the acoustical response of the side branch system. In these experiments the main pipe terminations were acoustically reflecting (open ends). An increase of the length of the downstream pipe segment, from $L_5 = 7cm$ to $L_5 = 17cm$, led to a resonator in which the pulsation amplitude decreased by an order of magnitude when the branches were detuned by 10%. It is interesting to note that in the case of a cross configuration with $L_1 = 49cm$ and $L_5 = 7cm$, detuning the side branches by 10% resulted in a 20% increase of the pulsation amplitude (Fig. 27-b).

For the special case of double side branches in tandem configuration separated by a well-tuned main pipe segment (Fig. 8-a, $L_2 = L_4 \approx L_3/2$),

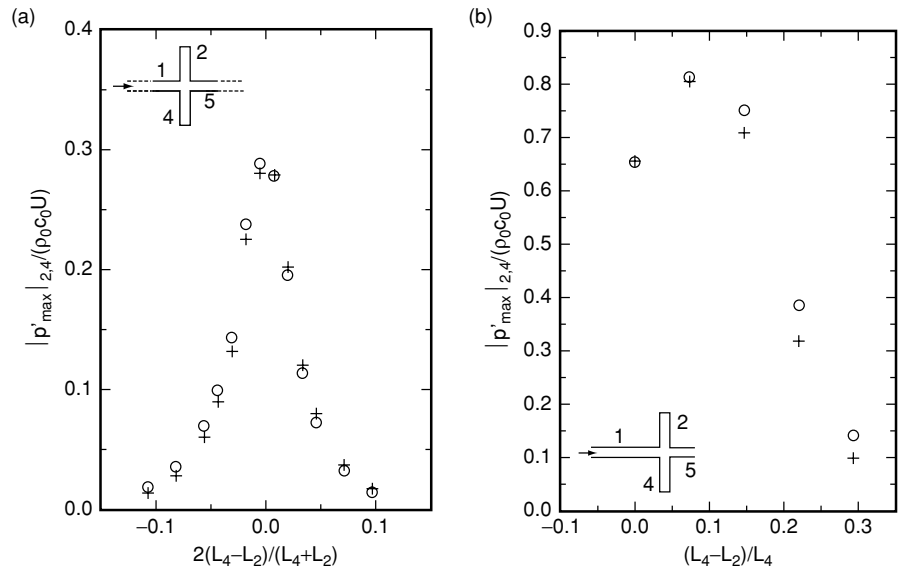


Figure 27: Dimensionless pulsation amplitude $|p'_{\max}|_{2,4}/(\rho_0 c_0 U)$ at the closed end of side branch L_2 (crosses) and L_4 (circles) in asymmetrical double side branch systems in cross configuration. (a) Side branch system with circular cross section of the pipes ($D_1 = D_5 = 89\text{mm}$, $D_2 = D_4 = 51\text{mm}$) and sharp edges. The length of one side branch is increased/decreased in steps while the other branch is shortened/elongated accordingly by an equal length ($L_2 + L_4 = 1.57\text{m}$) [71, 72]. (b) Side branch system with circular cross section of the pipes ($D_1 = D_2 = D_4 = D_5 = 33.6\text{mm}$) and rounded edges $r_{\text{up,down}}^{u,l} = 0.1D_2$. The length of one side branch L_2 is decreased in steps while the length of the other branch is kept constant $L_4 = 13\text{cm}$. The length of the upstream and downstream main pipe segments is $L_1 = 49\text{cm}$ and $L_5 = 7\text{cm}$ [158].

experiments by Bruggeman [58] indicate that detuning the length of the side branches becomes effective only for asymmetry of more than 20% (Fig. 28).

In the case of multiple side branches, the effect of detuning is more difficult to assess. Detuning the length of all the branches leads in general to a reduction of the pulsation amplitude. However, as shown by Tonon et al. [116], detuning the length of one side branch in a system composed by six side branches does not reduce much the pulsation levels. In 1958 Anderson [159] predicted that when a crystal is disordered enough (filled with a high concentration of defects) electron diffusion will cease. The phenomenon, called Anderson localization, explains the phase transition in a material that changes from a conductor to an insulator as disorder is increased and its electrons transform from diffusive,

delocalized waves into localized, or trapped, wavepackets [160, 161]. Dépollier et al. [162] observed that random irregularities in the length of the side branches of a multiple side branch systems induce acoustical Anderson localization, so that the system still displays trapped modes in spite of the randomness.

Finally, the length of the side branches can be designed in order to eliminate specific resonances [163]. This leads to the cancellation of the pulsation for specified conditions. An example of industrial application is the use of an additional side branch in safety valves to detune the resonance [11].

12.2. ANTI-VORTEX INSERT

Jungowski and Studzinski [164] developed and patented several anti-vortex devices which can be inserted

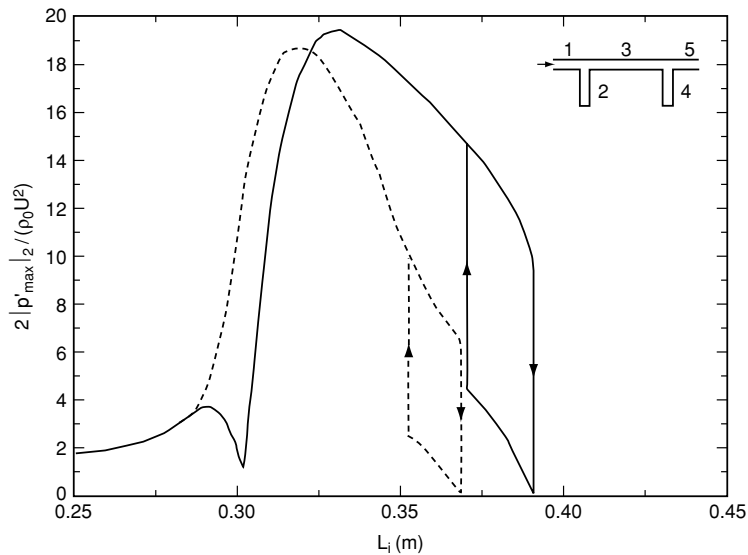


Figure 28: Influence of side branch length on the amplitude of self-sustained pulsations in the double side branch setup in tandem configuration of Fig. 8-a. The pipes have circular cross section ($D_1 = D_3 = D_5 = 30\text{mm}$, $D_2 = D_4 = 25\text{mm}$) and both upstream and downstream edges of the junctions are rounded $r_{\text{up,down}} = 0.12D_2$. The dimensionless pulsation amplitude $|p'_{\text{max}}|_2 / (1/2\rho_0 U^2)$ is measured at the closed end of the upstream side branch L_2 , varying the length of one side branch L_i , at fixed length of the other side branch. The solid line represents the results obtained with $L_3 = 2L_4 = 0.597\text{m}$ and varying the length L_2 , while the dashed line represents the results obtained with $L_3 = 2L_2 = 0.597\text{m}$ and varying the length L_4 .

into the mouth of closed branches. They consist of a single splitter plate, two plates in a cross configuration or three plates in a triangular arrangement. These inserts represent an attractive solution because they are very effective in suppressing the flow induced pulsations, do not interfere with the main flow and do not cause substantial increase in the pressure loss when the flow is diverted into the branches. The excellent performance of these inserts in suppressing flow induced pulsations appears to be due to several effects. They can reduce the formation of vortices inside the branch mouth; they change the length scale of the separated shear layer; and they introduce strong three dimensional effects.

12.3. SPOILER, SHARP TRAILING EDGE AND ORIFICE PLATE

Spoilers can be used to reduce self-sustained oscillations due to flow

separation in T-junction and cross-junction elements [46, 56]. Besides the advantage of reducing the pulsation amplitudes, they have the disadvantage of inducing flow losses.

The sharp trailing edge (upstream edge) suggested by Bruggeman et al. [56] is a type of spoiler that is very effective and only induces flow losses when the flow is turning into the side branch. In principle its effectiveness depends on the length l_s of the edge formed by a plate compared to the side branch diameter D_{sb} . In the experiments carried out by Bruggeman et al. [56] a ratio $l_s/D_{sb} \approx 0.2$ appeared to be very effective (Fig. 30).

An improvement of the spoiler, observed by Bruggeman et al. [56, 58] consists in using a zigzag edge rather than a straight edge normal to the flow. This reduces the coherence of the vortex shedding [165].

The effect of an upstream orifice plate on the acoustic resonance of side

branches in tandem and cross configurations was investigated by Ziada and Bühlmann [19]. When an orifice plate was positioned $5.5D_{sb}$ upstream of the branches, the pulsation amplitude was reduced to about 30% of its original value without the orifice plate, for both the tandem and the cross arrangements. In addition, the pulsations at the second hydrodynamic mode were eliminated for the tandem branches. Ziada and Bühlmann [19] attribute this mitigation effect to increased turbulence level in the main pipe, which disturbs the formation of coherent vortices at the branch mouth. A sharp bend, with a radius of curvature of $D_p/2$, appears to behave in a similar way as an orifice plate when it is placed few diameters upstream of a closed branch system. The drawback of these countermeasures is the increased pressure loss due to the restriction of the flow area.

12.4. ACTIVE CONTROL TECHNIQUES

Active control of flow induced pulsations has received considerable attention over the past two decades. Ffowcs Williams and Huang [166], Huang and Weaver [167] and Welsh et al. [168] used loudspeakers to counteract the resonant sound field of different types of resonators and thereby suppress the resonant oscillations. Later on, active suppression of flow induced pulsations in shallow cavities has been demonstrated, with a varying degree of success, by means of perturbing the shear layer at its separation location with the aid of oscillating flaps [169, 170], pulsed mass injection [169], piezoelectric actuators [171], or synthetic jets [172, 173]. It is also possible to use active control means to suppress acoustic resonances of closed branches, as demonstrated by Ziada [46, 174].

There are three different methods proposed in the literature to suppress self-sustained oscillations by active

means. The first involves externally forcing the shear layer at frequencies which are substantially different from that occurring during the resonance [169, 170]. In this approach, a continuous high level of power is needed to force the shear layer oscillation at a frequency different from the frequency of its natural instability. The other two active control methods are similar in that they employ a feedback control strategy, but differ in the type of the used actuator. In the first feedback control method [46, 166–168, 175], loudspeakers are used to counteract the acoustic resonance and thereby reduce the acoustic particle velocity below the critical level required to organize and synchronize the shear layer oscillation. This approach can be classified as active damping control of the acoustic mode because the actuator acts on the resonant acoustic mode rather than on the shear layer. In the other feedback control method [172–174], the shear layer is directly excited at the separation location to counteract the feedback generated by the resonant acoustic mode. This technique, therefore, can be described as feedback control of the shear layer oscillation. Since the actuators in both feedback control methods are activated by the system response, the energy consumption by the actuators decreases sharply after a short time period which is needed to suppress the resonance. This is in contrast with the external forcing of the shear layer at frequencies which are substantially different from that occurring during the resonance, which necessitates continuous high power level for the actuator.

13. SCALE MODELS

Scale model setups are convenient because they are more flexible and less expansive than real field setups. As the weight of a setup scales with the third power of the linear length scale, a

reduction of the length scale by a factor 10 reduces the cost of experiments by at least a factor 10^3 .

13.1. SIMILARITY

The key idea of scale modeling is that the dimensionless amplitude of self-sustained oscillation is a function of dimensionless parameters in which some of these parameters, such as the Mach number $M = U/c_0$ and the Reynolds number $Re_D = UD/\nu$ (D is the pipe diameter and ν is the kinematic viscosity of the gas), are not critical.

The square of the Mach number M^2 indicates the importance of compressibility on a steady flow. The Reynolds number Re_D indicates the importance of viscosity on the flow at the junction between the main pipe and a closed branch. For typical industrial gas flows, $M \leq 0.3$, and therefore the flow will not depend significantly on the Mach number. Furthermore, the Reynolds number is typically $Re_D \geq 10^5$, so that the flow is turbulent and does not depend critically on the specific value of the Reynolds number.

The choice of the dimensionless representation of experimental results is not unique. For a pipe system with resonant closed branches of diameter D_{cb} and length L_{cb} , the pressure p'_{\max} measured at an antinode, such as the closed end, can be written as a function F of the key dimensionless numbers: the Strouhal number $Sr_{W_{eff}} = fW_{eff}/U$ based on the effective cavity width W_{eff} (Sec. 3), the Helmholtz number $He_L = fL_{cb}/c_0$ based on the closed branch length L_{cb} , the product αL_{cb} of the branch length L_{cb} and the damping coefficient α for plane waves, and geometrical functions, such as the ratio r/D_{cb} of edge radius r to closed branch diameter D_{cb} of the junction between the closed branch and the main pipe (Fig. 14) and the ratio D_{cb}/D_p between the diameter of the closed branch D_{cb} and that of the main pipe D_p :

$$\frac{|p'_{\max}|}{\rho_0 c_0 U} = F(Sr_{W_{eff}}, He_L, \alpha L_{cb}, r/D_{cb}, D_{cb}/D_p) \quad (24)$$

For a laminar acoustic boundary layer, the damping coefficient α for plane waves [96] is given by:

$$\alpha = \frac{\delta_v \pi f}{D_{cb} c_0} \left(1 + \frac{\gamma - 1}{\sqrt{\text{Pr}}} \right) \quad (25)$$

where γ is the Poisson ratio c_p/c_v of specific heats at respectively constant pressure and constant volume, Pr is the Prandtl number and $\delta_v \approx \sqrt{\mu/(\rho_0 \pi f)}$ is the thickness of the viscous acoustic boundary layer.

For a resonant closed branch, the Helmholtz number is $He_L = (n + 1/2)/2$, with $n = 0, 1, 2, \dots$. In such a case the dimensionless pressure $|p'_{\max}|/(\rho_0 c_0 U)$ is a measure for the ratio $|\bar{u}'_{jun}|/U$ of the amplitude of the acoustical particle velocity $|\bar{u}'_{jun}|$ at the junction (sound source) and the main flow velocity U . From experiments on recorder flutes [142, 176] and Helmholtz resonators [105], it appears that the ratio $|\bar{u}'_{jun}|/U$ at the sound source (shear layer) is indeed a very good dimensionless representation of the pulsation amplitude.

As explained in Sec. 8.3, when visco-thermal and radiation losses become negligible, one reaches a high amplitude limit which is determined by geometrical parameters such as r/D_{cb} and the flow configuration. The amplitude $|\bar{u}'_{jun}|/U$ is then independent of αL_{cb} .

A scale model experiment will then accurately predict pulsations as long as geometrical details are accurate enough. Prediction is much easier for trapped modes than for global modes, because global modes require the accurate modeling of the acoustical boundary conditions of the pipe system (Sec. 1.2). This is not easy in scale model experiments.

In contrast to high amplitudes, $|\bar{u}'_{jun}|/U$ is not predicted by scale model experiments at low amplitudes. At these amplitudes, as discussed in Sec. 8.3, the local hydrodynamic pressure fluctuations induced by the shear layer oscillation are proportional to the acoustical forcing amplitude $|\bar{u}'_{jun}|$. The power balance determining the pulsation amplitude is extremely sensitive to minor changes in the experimental setup, because both the sound production and the sound dissipation are quadratic functions of $|\bar{u}'_{jun}|$.

In the following sections we will discuss the prediction of moderate amplitude pulsations by means of scale model experiments and some other aspects of scale modeling. Before doing so, we should stress the fact that exact geometrical scaling, including surface roughness, is not possible.

13.2. PREDICTING MODERATE AMPLITUDE PULSATIONS

At moderate amplitudes one expects that the sound source is only weakly dependent on the pulsation amplitude (Sec. 8.3). In such a case, the pulsation amplitude can be reasonably well predicted by using a power balance (Sec. 6) in which the acoustic source power $\langle P_{source} \rangle$ is determined from scale model experiments while visco-thermal $\langle P_{v-th} \rangle$ and radiation losses $\langle P_{rad} \rangle$ are estimated theoretically. This is the approach used by Bruggeman et al. [56] and Graf and Ziada [71, 72] (Sec. 9.1). This procedure will in general provide an overestimation of the pulsation amplitude because such a balance does not take into account wall vibrations, which provide additional damping and reduce the pulsation amplitudes. Furthermore, using for the damping coefficient a the approximation of Kirchhoff (Eq. (25)) we ignore the possibility of a transition from laminar to turbulent flow in the acoustic boundary layers in the closed branches.

Such a transition has never been demonstrated in laboratory experiments but could occur in industrial pipe systems when $\rho_0 \delta_v |\bar{u}'|/\mu > 350$ [130]. This transition would imply an increase in visco-thermal damping.

In contrast with high amplitude pulsations, it can be convenient to present scale model results for moderate amplitudes as the ratio $|p'_{max}|/(1/2\rho_0 U^2)$ of pressure fluctuation amplitude $|p'_{max}|$ and total head $1/2\rho_0 U^2$ of the main flow. This is due to the fact that at moderate amplitudes the local hydrodynamic pressure fluctuations induced by the shear layer are expected to scale with $1/2\rho_0 U^2$ so that the acoustic power production $\langle P_{source} \rangle$ scales with $1/2\rho_0 U^2 |p'_{max}|$. As the visco-thermal and radiation losses scale with $|p'_{max}|^2$, we expect $|p'_{max}|$ to be proportional to $1/2\rho_0 U^2$.

A problem with the moderate amplitude model is actually that it does not predict finite pulsation amplitudes independently of the magnitude of the damping. This implies that the power balance (Sec. 6) will not predict the sudden disappearance of pulsations when increasing the damping. This occurs when the pulsations reach the low amplitude level at which the source becomes amplitude dependant.

In scale models, losses can indeed become so large that self-sustained pulsations are not observed. In this case, the scale model results cannot be up-scaled because the self-sustained excitation mechanism and the resulting sound source are not reproduced in the model. This effect is demonstrated by the influence of the static pressure on the pulsation behavior of a single side branch resonator, observed by Bruggeman et al. [56, 58]. The measured dimensionless pressure $|p'_{max}|/(1/2\rho_0 U^2)$ is shown as a function of the Strouhal number $Sr_{W_{eff}}$ based on the effective cavity width, at both atmospheric pressure and at $p_0 = 5.2\text{bar}$ (Fig. 29). For the first hydrodynamic mode, around $Sr_{W_{eff}} \approx 0.4$, we do not

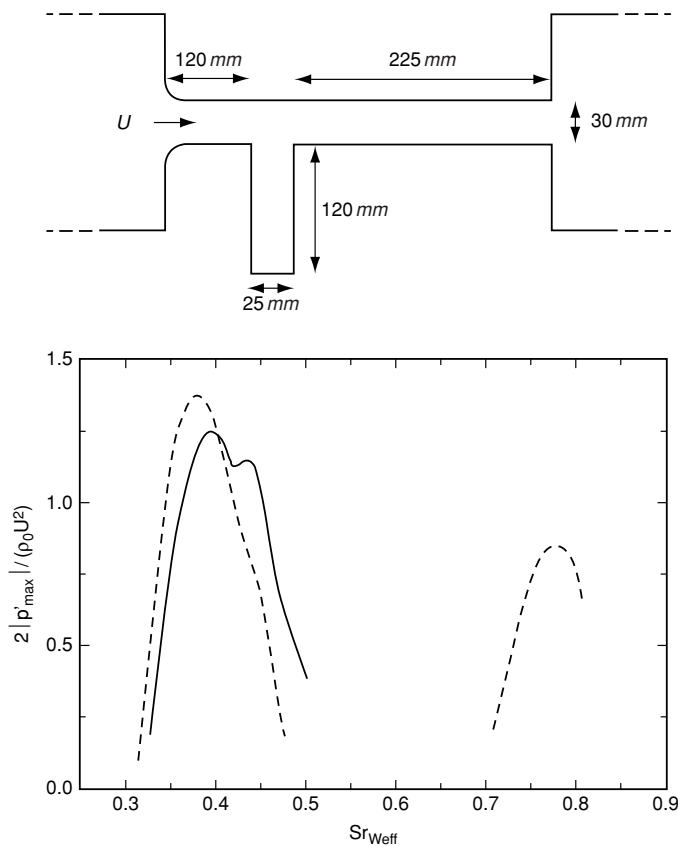


Figure 29: Influence of the static pressure of the gas p_0 on the dimensionless pulsation amplitude $|p'_{max}|/(1/2\rho_0 U^2)$. Single side branch configuration with circular cross section of the pipes and sharp edges of the junction. Solid line $p_0 = 1\text{bar}$, dashed line $p_0 = 5.2\text{bar}$.

observe a strong effect of the pressure. The second hydrodynamic mode, around $Sr_{Weff} \approx 0.8$ is only observed for $p_0 = 5.2\text{bar}$. A similar strong pressure dependency is illustrated in Fig. 30 for a double side branch system in tandem configuration. This graph presents the maximum of the dimensionless pulsation amplitude $|p'_{max}|_2/(\rho_0 c_0 U)$ as a function of the static pressure for $1\text{bar} \leq p_0 \leq 15\text{bar}$. Without spoilers we observe a strong increase of pulsation amplitude up to $p_0 = 5\text{bar}$, followed by a saturation. A spoiler placed upstream of the first side branch significantly reduces the pulsations at low pressures. Above a critical pressure, the pulsation amplitude suddenly rises, indicating a change in flow around the spoiler, which is probably related to the increase in Reynolds number. In this particular case we expect a transition from a laminar to a turbulent flow in the boundary layer around the teeth of the

spoiler. These examples clearly illustrate that the possibility to vary the pressure in a scale experiment will very strongly improve the reliability of the extrapolation of results to full scale.

13.3. PREDICTING THE ONSET OF PULSATIONS

In the previous sections we have been discussing the prediction of pulsations based on scale model experiments. We implicitly considered established pulsations. In engineering practice one would actually want to avoid pulsations. Hence, we seek for a prediction of the critical Strouhal number $Sr_{Weff,cri}$ below which pulsation occurs.

The main parameter that influence the Strouhal number at the onset of resonance $Sr_{Weff,cri}$ is the ratio D_{sb}/D_p between the diameter of the closed branch(es) D_{sb} and that of the main pipe D_p [49]. In a double side branch system

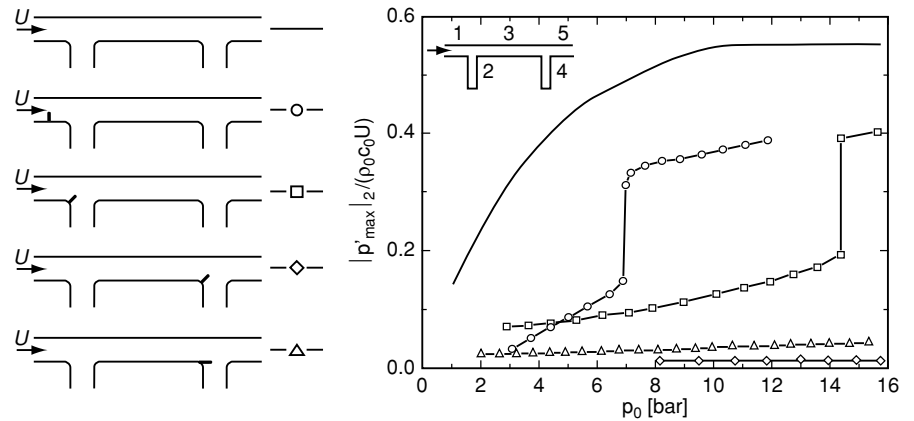


Figure 30: Influence of the static pressure of the gas p_0 on the dimensionless pulsation amplitude $|p'_{\max}|_2 / (\rho_0 c_0 U)$ measured at the closed end of the upstream side branch L_2 . Double side branch system in tandem configuration of Fig. 8-a ($L_3 = 2L_2 = 2L_4 = 0.597\text{m}$). The pipes have circular cross section ($D_1 = D_3 = D_5 = 30\text{mm}$, $D_2 = D_4 = 25\text{mm}$). Both upstream and downstream edges of the junctions are rounded $r_{\text{up,down}} = 0.12D_2$ in the reference configuration (solid line). Several remedial measures for the prevention of the self-sustained oscillations have been tested: a spoiler placed $1D_2$ upstream of the upstream T-junction (circles), a spoiler placed at the upstream edge of the upstream T-junction (squares), a spoiler placed at the upstream edge of the downstream T-junction (diamonds) and a sharp trailing edge of the downstream T-junction (triangles).

in tandem configuration, Ziada and Shine [49] observed an increase of the critical Strouhal number from $Sr_{W_{\text{eff},\text{cri}}} \approx 0.28$ up to $Sr_{W_{\text{eff},\text{cri}}} \approx 0.45$, as the diameter ratio was increased from $D_{sb}/D_p = 0.135$ up to $D_{sb}/D_p = 0.57$. Similar dependency of Strouhal number was found by Elder et al. [61] and Golliard [154] for grazing flow along orifices. For the (T-a1) limit case Nakiboglu et al. [152] predicts the same increase in Strouhal number with increasing D_{sb}/D_p . Although the radiation and the visco-thermal losses strongly influence the maximum pulsation amplitude and the width of the lock-in range of the resonance, they have a negligible effect on the critical Strouhal number $Sr_{W_{\text{eff},\text{cri}}}$ [49].

14. PERSPECTIVES

14.1. SOUND SOURCES

At the present time, we have obtained a fair qualitative understanding of the aeroacoustic behavior of pipe systems

with closed side branches, for the case of side branch diameter close to that of the main pipe $D_{sb} \approx D_p$. In such a case the flow at the junction is reasonably well described by a two-dimensional flow model. However, there is a need for more quantitative models, in particular for the case of junctions with rounded edges. Also the experimental information is mainly concerned with a grazing flow along the mouth of a closed side branch. There is little information on the other flow configurations (Fig. 15 and Fig. 16).

For the case of side branch diameter much smaller to that of the main pipe $D_{sb} \ll D_p$ we have only a reasonable understanding of the flow pulsations for the case of a grazing flow past a closed side branch. In this case a two-dimensional model remains reasonable. The reason why in this configuration the critical Strouhal number $Sr_{W_{\text{eff},\text{cri}}}$ depends on the diameter ratio D_{sb}/D_p should be studied more in detail. For the case of a main flow entering or

leaving a side branch, we do not have experimental data nor model describing the aeroacoustic behavior. In particular for the case of a flow leaving the side branch, one expects an essentially three-dimensional behavior due to the formation of a free jet.

14.2. THEORETICAL PREDICTION OF GLOBAL BEHAVIOR

The prediction of pulsations in complex systems has not yet been proven to be possible. Rules of thumb, such as an identification of resonators with a quality factor Q above 10 combined with a critical Strouhal number $Sr_{weff,cri}$ seem to predict in many cases pulsations which are not observed in industrial practice. As explained in Sec. 11 one possible reason for the reduction of pulsations in practice, is the damping due to wall vibrations. This should be verified.

Detuning of resonators, by choosing random lengths of the closed pipe segments, is certainly useful. It can however be expensive due to the increase in complexity of the pipe system. It does furthermore not give a guarantee that no acoustic trapped modes can appear (Sec 12.1).

At the present time, it is not clear how a scale model of a limited part of a pipe system can be used to predict the pulsation behavior of the whole (extended) system. In large pipe systems we can expect that several acoustic modes can interact. The simple energy balance based on the assumption that a single mode is dominant can fail. One may observe switching from one mode to another, rather than a stable limit cycle dominated by a single mode.

In many industrial systems, compressors are present. These compressors act as sound sources which can lock-in with flow induced pulsations or, on the contrary, impede these pulsations. This phenomenon has not been studied yet.

14.3. SCALE MODELS

Scale model experiments remain essential tools to study the behavior of complex systems. They can be used in the design phase in order to predict pulsations. Later they are most useful in order to test remedial measures, if flow induced pulsations appear as consequence of the modification of the operating parameters.

The possibility to vary the static pressure in a scale model is important in order to extrapolate the scale model results towards higher Reynolds numbers, as encountered at full scale. In general, scale models allow a large number of useful tests. Results should, however, always be confirmed by a number of full scale tests (Sec. 13.2) because up-scaling remains uncertain.

ACKNOWLEDGMENTS

This work is being sponsored by European Commission Marie Curie RTN Project AETHER (contract nbr MRTN-CT-2006-035713).

BIBLIOGRAPHY

- [1] Chen, Y.N. and Stürchler, R., Flow-induced vibrations and noise in the pipe system with blind branches due to coupling of vortex shedding, *Internoise 77*, 1977, Zurich, Switzerland.
- [2] Coffman, J.T. and Bernstein, M.D., Failure of safety valves due to flow induced vibration, *Journal of Pressure Vessel Technology*, 1980, 102, 112–118.
- [3] Baldwin, R.M. and Simmons, H.R., Flow-induced vibration in safety relief valves, *Journal of Pressure Vessel Technology*, 1986, 108, 267–272.
- [4] Gorter, J., Hirschberg, A., Wijnands, A. and Bruggeman, J.C., Flow induced pulsations in gas transport systems, *International Gas Research Conference*, 1989, Tokyo, Japan.

- [5] Jungowski, W.M., Botros, K.K. and Studzinski, W., Cylindrical side-branch as tone generator, *Journal of Sound and Vibration*, 1989, 131, 265–285.
- [6] Peters, M.C.A.M. and Riezebos, H.J., Analysis of the occurrence of flow-induced pulsations in a gas control station, *International Gas Research Conference*, 2001, Amsterdam, The Netherlands.
- [7] Lafon, P. Caillaud, S., Devos, J.P. and Lambert, C., Aeroacoustical coupling in a ducted shallow cavity and fluid/structure effects on a steam line, *Journal of Fluids and Structures*, 2003, 18, 695–713.
- [8] Hambric, S.A., Mulcahy, T.M., Shah, V.N., Scarbrough, T. and Wu, J., Acoustic loading on BWR steam dryers caused by valve singing, *9th NRC/ASME Symposium on Valves, Pumps and Inservice Testing*, 2000, Washington, D.C., United States.
- [9] DeBoo, G., Ramsden, K., Gesior, R. and Strub, B., Identification of Quad Cities main steam line acoustic sources and vibration reduction, *ASME Pressure Vessels and Piping Division Conference*, 2007, San Antonio, Texas, United States.
- [10] Takahashi, S., Ohtsuka, M., Okuyama, K., Ito, T. and Yoshikawa, K., Experimental study of acoustic and flow-induced vibrations in BWR main steam lines and steam dryers, *ASME Pressure Vessels and Piping Division Conference*, 2008, Chicago, Illinois, United States.
- [11] Ziada, S., Flow-excited acoustic resonance in industry, *Journal of Pressure Vessel Technology*, 2010, 132, 1–9.
- [12] Stoltenkamp, P.W., Bergervoet, J.T.M., Willems, J.F.H., van Uittert, F.M.R. and Hirschberg, A., Response of turbine flow meters to acoustic perturbations, *Journal of Sound and Vibration*, 2008, 315, 258–278.
- [13] Kergomard, J., Debut, V. and Matignon, D., Resonance modes in a one-dimensional medium with two purely resistive boundaries: Calculation methods, orthogonality, and completeness, *Journal of the Acoustical Society of America*, 2006, 119, 1356–1367.
- [14] Morse, P.M. and Ingard, K.U., *Theoretical acoustics*, Princeton University Press, Princeton, 1968.
- [15] Duan, Y., Koch, W., Linton, C.M. and McIver, M., Complex resonances and trapped modes in ducted domains, *Journal of Fluid Mechanics*, 2007, 571, 119–147.
- [16] Hein, S. and Koch, W., Acoustic resonances and trapped modes in pipes and tunnels, *Journal of Fluid Mechanics*, 2008, 605, 401–428.
- [17] Gorter, J., *Private communication*, 1987.
- [18] NRC, Additional flow-induced vibration failures after a recent power uprate, NRC Information Notice 2002-26, Supplement 2, January 9, 2004, *US Nuclear Regulatory Commission*, Washington, D.C., United States.
- [19] Ziada, S. and Bühlmann, E.T., Self-excited resonances of two side-branches in close proximity, *Journal of Fluids and Structures*, 1992, 6, 583–601.
- [20] Gillessen, R. and Roller, W., Verminderung und Beseitigung von Schwingungen an Rohrleitungssystemen (Reduction and elimination of vibration of piping systems), in: *Minderung von Rohrleitungsschwingungen*, VDI Berichte 748, VDI Verlag, Düsseldorf, 1989.
- [21] Powell, A., On the edgetone, *Journal of the Acoustical Society of America*, 1961, 33, 395–409.
- [22] Powell, A., Theory of Vortex Sound, *Journal of the Acoustical Society of America*, 1964, 36, 177–195.
- [23] Howe, M.S., Contributions to the theory of aerodynamic sound, with application to excess jet noise and the theory of the flute, *Journal of Fluid Mechanics*, 1975, 71, 625–673.
- [24] Blevins, R.D., *Flow-induced vibration*, Van Nostrand Reinhold, New York, 1977.

- [25] Blevins, R.D., Review of sound induced by vortex shedding from cylinders, *Journal of Sound and Vibration*, 1984, 92, 455–470.
- [26] Saffman, P.G., *Vortex dynamics*, Cambridge University Press, Cambridge, 1992.
- [27] Blake, W.K., *Mechanics of flow-induced sound and vibration*, Academic Press, Orlando, 1986.
- [28] Strouhal, V., Ueber eine besondere art der tonerregung, *Annalen der Physik*, 1878, 241, 216–251.
- [29] Fitzpatrick, J.A., The prediction of flow-induced noise in heat exchanger tube arrays, *Journal of Sound and Vibration*, 1985, 99, 425–435.
- [30] Ziada, S., Oengören, A. and Bühlmann, E.T., On acoustical resonance in tube arrays part I: experiments, *Journal of Fluids and Structures*, 1989, 3, 293–314.
- [31] Blevins, R.D., Experiments on acoustic resonance in heat exchanger tube bundles, *Journal of Sound and Vibration*, 1993, 164, 503–533.
- [32] Rockwell, D., Oscillations of impinging shear layers, *AIAA Journal*, 1983, 21, 645–664.
- [33] Rockwell, D. and Naudascher, E., Review – Self-sustaining oscillations of flow past cavities, *Journal of Fluids Engineering*, 1978, 100, 152–165.
- [34] Rockwell, D. and Naudascher, E., Self-sustained oscillations of impinging free shear layers, *Annual Review of Fluid Mechanics*, 1979, 11, 67–94.
- [35] Blake, W.K. and Powell, A., The development of contemporary views of flow-tone generation, in *Recent advances in aeroacoustics*, Springer-Verlag, New York, 1986.
- [36] Powell, A., Some aspects of aeroacoustics: from Rayleigh until today, *Journal of Vibration and Acoustics*, 1990, 112, 145–159.
- [37] Howe, M.S., Edge, cavity and aperture tones at very low Mach numbers, *Journal of Fluid Mechanics*, 1997, 330, 61–84.
- [38] Howe, M.S., Rayleigh conductivity and self-sustained oscillations, in *Theoretical and computational fluid dynamics*, Springer-Verlag, New York, 1998.
- [39] Howe, M.S., *Acoustics of fluid-structure interactions*, Cambridge University Press, Cambridge, 1998.
- [40] Gloerfelt, X., Cavity noise, *VKI Lecture: Aerodynamic noise from wall bounded flows*, 2009, Brussels, Belgium.
- [41] Howe, M.S., The dissipation of sound at an edge, *Journal of Sound and Vibration*, 1980, 70, 407–411.
- [42] Howe, M.S., *Theory of vortex sound*, Cambridge University Press, Cambridge, 2003.
- [43] Hirschberg, A. and Schram, C., A primitive approach to aeroacoustics, in: Y. Aurégan, A. Maurel, V. Pagneux (Ed.), *Sound-flow interactions*, Springer, Berlin, 2002.
- [44] Pierce, A.D., *Acoustics: an introduction to its physical principles and applications*, McGraw-Hill, London, 1991.
- [45] Peters, M.C.A.M., *Aeroacoustic Sources in Internal Flows*, PhD Thesis, Technische Universiteit Eindhoven, 1993.
- [46] Ziada, S., Flow-excited resonances of piping systems containing side-branches: excitation mechanism, counter-measures and design guidelines, *Seminar on Acoustic Pulsations in Rotating Machinery*, 1993, Toronto, Ontario, Canada.
- [47] Ziada, S., A flow visualization study of flow-acoustic coupling at the mouth of a resonant side-branch, *Journal of Fluids and Structures*, 1994, 8, 391–416.
- [48] Kriesels, P.C., Peters, M.C.A.M., Hirschberg, A., Wijnands, A.P.J., Iafrafi, A., Riccardi, G., Piva, R. and Bruggeman, J.C., High amplitude vortex-induced pulsations in a gas transport

- system, *Journal of Sound and Vibration*, 1995, 184, 343–368.
- [49] Ziada, S. and Shine, S., Strouhal numbers of flow-excited acoustic resonance of closed side branches, *Journal of Fluids and Structures*, 1999, 13, 127–142.
- [50] Dequand, S., Hulshoff, S.J. and Hirschberg, A., Self-sustained oscillations in a closed side branch system, *Journal of Sound and Vibration*, 2003, 265, 359–386.
- [51] Slaton, W.V. and Zeegers, J.C.H., Acoustic power measurements of a damped aeroacoustically driven resonator, *Journal of the Acoustical Society of America*, 2005, 118, 83–91.
- [52] Slaton, W.V. and Zeegers, J.C.H., An aeroacoustically driven thermoacoustic heat pump, *Journal of the Acoustical Society of America*, 2005, 117, 3628–3635.
- [53] Oshkai, P. and Yan, T., Experimental investigation of coaxial side branch resonators, *Journal of Fluids and Structures*, 2008, 24, 589–603.
- [54] Oshkai, P., Yan, T., Velikorodny, A. and VanCaesele, S., Acoustic power calculation in deep cavity flows: a semiempirical approach, *Journal of Fluids Engineering*, 2008, 130, 1–9.
- [55] Arthurs, D. and Ziada, S., Flow-excited acoustic resonances of coaxial side-branches in an annular duct, *Journal of Fluids and Structures*, 2009, 25, 42–59.
- [56] Bruggeman, J.C., Hirschberg, A., van Dongen, M.E.H., Wijnands, A.P.J. and Gorter, J., Self-sustained aero-acoustic pulsations in gas transport systems: experimental study of the influence of closed side branches, *Journal of Sound and Vibration*, 1991, 150, 371–393.
- [57] Ho, C.M. and Nosseir, N.S., Dynamics of an impinging jet. Part 1. The feedback phenomenon, *Journal of Fluid Mechanics*, 1981, 105, 119–142.
- [58] Bruggeman, J.C., *Flow induced pulsations in pipe systems*, PhD Thesis, Technische Universiteit Eindhoven, 1987.
- [59] Elder, S.A., Self-excited depth-mode resonance for a wall-mounted cavity in turbulent flow, *Journal of the Acoustical Society of America*, 1978, 64, 877–890.
- [60] Fletcher, N.H., Air flow and sound generation in musical wind instruments, *Annual Review of Fluid Mechanics*, 1979, 11, 123–146.
- [61] Elder, S.A., Farabee, T.M. and DeMetz, F.C., Mechanisms of flow-excited cavity tones at low Mach number, *Journal of the Acoustical Society of America*, 1982, 72, 532–549.
- [62] Nelson, P.A., Halliwell, N.A. and Doak, P.E., Fluid dynamics of a flow excited resonance, part II: flow acoustic interaction, *Journal of Sound and Vibration*, 1983, 91, 375–402.
- [63] Kook, H. and Mongeau, L., Analysis of the periodic pressure fluctuations induced by flow over a cavity, *Journal of Sound and Vibration*, 2002, 251, 823–846.
- [64] Den Hartog, J.P., *Mechanical Vibrations*, McGraw-Hill, London, 1956.
- [65] Batchelor, G.K., *An introduction to fluid dynamics*, Cambridge University Press, Cambridge, 1970.
- [66] Rayleigh J.W.S., *The theory of sound*, Dover Publications, New York, 1945.
- [67] Michalke, A., On spatially growing disturbances in an inviscid shear layer, *Journal of Fluid Mechanics*, 1965, 23, 521–544.
- [68] Freymuth, P., On transition in a separated laminar boundary layer, *Journal of Fluid Mechanics*, 1966, 25, 683–704.
- [69] Keller, J.J., Non-linear self-excited acoustic oscillations in cavities, *Journal of Sound and Vibration*, 1984, 94, 397–409.
- [70] Disselhorst, J.H.M. and van Wijngaarden, L., Flow in the exit of open pipes during acoustic resonance, *Journal of Fluid Mechanics*, 1980,

- 99, 293–319.
- [71] Graf, H.R. and Ziada, S., Flow induced acoustic resonance in closed side branches: an experimental determination of the excitation source, *International Symposium on Flow-Induced Vibration and Noise*, 1992, Anaheim, California, United States.
- [72] Graf, H.R. and Ziada, S., Excitation source of a side-branch shear layer, *Journal of Sound and Vibration*, 2010, 329, 2825–2842.
- [73] Hirschberg, A., Gilbert, J., Msallam, R. and Wijnands, A.P.J., Shock waves in trombones, *Journal of the Acoustical Society of America*, 1996, 99, 1754–1758.
- [74] Hofmans, G.C.J., *Vortex sound in confined flows*, PhD Thesis, Technische Universiteit Eindhoven, 1998.
- [75] Bruggeman, J.C., The propagation of low-frequency sound in a two-dimensional duct system with T joints and right angle bends: Theory and experiment, *Journal of the Acoustical Society of America*, 1987, 82, 1045–1051.
- [76] Howe, M.S., Mechanism of sound generation by low Mach number flow over a wall cavity, *Journal of Sound and Vibration*, 2004, 273, 103–123.
- [77] Ronneberger, D., Experimentelle Untersuchungen zum akustischen Reflexionsfaktor von unstenigen Querschnittänderungen in einem luftdurchströmten Rohr, *Acustica*, 1967, 19, 222–235.
- [78] Ronneberger, D., The acoustical impedance of holes in the wall of flow ducts, *Journal of Sound and Vibration*, 1972, 24, 133–150.
- [79] Cummings, A. and Eversman, W., High amplitude acoustic transmission through duct terminations: theory, *Journal of Sound and Vibration*, 1983, 91, 503–518.
- [80] Durrieu, P., Hofmans, G., Ajello, G., Boot, R., Aurégan, Y., Hirschberg, A. and Peters, M.C.A.M., Quasisteady aero-acoustic response of orifices, *Journal of the Acoustical Society of America*, 2001, 110, 1859–1872.
- [81] Ingard, U. and Ising, H., Acoustic nonlinearity of an orifice, *Journal of the Acoustical Society of America*, 1967, 42, 6–17.
- [82] Candel, S.M., Acoustic conservation principles and an application to plane and modal propagation in nozzles and diffusers, *Journal of Sound and Vibration*, 1975, 41, 207–232.
- [83] Davies, P.O.A.L., Practical flow duct acoustics, *Journal of Sound and Vibration*, 1988, 124, 91–115.
- [84] Peters, M.C.A.M., Hirschberg, A., Reijnen, A.J. and Wijnands, A.P.J., Damping and reflection coefficient measurements for an open pipe at low Mach and low Helmholtz numbers, *Journal of Fluid Mechanics*, 1993, 256, 499–534.
- [85] Boij, S. and Nilsson, B., Reflection of sound at area expansions in a flow duct, *Journal of Sound and Vibration*, 2003, 260, 477–498.
- [86] Boij, S. and Nilsson, B., Scattering and absorption of sound at flow duct expansions, *Journal of Sound and Vibration*, 2006, 289, 577–594.
- [87] Rämmal, H. and Åbom, M., Characterization of air terminal device noise using acoustic 1-port source models, *Journal of Sound and Vibration*, 2007, 300, 727–743.
- [88] Kooijman, G., Testud, P., Aurégan, Y. and Hirschberg, A., Multimodal method for scattering of sound at a sudden area expansion in a duct with subsonic flow, *Journal of Sound and Vibration*, 2008, 310, 902–922.
- [89] Boij, S., Flow effects on the acoustic end correction of a sudden in-duct area expansion, *Journal of the Acoustical Society of America*, 2009, 126, 995–1004.
- [90] Kooijman, G., Hirschberg, A. and Aurégan, Y., Influence of mean flow profile and

- geometrical ratios on scattering of sound at a sudden area expansion in a duct, *Journal of Sound and Vibration*, (2009), doi:10.1016/j.jsv.2009.09.021.
- [91] Benade, A.H., On the mathematical theory of woodwind finger holes, *Journal of the Acoustical Society of America*, 1960, 32, 1591–1608.
- [92] Keefe, D.H., Theory of the single woodwind tone hole, *Journal of the Acoustical Society of America*, 1982, 72, 676–687.
- [93] Keefe, D.H., Woodwind air column models, *Journal of the Acoustical Society of America*, 1990, 88, 35–51.
- [94] Nederveen, C.J., *Acoustical aspects of woodwind instruments*, Northern Illinois University Press, DeKalb, 1998.
- [95] Dubos, V., Kergomard, J., Khettabi, A., Dalmont, J.P., Keefe, D.H. and Nederveen, C.J., Theory of sound propagation in a duct with branched tube using modal decomposition, *Acta Acustica*, 1999, 85, 153–169.
- [96] Kirchhoff, G., Über den Einfluß der Wärnteilung in einem Gase auf die Schallbewegung, *Annalen der Physik und Chemie*, 1868, 134, 177–193.
- [97] Tijdeman, H., On the propagation of sound waves in cylindrical tubes, *Journal of Sound and Vibration*, 1975, 39, 1–33.
- [98] Kergomard, J., Comments on “wall effects on sound propagation in tubes”, *Journal of Sound and Vibration*, 1985, 98, 149–155.
- [99] Kergomard, J., Bruneau, M., Bruneau, A.M. and Herzog, P., On the propagation constant of higher order modes in a cylindrical waveguide, *Journal of Sound and Vibration*, 1988, 126, 178–181.
- [100] Ronneberger, D. and Ahrens, C.D., Wall shear stress caused by small amplitude perturbations of turbulent boundary-layer flow: an experimental investigation, *Journal of Fluid Mechanics*, 1977, 83, 433–464.
- [101] Allam, S. and Åbom, M., Investigation of damping and radiation using full plane wave decomposition in ducts, *Journal of Sound and Vibration*, 2006, 292, 519–534.
- [102] Selamet, A., Kurniawan, D., Knotts, B.D. and Novak, J.M., Whistles with a generic sidebranch: production and suppression, *Journal of Sound and Vibration*, 2002, 250, 277–298.
- [103] Ziada, S., McLaren, K.W. and Li, Y., Flow-acoustic coupling in T-junctions: Effect of T-junction geometry, *Journal of Pressure Vessel Technology*, 2009, 131, 1–14.
- [104] Panton, R.L., Effect of orifice geometry on Helmholtz resonator excitation by grazing flow, *AIAA Journal*, 1990, 28, 60–65.
- [105] Dequand, S., Luo, X., Willems, J. and Hirschberg, A., Helmholtz-like resonator self-sustained oscillations, Part 1: Acoustical measurements and analytical models, *AIAA Journal*, 2003, 41, 408–415.
- [106] Dequand, S., Hulshoff, S., Van Kuijk, H., Willems, J. and Hirschberg, A., Helmholtz-like resonator self-sustained oscillations, Part 2: Detailed flow measurements and numerical simulations, *AIAA Journal*, 2003, 41, 416–423.
- [107] Ingard, U. and Singhal, V.K., Effect of flow on the acoustic resonances of an open-ended duct, *Journal of the Acoustical Society of America*, 1975, 58, 788–793.
- [108] Bechert, D.W., Sound absorption caused by vorticity shedding, demonstrated with a jet flow, *Journal of Sound and Vibration*, 1980, 70, 389–405.
- [109] Hofmans, G.C.J., Boot, R.J.J., Durrieu, P.P.J.M., Aurégan, Y. and Hirschberg, A., Aeroacoustic response of a slit-shaped diaphragm in a pipe at low Helmholtz number, 1: quasi-steady results, *Journal of Sound and Vibration*, 2001, 244, 35–56.

- [110] Hofmans, G.C.J, Ranucci, M., Ajello, G., Aurégan, Y. and Hirschberg, A., Aeroacoustic response of a slit-shaped diaphragm in a pipe at low Helmholtz number, 2: unsteady results, *Journal of Sound and Vibration*, 2001, 244, 57–77.
- [111] Hirschberg, A., Bruggeman, J.C., Wijnands, A.P.J. and Smits, N., The whistler nozzle and horn as aeroacoustics sound source in pipe systems, *Acustica*, 1989, 68, 157–160.
- [112] Tonon, D., Willems, J.F.H., Hirschberg, A., Föller, S. and Polifke, W., Flow-induced pulsations in double closed branch systems, *16th AIAA/CEAS Aeroacoustics Conference*, 2010, Stockholm, Sweden.
- [113] Peters, M.C.A.M. and van Bokhorst, E., Flow-induced pulsations in pipe systems with closed branches, impact of flow direction, 7th *International Conference on Flow-Induced Vibration*, 2000, Lucerne, Switzerland.
- [114] Meissner, M., Acoustic modes induced by flow in a pipe with two closed side-branches, *Applied Acoustics*, 2002, 63, 1071–1083.
- [115] Smits, N.P.M., *Stromingsgeïnduceerde pulsaties in gastransportleidingen: modellen volle schaal experimenten*, Report TUE NT R-865-A, Technische Universiteit Eindhoven, 1987.
- [116] Tonon, D., Nakiboglu, G., Willems, J.F.H., Hirschberg, A., Leandro, R.E., Polifke, W. and Riezebos, H.J., Self-sustained aeroacoustic oscillations in multiple side branch pipe systems, *15th AIAA/CEAS Aeroacoustics Conference*, 2009, Miami, Florida, United States.
- [117] Geerssen, T.M., *Physical properties of natural gases*, N.V. Nederlandse Gasunie, Groningen, 1988.
- [118] Tonon, D., Landry, B.J.T., Belfroid, S.P.C., Willems, J.F.H., Hofmans, G.C.J. and Hirschberg, A., Whistling of a pipe system with multiple side branches: Comparison with corrugated pipes, *Journal of Sound and Vibration*, 2010, 329, 1007–1024.
- [119] Nakiboglu, G., Belfroid, S.P.C., Tonon, D., Willems, J.F.H. and Hirschberg, A., A parametric study on the whistling of multiple side branch system as a model for corrugated pipes, *ASME Pressure Vessels and Piping Division Conference*, 2009, Prague, Czech Republic.
- [120] Nakiboglu, G., Belfroid, S.P.C., Willems, J.F.H. and Hirschberg, A., Whistling behavior of periodic systems: corrugated pipes and multiple side branch system, *International Journal of Mechanical Sciences*, Article in press, DOI: 10.1016/j.ijmecsci.2010.03.018.
- [121] Elliot, J.W., Corrugated pipe flow, in: M.C.M. Wrigth (Ed.), *Lecture notes on the mathematics of acoustics*, Imperial College Press, London, 2005.
- [122] Ziada, S., Scott, A. and Arthurs, D., Acoustic excitation by flow in T-junctions, *Journal of Pressure Vessel Technology*, 2007, 129, 14–20.
- [123] Blevins, R.D., *Applied fluid dynamics handbook*, Krieger Publishing Company, Malabar, 1992.
- [124] Nelson, P.A., Halliwell, N.A. and Doak, P.E., Fluid dynamics of a flow excited resonance, part I: experiment, *Journal of Sound and Vibration*, 1981, 78, 15–38.
- [125] Knisely, C. and Rockwell D., Self-sustained low-frequency components in an impinging shear layer, *Journal of Fluid Mechanics*, 1982, 116, 157–186.
- [126] Ma, R., Slaboch, P.E. and Morris, S.C., Fluid mechanics of the flow-excited Helmholtz resonator, *Journal of Fluid Mechanics*, 2009, 623, 1–26.
- [127] Radavich, P.M., Selamet, A. and Novak J.M., A computational approach for flow-acoustic coupling in closed side branches, *Journal of the Acoustical Society of America*, 2001, 109, 1343–1353.
- [128] Nakiboglu, G. and Hirschberg, A., A numerical study of the aeroacoustic

- interaction of a cavity with a confined flow: effect of edge geometry in corrugated pipes, *ASME 3rd Joint US-European Fluids Engineering Summer Meeting and 8th International Conference on Nanochannels, Microchannels, and Minichannels*, 2010, Montreal, Canada.
- [129] Stokes, A.N. and Welsh, M.C., Flow-resonant sound interaction in a duct containing a plate, II: square leading edge, *Journal of Sound and Vibration*, 1986, 104, 55–73.
- [130] Verzicco, R. and Vittori, G., Direct simulation of transition in Stokes boundary layers, *Physics of Fluids*, 1996, 8, 1341–1343.
- [131] Coltman, J.W., Sounding mechanism of the flute and organ pipe, *Journal of the Acoustical Society of America*, 1968, 44, 983–992.
- [132] Rockwell, D., Prediction of oscillation frequencies for unstable flow past cavities, *Journal of Fluids Engineering*, 1977, 99, 294–300.
- [133] Elder, S.A., Forced oscillations of a separated shear layer with application to cavity flow-tone effects, *Journal of the Acoustical Society of America*, 1980, 67, 774–781.
- [134] Ronneberger, D., The dynamics of shearing flow over a cavity – a visual study related to the acoustic impedance of small orifices, *Journal of Sound and Vibration*, 1980, 71, 565–581.
- [135] Elder, S.A., The mechanisms of sound production in organ pipes and cavity resonators, *Journal of the Acoustical Society of Japan*, 1992, 13, 11–23.
- [136] Möhring, W., On flows with vortex sheets and solid plates, *Journal of Sound and Vibration*, 1975, 38, 403–412.
- [137] Crighton, D.G., The Kutta condition in unsteady flow, *Annual Review of Fluid Mechanics*, 1985, 17, 411–445.
- [138] Kooijman, G., Hirschberg, A. and Golliard, J., Acoustical response of orifices under grazing flow: Effect of boundary layer profile and edge geometry, *Journal of Sound and Vibration*, 2008, 315, 849–874.
- [139] Åbom, M., Karlsson, M. and Kierkegaard, A., On the use of linear aeroacoustic methods to predict whistling, *Noise and Vibration: Emerging Methods*, 2009, Oxford, United Kingdom.
- [140] Karlsson, M. and Åbom, M., Aeroacoustics of T-junctions – An experimental investigation, *Journal of Sound and Vibration*, 2010, 329, 1793–1808.
- [141] Fabre, B., Hirschberg, A. and Wijnands, A.P.J., Vortex shedding in steady oscillation of a flue organ pipe, *Acustica*, 1996, 82, 863–877.
- [142] Verge, M.P., Fabre, B., Hirschberg, A. and Wijnands, A.P.J., Sound production in recorderlike instruments. I. Dimensionless amplitude of the internal acoustic field, *Journal of the Acoustical Society of America*, 1997, 101, 2914–2924.
- [143] Hirschberg, A. and Rienstra, S.W., Elements of aero-acoustics, *VKI Lecture Series notes LS 94-04*, 1994, Brussels, Belgium.
- [144] Ito, H. and Imai, K., Energy losses at 90° pipe junctions, *ASCE Journal of the Hydraulics Division*, 1973, 99, 1353–1368.
- [145] Thompson, M.C., Hourigan, K., Welsh, M.C. and Soh, W.K., Prediction of vortex shedding from bluff bodies in the presence of a sound field, *Fluid Dynamics Research*, 1988, 3, 349–352.
- [146] Hourigan, K., Welsh, M.C., Thompson, M.C. and Stokes, A.N., Aerodynamic sources of acoustic resonance in a duct with baffles, *Journal of Fluids and Structures*, 1990, 4, 345–370.
- [147] Thompson, M.C., Hourigan, K., Welsh, M.C. and Brocher, E., Acoustic sources in a tripped flow past a resonator tube, *AIAA Journal*, 1992, 30, 1484–1491.

- [148] Chorin, A.J. and Bernard, P.S., Discretization of a vortex sheet, with an example of roll-up, *Journal of Computational Physics*, 1973, 13, 423–428.
- [149] Krasny, R., A study of singularity formation in a vortex sheet by the point-vortex approximation, *Journal of Fluid Mechanics*, 1986, 167, 65–93.
- [150] Krasny, R., Computation of vortex sheet roll-up in the Trefftz plane, *Journal of Fluid Mechanics*, 1987, 184, 123–155.
- [151] Martínez-Lera, P., Schram, C., Föller, S., Kaess, R. and Polifke, W., Identification of the aeroacoustic response of a low Mach number flow through a T-joint, *Journal of the Acoustical Society of America*, 2009, 126, 582–586.
- [152] Nakiboglu, G. and Hirschberg, A., A Numerical study of the aeroacoustics of corrugated pipes: Effect of the ratio of pipe diameter to cavity depth, *17th International Congress on sound & vibration*, 2010, Cairo, Egypt.
- [153] Binnie, A.M., Self-induced waves in a conduit with corrugated walls. II. Experiments with air in corrugated and finned tubes, *Proceedings of the Royal Society of London*, 1961, 262, 179–191.
- [154] Golliard, J., *Noise of Helmholtz-resonator like cavities excited by a low Mach-number turbulent flow*, PhD Thesis, University of Poitiers, 2002.
- [155] Föller, S., Polifke, W. and Tonon, D., Aeroacoustic characterization of T-junctions based on Large Eddy Simulation and System Identification, *16th AIAA/CEAS Aeroacoustics Conference*, 2010, Stockholm, Sweden.
- [156] Gloerfelt, X., Bailly, C. and Juvé, D., Direct computation of the noise radiated by a subsonic cavity flow and application of integral methods, *Journal of Sound and Vibration*, 2003, 266, 119–146.
- [157] Derks, M.M.G. and Hirschberg, A., Self-sustained oscillation of the flow along Helmholtz resonators in a tandem configuration, in: E. de Langre, F. Axisa (Eds.), *Proceedings of the 8th International Conference on Flow-Induced Vibration*, 2004, Ecole Polytechnique, Paris, 435–440.
- [158] Tonon, D., Willems, J.F.H. and Hirschberg, A., Flow-induced pulsations in pipe systems with closed side branches: study of the effectiveness of detuning as remedial measure, *20th International Congress on Acoustics*, 2010, Sydney, Australia.
- [159] Anderson, P.W., Absence of diffusion in certain random lattices, *Physical Review*, 1958, 109, 1492–1505.
- [160] Wilson, M., A photonic crystal localizes light in two dimensions, *Physics Today*, 2007, 60, 22–23.
- [161] Lagendijk, A., van Tiggelen, B. and Wiersma, D.S., Fifty years of Anderson localization, *Physics Today*, 2009, 62, 24–29.
- [162] Dépollier, C., Kergomard, J. and Laloe, F., Localisation d'Anderson des ondes dans les réseaux acoustiques unidimensionnels aléatoires (Anderson localization of the waves in the acoustic one-dimensional random networks), *Annales de Physique*, 1986, 11, 457–492.
- [163] Meissner, M.W. and Czechowicz, R., Experimental investigation of flow-induced acoustic oscillations in a piping system with closed branches, *Applied Acoustics*, 1995, 45, 359–375.
- [164] Jungowski, W.E. and Studzinski W., *United States Patent*, Patent Number: 4,867,190, 1989.
- [165] Amandolèse, X., Hémon, P. and REGARDIN, C., An experimental study of the acoustic oscillations by flows over cavities, *Journal of Vibration and Acoustics*, 2004, 126, 190–195.
- [166] Ffowcs Williams, J.E. and Huang, X.Y., Active stabilization of compressor surge, *Journal of Fluid Mechanics*, 1989, 204, 245–262.
- [167] Huang, X.Y., and Weaver, D.S., On the active control of shear layer oscillations across

- a cavity in the presence of pipeline acoustic resonance, *Journal of Fluids and Structures*, 1991, 5, 207–219.
- [168] Welsh, M.C., Hourigan, K., Alfredson, R.J. and Pan Di Lin, Active control of flow-excited acoustic resonance: Higher order acoustic modes, 1991, *International Conference on Flow-Induced Vibration*, Brighton, United Kingdom.
- [169] Sarno, R.L. and Franke, M.E., Suppression of flow-induced pressure oscillations in cavities, *Journal of Aircraft*, 1994, 31, 90–96.
- [170] McGrath, S. and Shaw, L., Active control of shallow cavity acoustic resonance, 27th *AIAA Fluid Dynamics Conference*, 1996, New Orleans, Louisiana, United States.
- [171] Cattafesta III, L.N., Garg, S., Choudhari, M. And Li, F, Active control of flow-induced cavity resonance, 28th *AIAA Fluid Dynamics Conference*, 1997, Snowmass Village, Colorado, United States.
- [172] Ziada, S., Control of fluid-structure-sound interaction mechanisms by means of synthetic jets, 2003, *JSME International Journal*, 46, 873–880.
- [173] Ziada, S., Ng, H. and Blake, C.E., Flow excited resonance of a confined shallow cavity in low Mach number flow and its control, *Journal of Fluids and Structures*, 2003, 18, 79–92.
- [174] Ziada, S., Interaction of a jet-slot oscillator with a deep cavity resonator and its control, *Journal of Fluids and Structures*, 2001, 15, 831–843.
- [175] Ziada, S., Feedback control of globally unstable flows: impinging shear flows, *Journal of Fluids and Structures*, 1995, 9, 907–923.
- [176] Dequand, S., Willems, J., Leroux, M., Vullings, R., van Weert, M., Thieulot, C. and Hirschberg, A., Simplified models of flue instruments: Influence of mouth geometry on the sound source, *Journal of the Acoustical Society of America*, 2003, 113, 1724–1735.

NO PLEASING SOME PEOPLE

T-mobile wants to erect a 125-foot cell tower in Bridgewater, NJ. To make it less obtrusive, they offered to design it as a flagpole. And now residents are complaining about the possibility of noise arising from the flapping of the flag, and the slapping of its ropes on flagpole.

BYPASS CONSTRUCTION COMPENSATION – SMALL

AROUND 60 people have received compensation after complaining about noise, dust and damage following the opening of a bypass near their homes. Stoke-on-Trent City Council has paid out the undisclosed sums after families living near the Tunstall Northern Bypass, in Sandyford, claimed the road has damaged their properties and created extra noise and dust. A further 25 claims have been assessed and will be paid out in the New Year. 370 more residents are still waiting for decisions on their claims. The council has set aside £180,000 to cover claims linked to the road which is officially known as James Brindley Way. Claims are being assessed under Part I of the Land Compensation Act 1973. The act states that compensation can be claimed by people who own or occupy a property which has been reduced in value by more than £50 by physical factors caused by a new or altered road which include noise and vibration. Assuming the Council's provision of £180,000 is realistic, and assuming all remaining claimants are successful, it appears that the average pay out will be around £400.